A Computational Model of Networked Small-Scale Fuel Synthesis Demonstrating Greater Production Flexibility and Specificity

Thomas Socci

Submitted in partial fulfillment of the
requirements for the degree of
Doctor of Philosophy
in the Graduate School of Arts and Sciences

COLUMBIA UNIVERSITY

2013

ABSTRACT

A Computational Model of Networked Small-Scale Fuel Synthesis Demonstrating Greater Production Flexibility and Specificity

Thomas Socci

The rapid pace of industrial change over the past hundred years has led to any number of paradigm shifts in the way business is conducted and technologies are applied, but economies of large scale have persisted in the energy sector. In an age of automation and mass-production of small units, however, complex networking of many small energy systems can permit novel application of established technologies. This dissertation explores how established fuel synthesis technologies might behave in an automated network in which familiar units are arranged in unfamiliar ways. The flexibility afforded by automation and small scale operation allows for potentially complementary means of exploiting the fungible nature of hydrocarbon resources. Beyond any benefits of small-scale incurred from mass production and learning, fuel synthesis is a process with sensitivities to input streams that a network could exploit in a nuanced way. The completed work demonstrates that a network of small-scale fuel synthesis reactors and thermal crackers, based on current industrial practices at large monolithic scale, can be networked to dramatically sharpen the chemical spectrum they produce. In order to study the behavior of such a network in ways that are unavailable in current software, a hierarchical numerical modeling code was developed to offer greater flexibility to nest and optimize network configurations within network configurations, reflecting the modularity of the networks it is meant to simulate. This new code is capable of simulating aggressively numerically constrained networks, dynamically substituting various configurations while optimizing them across user-specified variables. Various weighting schemes were developed to facilitate more rapid convergence to a

numerical solution so that highly constrained recycling schemes could be reconciled to a steady state that would produce the specified output spectrum. Modular units were coded to simulate the essential properties of real processes and technologies, with close attention paid to the sensitivity of these processes to input conditions, so that these units could be assembled in various configurations and subjected to user-specified constraints. Coded modules were designed under the principle that these individual units need not be custom-made or technologically ahead of their time; the benefits explored by network simulations are incurred not by dramatically upgrading the processes being simulated, but rather by directing and redirecting the chemical streams which are subject to those processes to tailor the outcome to the desired product. This principle was applied to chemical separation in an analytical framework in order to derive how unremarkable separators might be networked to produce remarkable precision of separation. Such precision is important because the direction and redirection of chemical streams is predicated on the ability to select the destination of a particular chemical. The effect of networking fuel synthesis reactors and thermal crackers was studied for unidirectional flows in order to understand how repeated applications of these units at smaller scale sharpen the spectrum relative to single large scale application. These fuel synthesis reactors and thermal crackers were also configured in aggressively recycled networks, imposing more severe constraints on the output spectrum. This work demonstrated that fuel synthesis at industrial output scales need not operate in monolithic units and can benefit dramatically from judicious networking, to the point that a network of units that would otherwise have produced a broad spectrum of chemical flavors can be configured to produce only a single user-specified output chemical.

TABLE OF CONTENTS

LIST OF CHARTS, GRAPHS, AND ILLUSTRATIONS

ACKNOWLEDGEMENTS

First and foremost, I owe a great debt of personal and intellectual gratitude to Professor Klaus Lackner, whose insight, advice, creativity, generosity and patience made this work possible. Professor Ah-Hyung (Alissa) Park, Professor Paul Duby, and Professor Tuncel Yegulalp were invaluably helpful and instructive in advising my thesis proposal; their input shaped the direction and success of my research. I want to thank them as well as Professor Juerg Matter for conducting my doctoral defense. Carey Russell's administrative work for the Lenfest Center for Sustainable Energy supported all of us who were studying and researching there and was enormously helpful to me.

DEDICATION

For my parents, Eliott and Cynthia Socci, who have been endlessly patient and supportive of my studies from infancy to dissertation defense. They raised three doctors.

Chapter 1

Introduction & Motivation

The rapid pace of industrial change over the past hundred years has led to any number of paradigm shifts in the way business is conducted and technologies are applied, but economies of large scale have persisted in the energy sector. In an age of automation and mass-production, however, complex networking of energy systems can permit novel application of established technologies. Mass production of small, modular units can reap the benefits of both technological learning incurred by the small scale approach and the cost savings of mass production. First, the technology itself will evolve as small-scale manufacturers learn, leading to the exponential growth already observed in such industries. Moreover, smaller units that are mass produced, modular, and operated in aggregate by cheap automation and control systems would represent a new approach to scale in energy production and conversion infrastructure. Mass production and low unit costs would no longer require these individual reactor units to be long-lived or robust. The modularity reduces reliability requirements, and allows for frequent replacement of existing parts by newer, improved components; individual subunits of a large aggregated reactor network need not be engineered to the same high standards as monolithic

plants. The prospect of this new paradigm is by itself exciting and potentially applicable to a wide range of applications, but of particular interest to this work are the possibilities offered by fuel synthesis. Recent work here at Columbia University demonstrated that the arguments underlying the assumption that “bigger is better” may no longer be relevant, and made the strong case that massively parallel systems of small-scale mass produced units could be just as cost-effective and efficient as large scale units [1]. If this is true, what further gains from networking that are specific to fuel synthesis might we find?

This dissertation explores how established fuel synthesis technologies might be enhanced in an automated network in which familiar units are arranged in unfamiliar ways. The completed work computationally investigated the combination of two well-understood industrial practices, namely fuel synthesis and the mass production of small-scale machines, into an entirely new energy processing method of running an automated network of small modular fuel synthesis reactors and crackers. Instead of the current paradigm of energy production that exploits the minimum on a cost optimization curve at which larger is cheaper, this modeled modular network explores how the chemical output spectrum might be sharpened if the loss of the economy of large unit scale were compensated by the gain in economy of smaller, more flexible, mass produced units. Because fuel synthesis as a process is highly sensitive to its reaction conditions as well as the stoichiometry of its feedstock, the synthesis will particularly benefit from the small-scale paradigm in which the conditions of each individual unit could be customized, optimized, and automated, perhaps even in real-time, to obtain the desired distribution of conventional or designer hydrocarbon fuel products. Perhaps more effectively, however, each

unit need *not* be customized but rather the streams that are directed to various units are more carefully navigated. In this way gains are observed from the way streams are directed, rather than tailoring the units they are being directed through. The network is complex because it breaks a known process into sub-processes with feedback loops. Optimization referred to a system of penalties that assessed the value and performance of the network according to design criteria.

The flexibility afforded by automation and small scale operation allows for potentially complementary means of exploiting the fungible nature of hydrocarbon resources. The fuel synthesis network demonstrated here offers customizable and automated conversion of various indiscriminate sources of carbon to its most energetically dense form. Presently investigated is a simplified fuel production process based on the Fischer-Tropsch synthesis, a chemical process by which an array of liquid hydrocarbon fuels is produced from carbonaceous synthesis gas. Fuel synthesis, and particularly the Fischer-Tropsch process, is a currently viable and commercially available catalytic process at a minimum on the cost optimization curve at which larger is cheaper. At a lower point on the same curve it may well be possible that the loss of the economy of large singular scale is compensated for by the gain in economy of smaller, more flexible, mass produced units. If this is possible then one can ask the question how such smaller units can be networked to sharpen the chemical spectrum produced? This work assumes a black box syngas production step external to the network that provides CO and H_2, which in the original large-scale version were sole chemical inputs, but network manipulation of the throughput will alter and diversify the input compositions to provide optimum feedstock for the proposed small scale reactor units, which play off of one another as optimized by modeled command and control.

First developed in 1923 and in expanding but niche commercial use today, the Fischer-Tropsch process consists of the hydrogenation of adsorbed CO to form $–CH_2–$ “monomers” for stepwise oligomerization on catalyst surfaces. The source of the reactants is a synthesis gas of carbon monoxide and hydrogen, which are adsorbed onto the surface of a catalyst and polymerized into a spectrum of mostly non-branched hydrocarbons ranging in carbon number from methane to heavy wax. Fuel synthesis reactors designed for this process can grow these carbon chains, and thermal crackers can break them down.

The generic benefits of mass production of small-scale units certainly could apply to fuel synthesis; in one case of Fischer-Tropsch, for example, a slurry bubble column reactor must be taken entirely off-line for reactor-level maintenance, and although catalyst loading and off-loading is possible without shutting down such systems, catalyst poisoning rapidly spreads system-wide. Individual reactor units in a network can promptly and non-disruptively be taken off-line while feedstock is redirected; the cost here is, at most, the time constant to reach a new steady state in downstream affected reactors and any inefficiencies that are incurred during that transition. Here automation as modeled by the network code will play a particularly important role in optimizing that transition. Thus the failure of one single component out of many will not have the same catastrophic effects as the equivalent failure of a single big unit. Even in a steady-state system however, the parameters of these synthesizers and crackers exert great influence over the outgoing products, and different input feeds produce different outputs. They are therefore ripe for examination of their behavior in a network of such units receiving and producing judiciously directed chemical streams.

Flexibility of scale also permits optimization of flow regimes; a large scale plug flow reactor (PFR) setup can be approximated as a series of small slices of continuously stirred tank reactors (CSTR), only those small CSTR processes can be individually optimized with respect to its input and output streams to perform as dramatically enhanced PFR process when viewed as a single aggregated process. The Fischer-Tropsch reaction as a particular fuel synthesis option takes these potential advantages of smaller units one step further, given the sensitivity of this process to temperature, pressure, input gas stoichiometric ratios of carbon and hydrogen, catalyst type, and promoters. Existing reactors separate and recycle the output streams back into their own input stream to maximize conversion, but a network of smaller scale reactors allows output streams to be refined in terms of these parameters and redirected to different small-scale units whose conditions are optimized for the products of choice. These smaller units host reactions of shorter residence time, but are operated by process automation that can make decisions in real-time redirecting the small-unit tailgas to optimal reaction conditions. Of particular importance is the study and management of the secondary reactions that occur in a Fischer-Tropsch reactor, as recycled olefins have been demonstrated to be catalytically reabsorbed for further transformation and synthesis [2]. Understanding the conditions under which this occurs and the effect of various operating conditions on selectivity of products informs a networking control strategy through which the advantages of an aggregate network might be realized; enhanced control of reactants allows more selective control of products. Recent research suggests that running Fischer-Tropsch reactors in concert may be an ever more plausible approach [3]. In one joint study between the University of Tehran and the Irani Research Institute of Petroleum Industry, a dual-bed reactor was studied using different cobalt catalysts. An alkali-promoted cobalt catalyst was used in the

first bed of a fixed-bed reactor followed by a Ruthenium promoted cobalt catalyst in the second in order to assess the activity, product selectivity and system deactivation. Compared to a single-bed reactor, methane selectivity was 18.9 % lower, selectivity for hydrocarbons C5+ was 10.9 % higher, and accelerated deactivation 42 % lower. Catalyst recovery after regeneration was also favorable. These results hint at the possibility and promise of Fischer-Tropsch synthesis from a network of customizable reactors, reflecting optima unique to this process. The generalized advantages conferred by re-optimization of scale may further compound these gains.

As a final note, these arguments point towards an innovative and efficient production model for producing familiar liquid hydrocarbons in a novel way, but at the same time questions and does not explicitly rely on the assumption of gasoline and diesel as the ultimate choice of transportation fuels. These convenient products of oil refining are the status quo among transportation energy carriers, but in a post-oil world the reliance on these particular carbon chains may no longer be necessary. The Fischer-Tropsch process itself is evidence of the fungible nature of carbon resources, and is readily able to produce whatever flavor of hydrocarbon is de rigueur. For example, it has been shown in processes that can generate 90% gasoline in the product suite that DME generation in the presence of certain catalysts is highly effective in promoting the Fischer-Tropsch synthesis reactions [4]. However DME could in turn become the desired product, and its production from methanol synthesis units can be either inhibited where methanol is the product of choice or encouraged via dehydration. DME has been demonstrated to be an efficient choice of turbine fuel, a competitive automotive fuel, functional as residential fuel for heating and cooking, non-toxic and non-carcinogenic [5]. The network

simulated here focuses on the conventional fuels, as their introduction does not require changes in the existing infrastructure. However, as time goes on, this network would expect and accommodate an increasing focus on advanced designer fuels. There are no intrinsic constraints on the system in this regard. Automated process control of process conditions and feedstock parameters and astute choices of catalysts can easily handle this transition from one fuel to another, or indeed from one catalytic process to another. Nor are the behaviors and improvements simulated here unique to Fischer-Tropsch. Another process readily applied to the automated network concept could be methanol synthesis followed by methanol-to-gasoline transformation. Generally speaking, any "catalysis-in-a-box" that demonstrates sensitivity to conditions and input streams could stand to benefit if these streams were networked under a command and control algorithm designed to harness the marginal improvements to output as streams are navigated more judiciously.

Having motivated the study undertaken here, Chapter 2 of this dissertation will review the history and recent developments of the Fischer-Tropsch process in particular, with special attention paid to reactor selection and research with respect to scale. It will be clear that currently available Fischer-Tropsch technologies perform at small scale, and are therefore consistent with the assumption that off-the-shelf technologies could produce dramatically more specific outputs under clever network configurations. Chapter 3 reviews the design improvements coded into the numerical solver in order to enable more robust and computationally efficient reconciling of constraints and conservation laws. The tool developed here is applicable beyond the specific modeling for which it was employed for this dissertation. Chapter 4 justifies the matrices and

algorithms that were coded to reconcile the incoming and outgoing streams for each unit of the network. Presently observed process behaviors and typical parameters for fuel synthesis and thermal cracking were coded into matrices that map incoming reactant to chemicals into outgoing product chemicals (and vice versa), and this chapter details the way in which these matrices are constructed depending on user-specified parameters and actual chemical streams encountered by these units in real time. Chapter 5 is an analytical exploration of how simple separation units behave when networked under various configurations of continuous chains with and without internal recycle of chemicals. Here, again, the design objective is to make unremarkable units interact in such a way as to produce outputs that are dramatically more specific to the needs of the user without dramatic improvements to the individual underlying units. Chapter 6 is a presentation of the results of the network simulations under configurations of unidirectional cascades of reactors and more tightly arranged and looped recycle schemes. Outputs are shown to dramatically sharpen under the influence of networking as compared to once-through operation, and even recycled operation is shown to perform better when more recycling units, accomplishing less per unit, replace a single recycling unit that accomplishes more per unit. Chapter 7 concludes the dissertation with a review of these results.

References

1. Dahlgren, E., *Rescaling Capital: The Impact of Small-Scale Physical Capital in the Energy and Materials Processing Industries*, in *Earth & Environmental Engineering*. 2013, Columbia University: New York.

2. van der Laan, G.P. and A.A.C.M. Beenackers, *alpha-Olefin readsorption product distribution model for the gas-solid Fischer-Tropsch synthesis.* Natural Gas Conversion V, 1998. **119**: p. 179-184.

3. Tavasoli, A., A. Nakhaeipour, and K. Sadaghiani, *Raising Co/Al2O3 catalyst lifetime in Fischer-Tropsch synthesis by using a novel dual-bed reactor.* Fuel Processing Technology, 2007. **88**(5): p. 461-469.

4. Zonetti, P.C., *Fischer-Tropsch synthesis and the generation of DME in situ.* Fuel Processing Technology, 2009: p. 7.

5. Semelsberger, T.A., R.L. Borup, and H.L. Greene, *Dimethyl ether (DME) as an alternative fuel.* Journal of Power Sources, 2006. **156**(2): p. 497-511.

Chapter 2

A History and Process Overview of Fischer-Tropsch Fuel Synthesis

I. Process Overview

The Fischer-Tropsch process was first investigated at Franz Fischer's laboratories at the Kaiser Wilhelm Institute for Coal Research (currently the Max Plank Institute) in collaboration with the Ruhrchemie Company. The strategic value of liquid fuel production from coal outweighed any economic imperative, and industrial capacity in 1945 was 600,000 tons per year.

Historically, throughout the industrial developments outlined below, research and development of industrial fuel synthesis processes assumed singular, large scale structures, embracing and discarding various reactor designs under the assumption that the ability to scale-up to larger and larger reactor units was a critical criterion for reactor choice [1]. The exothermic nature of the reaction requires that scale-up designs have sufficient heat exchange to maintain an exothermic reaction environment; large cooling areas are required to shed this heat. The issue of pressure drop with increasing bed length is also a scale-up concern, as is observed in the long,

narrow reaction chambers of multi-tubular fixed bed reactors, or in re-circulating reactors that employ multiple passes of gaseous streams to maximize the conversion of syngas to hydrocarbon product. Maintaining these process conditions is of critical importance for the Fischer-Tropsch synthesis, as increased temperature favors selective methane formation (an undesired product), deposition of catalyst-damaging carbon, and reduced chain length of products. Thus the most prolific reactor design in commercial use today is the slurry bubble column reactor, which exhibits on large scales the requisite low pressure drop, excellent heat transfer characteristics for stable reactor temperatures, no diffusion limitations, continuous online refreshment of catalyst particles, and relatively simple construction at low investment capital cost [2]. To this day, the slurry bubble column and the multi-tubular reactor design are the only two Fischer-Tropsch models with significant market share [3].

I.1. Early History

Fischer-Tropsch synthesis development and research has been driven by environmental, political, and economic circumstances of the last 70 years evolving as an adaptation to energy niches. Remote natural gas reserves can be deemed "stranded" if they are too far to be cost-effectively transported. Fischer-Tropsch synthesis at these sites enables shipment of liquid fuels, but energy savings policies, carbon emissions awareness, and the taxing or outright prohibition of flaring can result in natural gas incurring even negative value on-site. Heavy oils are often better converted to syngas to produce clean diesel. With access to the global oil market, South African fuel synthesis has been redirected towards more valuable olefins rather than gasoline [4]. (Note that the ability to alter the intended chemical products of the facility, which is a

cumbersome at large monolithic scale, becomes simply a redirection of chemical streams in a small-scale network.)

From 1945-1955, large coal reserves, increasing liquid fuel demands and oil reserve uncertainty propelled interest in Fischer-Tropsch. Storch, Golumbic and Andserson evaluate German FT wartime activity for the US Bureau of Mines, the fluid bed process was developed in Brownsville, the circulating catalyst process at Kellog, the fixed bed, multi-tubular Arge process at Ruhrchemie-Lurgi, and the slurry process by Kölbel at Rheinpreußen. South Africa constructed and improved its Fischer-Tropsch synthesis as energetic necessity.

From 1955-1970, the world exploited large oil fields in Saudi Arabia, the North Sea and Alaska, so cheap and abundant oil generally marginalized interest in Fischer-Tropsch synthesis. South African activity continued at Sasol due to extremely cheap domestic coal and favorable state energy policies.

From 1970-1990, alarming forecasts about diminishing oil reserves and major oil boycotts spurred the United States, Japan, and Europe to develop coal-based Fischer-Tropsch processes. There was a desire for coal and heavy oil power plants with an integrated gasification and gas cleaning stage to produce clean syngas for methanol and Fischer-Tropsch synthesis. German research targeted Fischer-Tropsch synthesis of C_2, C_4 olefins.

Below is a summary of commercially deployed low-temperature (LTFT) and high-temperature (HTFT) Fischer-Tropsch synthesis facilities, which have only been catalyzed by iron and cobalt at large scale.

Fe-HTFT	Fe-LTFT	Co-LTFT
Fixed fluidized bed (1951, Hydrocol)	Fixed bed (1955, Arbeitsgemeinschaft Ruhrchemie-Lurgi)	Fixed bed (1936, German normal-pressure)
Circulating fluidized bed (1955, Kellogg Synthol)	Slurry bed (1993, Sasol slurry bed process)	Fixed bed (1937, German medium-pressure)
Circulating fluidized bed (1980, Sasol Synthol)		Fixed bed (1993, Shell middle distillate synthesis)
Fixed fluidized bed (1995, Sasol Advanced Synthol)		Slurry bed (2007, Sasol slurry bed process)

Figure 2.1: Industrially applied Fischer-Tropsch technologies, from de Klerk [5].

There has been increasing movement in recent years towards developing Fischer-Tropsch reactors that operate individually at smaller scale, in part because the existence of stranded or small natural gas fields that are too small to be viably developed using current commercial scales of reactor technology and too remote for pipelines [6]. Although this movement towards smaller scale eyes individual and decentralized operation, it creates further opportunity for the application of smaller synthesis technologies for use in series and parallel networks.

I.2. Syngas Preparation Overview

Although the network simulated in this work presupposes syngas preparation, a brief overview is worthwhile. Generally, fuel can be synthesized from any carbon-based feedstock, whether it be coal, petroleum coke, biomass, natural gas. Industrial production of syngas in currently commercially significant operations is most commonly the result of coal gasification,

though syngas can be produced more efficiently using natural gas via catalytic steam reforming, auto-thermal reforming, partial oxidation, and heat exchange reforming. Burgeoning natural gas development in the U.S. presents an abundant source of carbon and hydrogen to pass through a syngas intermediary towards fuel synthesis.

Syngas preparation, the lion's share of typical Fischer-Tropsch plants, accounts for 60-70% of the capital and operating costs [7]. This cost is incurred in no small part due to materials handling, ash removal, and purification of input fossil fuels and their concomitant sulfur, nitrogen, and soot content [8]. One of many advantages of synthetic fuel production subsequent to this step is that these impurities have been removed previous to network operation, improving the quality of the product and reducing decontamination costs associated with crude oil refining. The chemical profile of this feedstock will be revisited below, but it is important to note and this assumes the interchangeability of CO and CO_2 via the exothermic water-gas shift reaction (WGS, shown below) and its reciprocal, the reverse water-gas shift reaction (RWGS) which exchange an oxygen atom between hydrogen and water molecules:

$$CO + H_2O \rightarrow CO_2 + H_2 + 41.3\ kJ \qquad (1)$$

This reaction takes place under common catalytic conditions of the synthesis reactors downstream. Although Fischer-Tropsch fuel synthesis refers specifically to the modularity and small scale of the fuel synthesis reactors themselves, cracking and refining these outputs are critical components of the overall fuel production process, and specifically thermal cracking and hydrotreating were also investigated as modular components. In fact there is no reason to believe that the syngas preparation step itself couldn't one day be included in modular fashion. One

example of a process that has been demonstrated to be readily and favorably available at small scale is the CO_2-consuming RWGS reaction, which while only mildly endothermic, requires high temperatures for favorable kinetics, but recent work here at Columbia University by Professor Marco Castaldi suggested the availability of a highly effective means of conducting this reaction that could function within a modular network and at the appropriate scales. High temperature reactions are mass-transfer controlled, as discussed below with respect to reactor conditions, and so the choice of substrate is an important determinant of reactor performance and size. The short contact time (SCT) approach is to pass a rich fuel/air mixture over the catalyst at very high flow velocities such that the contact times are on the order of milliseconds, producing very high selectivities. The extremely short channel length of these substrates is a perfect fit for a network of aggregated small units and avoids the boundary layer buildup observed in conventional long channel monoliths. Relevant heat and mass transfer coefficients also depend on the boundary layer thickness. In a long-channel monolith a fully developed boundary layer is present over a considerable length of the device. The SCT technology would replace the long channels of a monolith with a series of short channel lengths, each short enough to avoid significant boundary layer build-up. The high heat and mass transfer rates allow extremely small reactor sizes – up to $1/20^{th}$ the size of conventional monoliths for equivalent conversion. The conversion per unit of geometric surface area of the SCT substrates can also be up to an order of magnitude higher than conventional monolith substrates under mass transfer limited conversion which can lead to significant cost reductions especially when using precious metal catalysts. Convective heat exchange with the gas phase is also strongly dependent on the boundary layer build-up, and the excellent convective heat transfer and low thermal mass of the SCT substrate results in rapid heat

exchange with the gas, allowing equilibrium conditions to be quickly achieved. In addition, reactors designed for using the SCT substrates offer equivalent conversion at a fraction of the volume with similar pressure drops as conventional monolithic substrates.

The RWGS approach is effective as a producer of feedstock for the Fischer-Tropsch synthesis, for which the optimal syngas consists of CO and not CO_2, due to the low conversion efficiencies with H_2-poor or CO_2-rich feedstock. However it is not necessarily the case that CO_2 as an output of syngas preparation needs to be converted to CO. Methanol can be synthesized from either partially or fully oxidized carbon with comparable free energies and enthalpies of reaction, and even as regards Fischer-Tropsch, recent research trends in hybrid catalyst systems point to the hydrogenation of CO_2 as a means of deploying that feedstock, enhancing the flexibility of the fuel synthesis step in response to its inputs [9, 10].

I.3. Fuel Synthesis Overview

I.3.1. The Fischer-Tropsch Process

First developed in 1923 and in expanding but niche commercial use today, the Fischer-Tropsch process consists of the hydrogenation of adsorbed CO to form $–CH_2–$ "monomers" for stepwise oligomerization on catalyst surfaces. The source of the reactants is a feedstock comprised by the synthesis gas of carbon monoxide and hydrogen introduced above along with any other hydrocarbon chemical streams that are revisiting the synthesis step. Favored species of this chemical stream are adsorbed onto the catalyst and undergo the overall exothermic synthesis reaction summarized as

$$CO + 2\,H_2 \rightarrow -CH_2- + H_2O + 165\ kJ \quad (2)$$

At each stage, the newly formed adsorbed hydrocarbon can desorb, hydrogenate, or continue chain growth with the adsorption of another monomer. Hydrogenation at termination produces *n*-alkanes while reductive abstraction produces 1-alkenes. Specifically, the most important reactions and products of the Fischer-Tropsch synthesis are [5]:

Alkanes: $n\,CO + (2n+1)\,H_2 \rightarrow H(CH_2)_nH + n\,H_2O$ (3)

Alkenes: $n\,CO + 2n\,H_2 \rightarrow (CH_2)_n + n\,H_2O$ (4)

Alcohols: $n\,CO + 2n\,H_2 \rightarrow H(CH_2)_nOH + (n-1)\,H_2O$ (5)

Carbonyls: $n\,CO + (2n-1)\,H_2 \rightarrow (CH_2)_nO + (n-1)\,H_2O$ (6)

Carboxylic acids: $n\,CO + (2n-2)H_2 \rightarrow (CH_2)_nO_2 + (n-2)\,H_2O$, $n > 1$ (7)

Water gas shift: $CO + H_2O \rightarrow CO_2 + H_2$ (8)

As indicated schematically below, desorption or chain growth proceeds according to some probability parameter (here *d*, α, respectively). The result is a suite of hydrocarbon paraffin waxes and olefins of varying chain length and industrial applicability, particularly gasoline and diesel. Synthetic fuels produced by this process are sulfur-free and nitrogen-free, and are therefore chemically cleaner than those produced from crude oil and obviate the need for extensive waste processing by the fuel synthesis network facility.

Stoichiometric ratios are critical to determining the per pass conversion and success of the above synthesis reactions, which is a consideration of syngas preparation for (a) the initial feed, (b) reactor and catalyst choice for management of the water-gas shift between H_2 and CO_2 ,

and (c) determination of selectivity and kinetics. While an H_2:CO ratio of ~2 is typically ideal, water-gas shift activity demands instead that the following ratios hold true:

$$\text{Stoichiometric ratio: } (H_2 - CO_2) / (CO + CO_2) \approx 2 \quad (9)$$

$$\text{Ribblett ratio: } (H_2) / (2\,CO + 3\,CO_2) \approx 1 \quad (10)$$

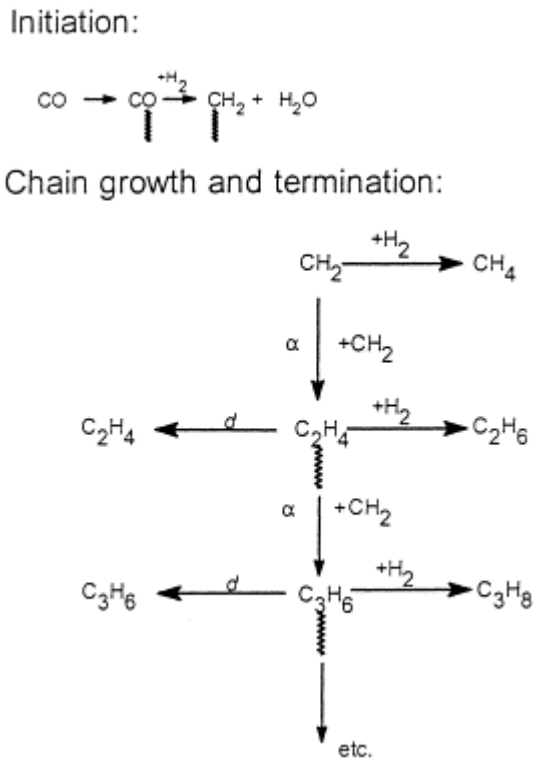

Figure 2.2: Illustration of chain growth and termination [7].

For probability of chain growth α, the distribution of carbon products of chain length *n* in the resulting carbon spectrum is given by the work of Anderson, Shulz, and Flory to model what is

known as the Anderson-Schulz-Flory (ASF) distribution of carbon number in the Fischer-Tropsch output. In terms of the mole fraction x_n of the spectrum, the equation given by [11]

$$x_n = (1 - \alpha) \cdot \alpha^{(n-1)} \tag{11}$$

In terms of the weight fraction W_n, the distribution is given by [12]

$$W_n = (\ln^2 \alpha) \cdot n \cdot \alpha^n \tag{12}$$

Also worth noting for computational purposes is a rearrangement of the above to enable empirical calculation of α from any two mole fractions according to

$$\frac{x_n}{x_j} = \alpha^{(n-j)} \tag{13}$$

The simplicity of this relation is appealing, but it is a model from which actual fuel synthesis deviates. Most significant are deviations in methane selectivity, deviations in C_2 selectivity, and the apparent bifurcation of the spectrum into two values of α [11].

Methane selectivity tends in practice to exceed that predicted by the above model. Proposed explanations for this in the literature include mass transfer limitations that permit the thermodynamic favorability of methane to prevail. The more rapid diffusion of H_2 depletes the relative CO content within the catalyst particle, increasing methane selectivity and hydrogenation to short chain-length products [13]. Also offered as explanation are heat transfer limitations of what is ideally an isothermal environment for this exothermic process to create “hot spots” in the reaction chamber which favor methane yield, and surface mobility or hydrogenation arguments that are specific to the reaction mechanism.

C_2 selectivity, by contrast, is overestimated by the ASF model, and the production of ethene relative to ethane is less than other analogous alkene/alkane ratios. Explanations for this behavior include the formation of M–CH_2–CH_2–M intermediates [5] that are capable of chain propagation at either end as well as secondary reactions via readsorption or hydrogenation to ethane. Secondary reactions of this nature, in which hydrocarbon products are adsorbed downstream to react further, is a particular area which the fuel synthesis network aims to exploit in order to sharpen the ultimate distribution of products. Secondary reactions occur with increasing frequency in Fe, Ru, and Co catalysts, respectively [11]. Both ethene and propene have been observed to readsorb more readily than other olefins [14], though in general olefins readsorb better at higher carbon numbers due to decreased mobility [15].

The apparent splitting of the product spectrum into two values of α is a feature of low-temperature (LTFT) processes, in which carbon products shorter than C_8 behave according to a chain growth probability α_1 while carbon products greater than C_{12} behave with probability α_2 [5]. In between these sizes, the mole fractions behave approximately according to the weighted average

$$x_n = \kappa_1 \cdot \alpha_1^{(n-1)} + \kappa_2 \cdot \alpha_2^{(n-1)} \tag{14}$$

The Botes equation was developed to express the chain-length dependence of α more accurately, recognizing that the model of a single growth probability, while mathematically convenient and remarkably close considering, does not explain increase with chain length *n* and plot curvature [16]:

$$\alpha_n = \frac{1}{1 + \tau_P + \tau_O \cdot \mathrm{e}^{-k \cdot n}} \tag{15}$$

Here, τ_P and τ_O are model parameters that are functions of the rate constants for hydrogenation (k_h), desorption (k_d), and growth rate (k_g) of paraffins and olefins respectively:

$$\tau_P = \frac{k_h}{k_g} \quad \text{and} \quad \tau_O = \frac{k_d}{k_g} \tag{16}$$

Because parameters τ_P and τ_O depend on rate constants, they are functions of the reaction conditions of temperature and reactant partial pressure. This model predicts the ratio of the production of alkenes (O) to alkanes (P) as function of chain length and of a parameter *k* that is independent of process conditions but depends on the properties of the catalyst:

$$\left(\frac{O}{P}\right)_n = \frac{\tau_P}{\tau_O} e^{-k \cdot n} \tag{17}$$

The chain length dependency of the olefin to paraffin ratio, O_n/P_n, has been attributed to diffusivity, solubility, and physisorption [11]. Diffusion limitations have been a subject of some debate in the literature in terms of how far they really go towards explaining such deviations in the product spectrum, but while they are crucially important towards determining activity and selectivity, more recent work has demonstrated that they do not primarily explain secondary reactions of olefins [13]. A model has been derived that accounts for solubility and physisorption as well as diffusivity [17], finding exponential dependence on chain length even using foils without diffusivity limitations. That research reported that in the diffusion limiting case the ratio, expressed this time as P/O, is

$$\frac{P_n}{O_n} \propto \frac{d}{D_n} \exp\left(\frac{n\Delta G_{1Phys}}{RT}\right) \propto \exp\{(0.2 \pm 0.1)n\}\, n^{0.6} \tag{18}$$

in which the free energy term is the Gibbs free energy of physisorption for a $–CH_2–$ monomer, d is the diffusion distance and D_n is the olefin chain-length-dependent diffusivity.

Solubility issues arise because liquid infused slurries are sensitive to vapor-liquid equilibria, and also tends to increase exponentially with carbon number [11]. Therefore, longer chains of hydrocarbons are favored for readsorption. Physisorption effects refer to a state in between chemisorptions and vapor, are governed by Van der Waals forces, and have enthalpies that are linear in carbon number.

These model considerations are included because secondary reactions of olefins stand to be an important tuning mechanism in the network for improving the specificity of the resulting product spectrum. Initially, however, most useful for determining the performance of the network's reactor units will be empirical parameters and maps that have been observed in known reactors at investigated scales.

To return to overall product selectivity, there is some flexibility within the constraint of the ASF distribution described above including within the spectrum of products of a given carbon number [5]. Temperature is important because endothermic desorption and hydrogenation are both enhanced by higher temperatures, overall lowering chain growth and producing shorter products, while the relative change in hydrogenation versus desorption determines olefin production relative to paraffins. Pressure and syngas composition affect the relative partial pressures of CO and H_2, which affects production since chain growth is favored by greater CO

adsorption. Pressure also favors iron catalyst productivity over that of cobalt catalysts. Space velocity is important because increasing that flow reduces secondary reactions; faster products spend less time in contact with potentially readsorbing catalysts. Furthermore, space velocity reduces conversion of CO, and higher outlet CO partial pressure is more competitive with the olefins that might be readsorbed.

I.3.2. Applicability to Methanol Synthesis

Methanol synthesis is another industrially significant and already well-established catalytic process by which oxidized carbon is hydrogenated by either of the following reactions [18]:

$$CO + 2\,H_2 \rightarrow CH_3OH \tag{19}$$

where $\Delta H_{600K} = -100$ kJ/mol and $\Delta G_{600K} = +45$ kJ/mol, and

$$CO_2 + 3\,H_2 \rightarrow CH_3OH + H_2O \tag{20}$$

where $\Delta H_{600K} = -62$ kJ/mol and $\Delta G_{600K} = +62$ kJ/mol. Subsequent dehydration can lead to dimethylether (DME) production via

$$2\,CH_3OH \rightarrow CH_3OCH_3 + H_2O \tag{21}$$

where $\Delta H_{600K} = -21$ kJ/mol and $\Delta G_{600K} = -11$ kJ/mol, as methyl alcohol is thermodynamically uphill of higher alcohols and hydrocarbons (which, happily, are ideal outputs of this unit). As in the Fischer-Tropsch process above, proper choice of catalyst can either inhibit or

thermodynamically lubricate this chain of hydrogenation reactions, which in industry successfully produces almost pure methanol but in this reactor network can be optimized to produce whatever hydrocarbon is desired or whatever input stream is desired for subsequent reactor units.

Like Fischer-Tropsch, the similarly highly exothermic methanol-to-gasoline reaction attracted a great deal of attention in the 1970s when cheap oil no longer looked limitless, and conversion to synthetic fuel over zeolite catalyst is well documented [19]. The Motunui synthetic petroleum plant was the first of its kind, converting methanol into liquid hydrocarbons from 1987 to 1997 using the Mobil-designed MTG process over ZSM-5 zeolite catalyst with a design capacity of 2,200 tons of gasoline per day, or 1 GW. The most recent addition to the industry is a Lurgi plant converting methanol to the light olefin propene (MTP) [20]. Lurgi is producing propene from methanol at a rate of 474 kt/a, along with 41 kt/a of LPG and 185 kt/a of gasoline. Here, again, the completed work investigated a process that is well-established in the literature and in industry, but instead with an eye towards modularity and scaling. A future optimization objective is to assess the relative representation of MTG and Fischer-Tropsch process units comprising the catalytic fuel synthesis network.

There have been particularly promising recent developments in the current state of the art of MTG. For example consider the Topsoe Integrated Gasoline Synthesis (TIGAS) process, developed by Haldor Topsoe to integrate methanol synthesis and MTG into a single loop [21]. In contrast with Mobil's MTG process in which different pressures are optimal for production of syngas, methanol synthesis, and MTG, the TIGAS process levels out these variations via catalyst

alteration (customization) and in doing so invites modular deployment. Intermediate DME synthesis levels out the stoichiometry and leads to one recycle loop, but any recycle loops can be considered in an integrated fuel synthesis network to be throughput to a subsequent unit. Furthermore, demonstrated flexibility in syngas compositions in the TIGAS process is similarly compatible with an aggregated network in which a variety of throughput compositions may simultaneously flow, and demonstrated 60% per-pass conversion efficiencies can be readily compounded by an integrated system [22]. Far from being merely speculative, the TIGAS process was first introduced in the mid-1980s, and has as recently as the past 6 months been funded by the Department of Energy to synthesize transportation fuel from wood biomass in the United States.

I.4. Catalyst Overview

Remarkably, Fischer and Tropsch published their 1926 work in reference to iron and cobalt catalysts, and these remain the most viable in industrial application to this day. Nickel and ruthenium are also effective catalysts of the Fischer-Tropsch synthesis, producing even higher molecular weight hydrocarbons. Nickel tends to form nickel carbonyl at higher pressures, and with increasing reaction temperature the selectivity tilts primarily towards methane, as is also true to a lesser extent with cobalt and ruthenium. Ruthenium is the most active catalyst, working at the lowest reaction temperatures (~150°C) and highest molecular weight products (up to 10^6 g/mol), as in polyethylene synthesis. However ruthenium is merely of scientific and not commercial interest. Even though it catalyzes FT as a pure metal, without promotors, providing

the simplest catalytic system and the cleanest mode of chain growth, it is too expensive and rare for industrial application. However it is used as an additive to more economical catalytic structures [4].

Choice of catalyst for the fuel synthesis reactors in the simulated network must strike a balance between economics and chemical effectiveness. Any suitable catalyst must be active for hydrogenation reactions and capable of forming metal carbonyls. Fischer-Tropsch pressure and temperature conditions are thermodynamically close to conversion of metals into metal carbonyls, so it is believed that "surface carbonyls" play a major mechanistic role in hydrocarbon production. The catalyst must be capable of meeting varying targets for the production of gasoline, diesel, waxes, or chemicals (olefins & alcohols) in the desired product spectrum. It must convert CO/H_2 mixtures to aliphatic (long-chain) hydrocarbons in a one-step reaction, which is to say that reaction intermediates are not prematurely desorbed from the catalyst surface.

Given the guiding principle that the network be cheap at the unit level, and representative of known economical and chemical value, the fuel synthesis units will clearly be using some combination of iron and cobalt catalysts for maximum flexibility of output and predictability of behavior. Of course characterization of catalysts does not stop with choice of metal, and even optimization of catalyst particle size is confounded by the tradeoff between pressure and diffusion length. Whatever combination of iron and cobalt catalysts are employed, known setups and supports with verified data and behavior will be assumed in the investigation of the reactor network.

In the case of iron catalysts, tail gas recycling is an important technique, since water-gas shift (WGS) behavior over iron leads to water inhibition of the conversion. Naturally the networking of the process is to feed streams from unit to unit, which is effectively recycling. As to the WGS activity, this is favorable for synthesis with CO-rich syngas from high temperature coal- or heavy-oil-gasification through partial oxidation, or from a previous unit that produced a syngas rich stream. WGS is undesirable with hydrogen-rich syngas, as for example that produced from natural gas.

Carbon deposition and accumulation in the iron catalyst has a deactivating effect and must be avoided, though that risk is mitigated by the ease with which the units can be substituted on- and off-line. Iron has been shown to feature relatively low methane selectivity, even at the high temperatures of the Synthol process (~340°C). The network model need not be overly concerned with techniques of catalyst promotion and support, since behavior will mimic known reasonable expectations, but it should be noted that iron needs alkali promotion to attain high activity and stability, copper for reduction promotion, silicon and aluminum oxides for structural promotion and possibly manganese for selectivity control with respect to olefins. Relative to cobalt, iron is considerably less active for hydrogenation.

Iron is appealing for its flexibility of use, in that it is commercially applied at both low and high temperatures. In the low temperature case, high activity produces a hydrocarbon stream in the liquid phase under reaction conditions. Wide pores allow ease of reactant mass transfer and fill with liquid product. Paraffin wax is a significant product fraction that Sasol refines to marketable waxes, and can also be hydrocracked selectively into high quality diesel. Under high

temperature operation, low molecular weight olefinic hydrocarbons are favored, produced by Sasol Synthol either in an entrained phase or fluid bed. The average molecular weight is so low that there is no liquid product phase, the catalysts are small (~100 μm) with small pore diameters. Sasol employs these and oligomerizes C_3, C_4 olefins to maximize overall yield of gasoline yield, while polymerization recovers olefins for commodity chemical use. It should be noted that conversion of light hydrocarbons into petrochemicals is similarly possible and practiced over zeolite catalysts, suggesting that producing methanol from syngas has real advantages which the network strategies studied here could exploit [19, 23].

In contrast to iron, cobalt catalysts do not suffer from water inhibition as they permit only negligible WGS activity. Relative to iron, cobalt offers greater per-pass conversion, and less risk of carbon deposition which allows longer running time. It is much more active for hydrogenation, so CO partial pressure needs to be high to avoid excessive methane selectivity particularly in the center of the catalyst particle. Cobalt catalysts allow olefin readsorption on the adsorption sites, contributing to high wax selectivity. Olefin secondary hydrogenation and double bond shift should be kept low. Cobalt has been successfully employed in service of diesel fuel selectivities approaching 80% with a hydrocracking process following the Fischer-Tropsch synthesis.

II. Refinery Discussion

Crude oil refinery is constrained by the specificity of current applications. Fuels produced for industrial and transportation applications must meet standards of quality that are specific to end-use as dictated both by technology and by applicable regulations, since end-use performance parameters are not necessarily intrinsic qualities of the fuel. Petrochemicals sold as commodities are valued based on intrinsic qualities, but of course there exists a wide array of chemicals valued by the marketplace. Furthermore, the requirements for such chemicals have varied over time based on regulatory and technological changes. Major shifts in the way crude oil was refined throughout its history can be tied directly such changes [5]. The fuel quality demands of a new and burgeoning airline industry coupled with the switch from kerosene- to electricity-driven lighting led to the addition of thermal reforming units. Vacuum distillation and residue upgrading were responses to spikes in oil prices. Upgrading of all fractions of the crude oil was driven by changes in air quality standards.

There has been similar historical variation in the design of Fischer-Tropsch refineries, which have produced both transportation fuels and commercial chemicals in a way that reflects their own technological and regulatory environment [24]. The possibility of such evolution presents a major investment risk for fuel synthesis facilities, but also a major advantage to a flexible modular network. The adaptability of network design specificity towards production of either a certain chemical commodity or a fuel designed for specific purposes and properties can only be an asset. Furthermore the specificity of fuel synthesis refiners would be an efficiency

gain regardless of networking opportunities, since much of the existing technology is inherited from and better suited to crude oil refining than syncrude [25],[26].

The value of an automated network to syncrude refining is that feed selection and gas loop design are crucial determinants of refinery design. A variety of feeds and loops naturally invite a variety of refiners. High temperature Fischer-Tropsch (HTFT) facilities produce gaseous products which upon cooling lead to more than one product phase. Large HTFT refining facilities cryogenically separate H_2, CH_4, ethylene, and ethane, while smaller HTFT facilities tend not to recover carbon chains C_2 and lighter. Meanwhile, low temperature Fisher-Tropsch (LTFT) facilities produce a chemical spectrum that consists of four different phases at ambient conditions, namely gaseous tail gas, organic liquid condensates, organic solid wax, and aqueous products [26].

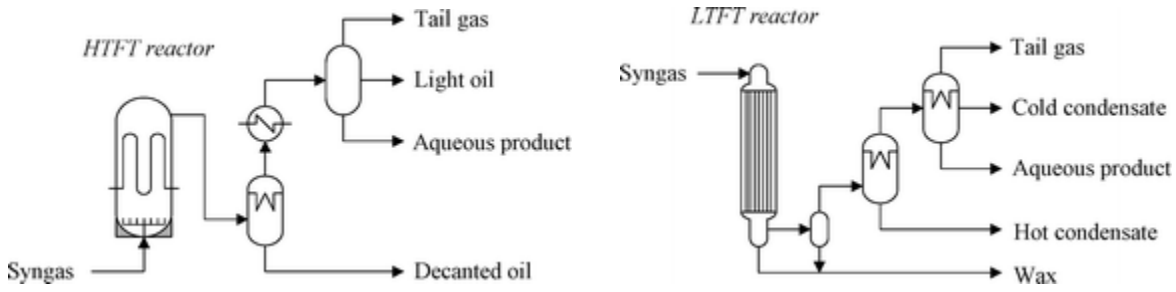

Figure 2.3: Refiner feedstock from high and low temperature reactors [26].

Recent work on refinery design specifically for syncrude notes that processes that are common to crude oil refining are incompatible with the needs of syncrude refining [26],[27]. Fluid catalytic cracking, thermal cracking, $Pt/Cl^-/Al_2O_3$ catalytic reforming and aliphatic alkylation are crucial crude refining choices that are not as effective in a syncrude refining, as the

molecular composition of syncrude is markedly different from that of fossil crude. The most important technologies in the case of Fischer-Tropsch synthesis are olefin dimerization/oligomerization, aromatic alkylation, pentene skeletal isomerization with etherification, hydrotreating of oxygenates and olefins, hydroisomerization, hydrocracking, nonacidic Pt/L-zeolite reforming, and alcohol dehydration [26]. This list of resident processes in a standalone refinery coud instead be thought of as flavors of refining units in a simulated fuel synthesis network. As the results will demonstrate, refining units were not necessary in this case to tune the chemical output spectrum to precisely and solely the user-specified chemical, but one can imagine that more complex processes or alternative requirements for the output spectrum might invite networked refining units into the process.

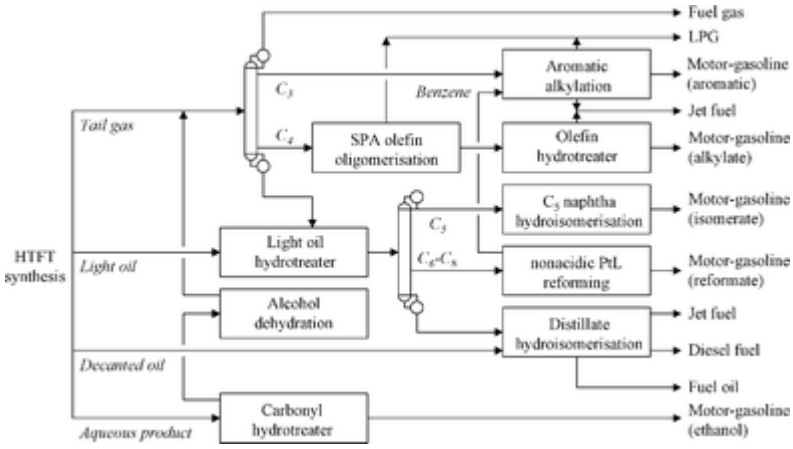

Figure 2.4: De Klerk's Fischer-Tropsch refinery design [26].

III. Reactor Discussion

The choice of reactor for the Fischer-Tropsch fuel synthesis network must balance the conflicting needs of the process. For example, short diffusion distances are preferable for fuel synthesis, as they benefit reactant transport, and for high α-olefin production for use as base chemicals downstream in the network, but small catalyst particles are problematic [28]. An appropriate reactor for a given set of intended products must be coupled with and conducive to the desired operating conditions of temperature, pressure, space velocity, and syngas composition.

Mass and heat transfer characteristics within the synthesis reactor are crucial design considerations. Mass transfer issues can lead directly to selectivity issues if transport of CO relative to H_2 alters the stoichiometric ratios, or if slow product transport inhibits the occurrence of secondary reactions. Reactors containing a liquid phase are subject to greater mass transfer limitation, and so this can be problematic for low-temperature Fischer-Tropsch (200-230 °C, LTFT) processes in which the liquid phase is present relative to high-temperature (320-340 °C, HTFT) process in which only the gas phase is present. The highly exothermic nature of the Fischer-Tropsch synthesis invites heat transfer challenges as well, which preferences HTFT processes over LTFT processes, as the most common method of heat removal is steam, which at HTFT temperatures is more highly pressurized than at LTFT temperatures [5].

There are three primary types of reactor that are commercially employed for Fischer-Tropsch, though it is crucial to note that these are the reactor types that have survived historically prevalent demands for scaling up in size which may not be intrinsically required by the process.

These types are fixed bed, slurry bed, and fluidized bed, and each has advantages and drawbacks depending on the purpose. Small scale versions of these and others not commercially deployed at scale as of yet will be modeled in the network to investigate their performance in a modular framework [29].

Multi-tubular and multichannel fixed bed reactors operate in the plug flow reactor (PFR) regime, meaning that conditions and composition change axially along the reactor but minimally in the radial direction. Of the three, this type is most efficient in absence of heat and mass transfer issues, but this is not a negligible problem [5]. Multi-tubular fixed bed reactors suffer too much pressure drop in use with small catalyst particles, and they present a challenge to heat removal [28],[30]. They are however the most obviously scale-able up and down, since a multiplicity of tubes each behave as an individual tube would, except that heat removal challenges don't scale as cleanly. Catalyst design requires that the catalyst particles have sufficient crushing strength to withstand initial construction, but once they are loaded in the bed the operation of the reactor is not mechanically abusive, which aids design flexibility. Catalyst separation is not an issue, since it is embedded in the walls. Disturbance in syngas production or deactivation of catalysts in a fixed bed setup has a local but not a global effect, which is a benefit of the small scale approach. The stability of a fixed bed reactor is not undermined by a drop in the feed, which is an important consideration for a network in which traffic may be redirected. The abundance of literature and empirical data on multi-tubular reactors combined with the applicability of that data to a smaller scale setup allows for reliable and realistic network modeling in the coded reactor units.

Slurry and fluidized bed reactors behave in a manner more closely following the continuously stirred tank reactor (CSTR) regime, in which the assumption of perfect mixing assumes that conditions and composition throughout the reactor are identical to outlet conditions and composition. Both fluidized and slurry reactors tend to produce chemicals that are significantly less hydrogenated, and therefore contain more olefins and oxygenates. Both place demands on the mechanical strength of the catalyst particles, since they are constantly in motion and colliding. Both require separation steps to remove catalysts from the output.

Among fluidized beds, the fixed version is more well-mixed than the circulating version. Fluidized bed reactors are particularly effective in the production of gasoline and base chemicals, but they are resistant to operation at high chain growth probabilities. This is because high chain growth ($\alpha > 0.7$) leads to condensed products, and the setup is necessarily gaseous [5]. Gas-solid separation is easier than gas-liquid separation, and is accomplished via cyclones on fluidized bed setups.

Slurry bubble column reactors offer excellent heat transfer, and function well with 100 μm particles to provide short diffusion lengths, but catalysts of that size are more difficult to separate and more susceptible to attrition [28],[30]. Conversely to fluidized beds, slurry beds require high values of α in order to guarantee sufficient chain growth to maintain the liquid phase in the reaction chamber. The slurry bed is advantageous over the multi-tubular model in terms of mass transfer issues because of the liquid phase moves more freely at low temperatures (LTFT). Hydrodynamic considerations are more important in the slurry bed. Catalyst separation from the liquid is a liability, and an important consideration before selecting slurry technology.

Because slurry technology is so commercially important historically, there is a wealth of historical and recent information about its operation and behavior, including intrinsic bench scale reaction behavior, which will inform the modeling of small modular units of slurry reaction [31]. That said, slurry is made for scale-up, and it is unlikely to confer its current advantages in the same way at small scale.

Description	Fixed Bed		Slurry bed	Fluidized bed	
	Multi-tubular	Microchannel		Fixed fluidized	Circulating
Nature of the reactor	PFR	PFR	CSTR	CSTR	CSTR
Reaction phase	g or g+l	g or g+l	g+l	g	g
Catalyst particle size (mm)	>2	<0.1	<0.1	<0.1	<0.1
Mass transfer limitation	High	Low	Medium	Medium-low	Medium-low
Heat transfer limitation	High	Low	Low	Medium-low	Medium-low
On-line catalyst replacement	No	No	Possible	Possible	Possible
Catalyst mechanical strength	Low	Low	Medium	High	High
Catalyst–product separation	Easy	Easy	Difficult	Fairly easy	Fairly easy
Scale-up risk (lab to plant)	Low	Low	Medium	Medium	Medium
Scale-up economy of scale	Medium-Low	Low	High	Very high	High
Feed poisoning	Local	Local	Global	Global	Global
Feed turn down limitation	None	None	Catalyst setting	Defluidization	Defluidization

Figure 2.5: Main reactor characteristics, taken from de Klerk [5]

III.1. Monolithic Loop Reactors

There has been a great deal of work in recent years directed toward microstructured reactors, as they offer the chemical benefits of fuel synthesis that actually improve when scaled downward, such as transport of heat from the reaction chamber, mass transport of mixing species, greater boundary layers that come with small channel dimensions [32],[33].

One possible solution to some of the challenges of large scale outlined above that fits well in the small-scale paradigm is the monolith. Inherently small-scale and modular but not yet

applied at industrial output scale, this reactor type can be investigated as a network option with particular interest in the proposed thesis.

Monoliths are ceramic structured catalysts with small axial channels of 0.5-3 mm internal diameter partitioned by 60-300 μm walls of a washcoated catalyst support on cordierite for low catalyst fractions per unit volume or of an alumina or silica support material to provide high catalyst fractions per unit volume. The variety of options for catalyst support and activity on the surface of the channel walls and variability of cell density permit a high degree of control over the characteristic diffusion lengths discussed above.

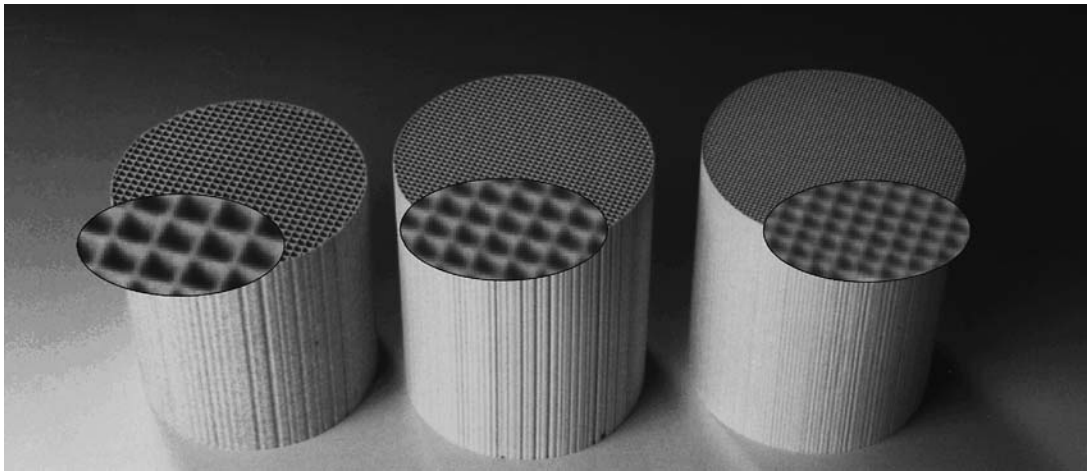

Figure 2.6: Monolithic structures at 200, 400, and 600 cells per square inch [28].

Early experimentation on these monolithic structures has demonstrated that changes to the stoichiometric syngas ratio can produce either much lower activity and higher growth probability or, at higher H_2 ratios, activity comparable to the literature but with higher methane yields [28]. Modeling fuel synthesis through a monolith channel is quite similar to the Fischer-Tropsch models in more common reactors, and so it is included here as an example of a set of traditional

modeling equations. For each component *i* of the chemical stream, there is an axial mass balance in the gas phase of

$$\frac{\partial(u_G C_{i,G})}{\partial z} = -k_{GL}a_{GL}\left(C_{i,sat} - C_{i,L}\right) - k_{GS}a_{GS}\left(C_{i,sat} - C_{i,L}\right) \tag{22}$$

subject to $C_{i,G}\big|_{z=0} = C_{i,G,0}$,and in the liquid phase of

$$u_L \frac{\partial C_{i,L}}{\partial z} = k_{GL}a_{GL}\left(C_{i,sat} - C_{i,L}\right) - k_{LS}a_{LS}\left(C_{i,L} - C_{i,s}\right) \tag{23}$$

subject to $C_{i,L}\big|_{z=0} = C_{i,L,0}$, an axial energy balance of

$$u_L \frac{\partial T}{\partial z} = \frac{\Delta H_R}{\rho_L C_{p_L} L_C}\int_0^{L_C} \rho_s v_{CO} r_{syngas} dy \tag{24}$$

subject to $T|_{z=0} = T_0$, and a momentum balance of

$$\frac{\partial p}{\partial z} = -f\frac{1}{2}\rho_L u_{TP}^2 \frac{4}{d_h} + \epsilon_L \rho_L g - \epsilon_L \rho_L u_{TP}\frac{\partial u_{TP}}{\partial z} \tag{25}$$

subject to $u_G|_{z=0} = u_{G,0}$ [30]. After some modeling with these equations in preparation for this proposed work, they have yielded to the unit reconcile methods described below in conjunction with the network numerical model description.

A means of incorporating monoliths into a reactor has been investigated in the form of the monolith loop reactor, in which liquid is pumped through a monolith catalyst and recycled through a heat exchanger while gas-phase material is driven by pressure drop [34].

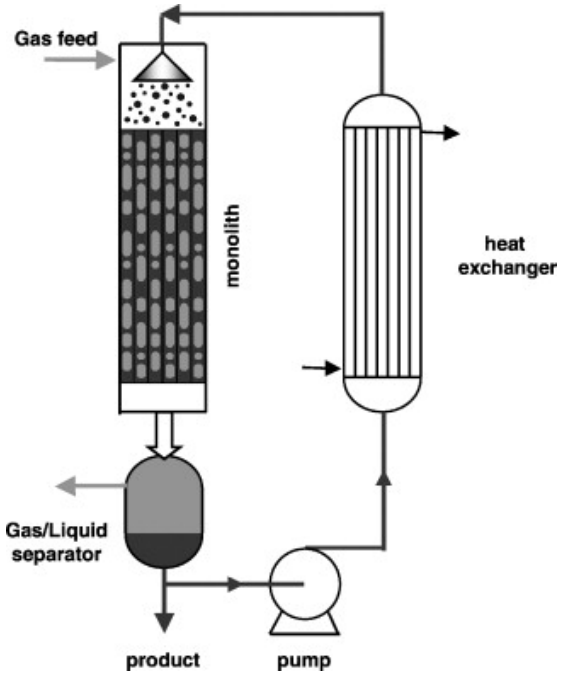

Figure 2.7: Monolithic loop reactor with liquid recycle [30].

Recalling that isothermal plug flow is the optimal regime for Fischer-Tropsch reactants, the monolith loop reactor drives the recycled liquid concurrently with once-through gas-phase material with approximately the uniform cross-sectional velocity and absent boundary layer required of plug flow. While some temperature rise is to be expected in recycled liquid heat removal, the gradient can be kept to ~15 °C in ~240 °C operation. In a side-by-side study of a modeled monolithic loop reactor and a 4410 m^3 slurry bubble column reactor both producing 5000 ton middle distillates per day (C_{11+}), it was found that the required scale of the monolithic loop is 3350 m^3, though the slurry bubble column includes its heat exchanger [30].

Other recent work has investigated monoliths whose wall surfaces are coated with a microporous ceramic membrane, for which the variables of membrane composition, pore size,

tortuosity, thickness may be optimized. Comparison between a monolithic loop catalytic membrane reactor, a tubular catalytic membrane reactor, and a tubular fixed bed reactor revealed that paraffin selectivity and yield per unit mass of catalyst in a tubular membrane reactor exceed that of a tubular fixed bed, but the membrane monolith seemed to be mass transfer limited and of inferior yield relative to the tubular models [6].

Given the greater productivity of the monolithic loop reactor in plug flow and accompanying absence of problems of catalyst attrition and separation, the looping of feedstock, and the obvious scalability to reduced size, the structured monolith is an appealing candidate for the reactor of choice in a fuel synthesis network. A network of small reactors, in which less syngas can be fed through at lower inlet velocities, would permit lower conversion levels. These are advantageous in the monolithic loop because lowering conversion (a) reduces the gas-phase water inhibition which tends to lower activity; (b) decreases pressure drop due to lower liquid flow rates required to maintain isothermicity (c) decreases the reactor length [30]. The ability to tune the wall thickness of a monolith has great affect on diffusion characteristics and pressure drop, and therefore on activity and selectivity. This flexibility in design of a particular reactor readily translates to flexibility in a reactor network, in which chemical flows can be directed to appropriate monoliths.

III.2. The Gas-lift Reactor

A gas-lift reactor is another new technology that has recently been proposed [35]. It consists of bubbling syngas up through a slurry of catalyst particles and liquid products not

unlike what is found in a slurry bubble column reactor, while slurry actually flows down through the reactor and into a heat exchanger before being fed back through the top. Unconverted syngas and gaseous products are removed from the top. The system is considered advantageous because it operates in the plug flow regime, permitting staged feeding of gases, while re-circulating liquid can be considered well mixed and therefore stabilizing isothermal conditions. The axial gradient of catalyst distribution is gentler in this setup than in traditional slurry bubble columns. Gas-lift research is directed toward retrofitting large scale slurry systems, but it is interesting and relevant to this proposed work that large scale systems are attempting to simulate the staged feeding of gases that a small-scale modular synthesis network naturally invites.

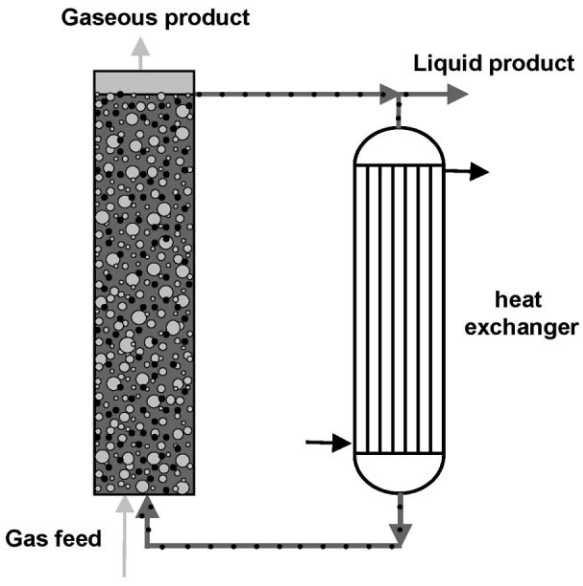

Figure 2.8: Gas lift reactor [35]

IV. References

1. Steynberg, A.P., et al., *Fischer-Tropsch reactors.* Fischer-Tropsch Technology, 2004. **152**: p. 64-195.

2. Wang, T.F., J.F. Wang, and Y. Jin, *Slurry reactors for gas-to-liquid processes: A review.* Industrial & Engineering Chemistry Research, 2007. **46**(18): p. 5824-5847.

3. van Vliet, O.P.R., A.P.C. Faaij, and W.C. Turkenburg, *Fischer-Tropsch diesel production in a well-to-wheel perspective: A carbon, energy flow and cost analysis.* Energy Conversion and Management, 2009. **50**(4): p. 855-876.

4. Steynberg, A.P., *Introduction to Fischer-Tropsch technology.* Fischer-Tropsch Technology, 2004. **152**: p. 1-63.

5. de Klerk, A., *Fischer-Tropsch Refining*. 2011: Wiley-VCH Verlag GmbH & Co. KGaA. 620.

6. Bradford, M.C.J., M. Te, and A. Pollack, *Monolith loop catalytic membrane reactor for Fischer-Tropsch synthesis.* Applied Catalysis a-General, 2005. **283**(1-2): p. 39-46.

7. Dry, M., *The Fischer-Tropsch process: 1950-2000.* CATALYSIS TODAY, 2002: p. 227-241.

8. Wilhelm, D.J., et al., *Syngas production for gas-to-liquids applications: technologies, issues and outlook.* Fuel Processing Technology, 2001. **71**(1-3): p. 139-148.

9. James, O.O., et al., *Increasing carbon utilization in Fischer-Tropsch synthesis using H-2-deficient or CO2-rich syngas feeds.* Fuel Processing Technology, 2010. **91**(2): p. 136-144.

10. Riedel, T., et al., *Comparative study of Fischer-Tropsch synthesis with H-2/CO and H-2/CO2 syngas using Fe- and Co-based catalysts.* Applied Catalysis a-General, 1999. **186**(1-2): p. 201-213.

11. Van der Laan, G.P. and A. Beenackers, *Kinetics and selectivity of the Fischer-Tropsch synthesis: A literature review.* Catalysis Reviews-Science and Engineering, 1999. **41**(3-4): p. 255-318.

12. Puskas, I. and R.S. Hurlbut, *Comments about the causes of deviations from the Anderson-Schulz-Flory distribution of the Fischer-Tropsch reaction products.* Catalysis Today, 2003. **84**(1-2): p. 99-109.

13. Kapteijn, F., R.M. de Deugd, and J.A. Moulijn, *Fischer-Tropsch synthesis using monolithic catalysts.* Catalysis Today, 2005. **105**(3-4): p. 350-356.

14. Aaserud, C., et al., *Hydrogenation of propene on cobalt Fischer-Tropsch catalysts.* Catalysis Letters, 2004. **94**(3-4): p. 171-176.

15. Iglesia, E., S.C. Reyes, and R.J. Madon, *TRANSPORT-ENHANCED ALPHA-OLEFIN READSORPTION PATHWAYS IN RU-CATALYZED HYDROCARBON SYNTHESIS.* Journal of Catalysis, 1991. **129**(1): p. 238-256.

16. Botes, F.G., *Proposal of a new product characterization model for the iron-based low-temperature Fischer-Tropsch synthesis.* Energy & Fuels, 2007. **21**(3): p. 1379-1389.

17. Kuipers, E.W., I.H. Vinkenburg, and H. Oosterbeek, *CHAIN-LENGTH DEPENDENCE OF ALPHA-OLEFIN READSORPTION IN FISCHER-TROPSCH SYNTHESIS.* Journal of Catalysis, 1995. **152**(1): p. 137-146.

18. Klier, K., *Methanol Synthesis.* Advances in Catalysis, 1982. **31**: p. 243-313.

19. Zaidi, H.A. and K.K. Pant, *Catalytic conversion of methanol to gasoline range hydrocarbons.* CATALYSIS TODAY, 2004. **96**(3): p. 155-160.

20. Bjorgen, M., et al., *Methanol to gasoline over zeolite H-ZSM-5: Improved catalyst performance by treatment with NaOH.* Applied Catalysis a-General, 2008. **345**(1): p. 43-50.

21. Spath, P.L. and D.C. Dayton, *Preliminary Screening - Technical and Economic Assessment of Synthesis Gas to Fuels and Chemicals With Emphasis on the Potential for Biomass-Derived Syngas*. 2003. p. 160.

22. Rostrup-Nielsen, T., et al. *Polygeneration – Integration of Gasoline Synthesis and IGCC Power Production Using Topsoe's TIGAS Process*. in *Risø International Energy Conference*. 2007. Risø National Laboratory DTU.

23. Wu, W., et al., *Methanol conversion to olefins (MTO) over H-ZSM-5: Evidence of product distribution governed by methanol conversion.* Fuel Processing Technology, 2013. **108**(0): p. 19-24.

24. De Klerk, A., *PETR 29-Refining of Fischer-Tropsch syncrude: Lessons from the past.* Abstracts of Papers of the American Chemical Society, 2008. **236**.

25. de Klerk, A., *Environmentally friendly refining: Fischer-Tropsch versus crude oil.* Green Chemistry, 2007. **9**(6): p. 560-565.

26. de Klerk, A., *Fischer-Tropsch refining: technology selection to match molecules.* Green Chemistry, 2008. **10**(12): p. 1249-1279.

27. de Klerk, A., *Fischer-Tropsch fuels refinery design.* Energy & Environmental Science, 2011. **4**(4): p. 1177-1205.

28. de Deugd, R.M., F. Kapteijn, and J.A. Moulijn, *Using monolithic catalysts for highly selective Fischer-Tropsch synthesis.* Catalysis Today, 2003. **79**(1-4): p. 495-501.

29. Sie, S.T. and R. Krishna, *Fundamentals and selection of advanced Fischer-Tropsch reactors.* Applied Catalysis a-General, 1999. **186**(1-2): p. 55-70.

30. de Deugd, R.M., et al., *Is a monolithic loop reactor a viable option for Fischer-Tropsch synthesis?* Chemical Engineering Science, 2003. **58**(3-6): p. 583-591.

31. Jung, H., et al., *Investigation of Fischer-Tropsch synthesis performance and its intrinsic reaction behavior in a bench scale slurry bubble column reactor.* Fuel Processing Technology, 2010. **91**(12): p. 1839-1844.

32. Klemm, E., et al., *Microstructured reactors in heterogeneous catalysis.* Chemical Engineering & Technology, 2007. **30**(12): p. 1615-1621.

33. Knochen, J., et al., *Fischer-Tropsch synthesis in milli-structured fixed-bed reactors: Experimental study and scale-up considerations.* Chemical Engineering and Processing, 2010. **49**(9): p. 958-964.

34. Heiszwolf, J.J., et al., *Hydrodynamic aspects of the monolith loop reactor.* Chemical Engineering Science, 2001. **56**(3): p. 805-812.

35. de Deugd, R.M., F. Kapteijn, and J.A. Moulijn, *Trends in Fischer-Tropsch reactor technology - opportunities for structured reactors.* Topics in Catalysis, 2003. **26**(1-4): p. 29-39.

Chapter 3

Coding the Numerical Solver

I. Coding the Network Model

This completed work employed and substantially advanced the code developed by Klaus Lackner, Ian Katz, and Xinxin Li for observing and optimizing the properties of a complex network. The design of the code is to be as general and therefore as versatile as possible, establishing a structure of streams and blocks that could represent any process being studied by the end-user. In order to study the behavior of such a network in ways that are unavailable in current software, the hierarchical numerical modeling code was developed to offer greater flexibility to nest and optimize network configurations within network configurations, reflecting the modularity of the networks it is meant to simulate. The modularity of the code structure is a perfect fit for the modularity of a fuel synthesis network, as the network itself views the component parts of the process as discrete units among which the flow of chemicals can be directed and redirected. This new code is capable of simulating aggressively numerically constrained networks, dynamically substituting various configurations while optimizing them across user-specified variables.

The basic modules of this numerical modeling code are the aforementioned streams and blocks. Streams are material or energetic flows that are defined by the user. They could be heat, work, steam, water, coal, flue gas, or as in the case of this work, hydrocarbons. These streams are like connective pipes in the code that are attached to the ports of the other basic modules of the code, the blocks. Furthermore, the streams are "dumb" pipes, which is to say that they contain no process operations save the requirement that the stream flowing through a pipe is identical in every respect at both ends of that pipe. No gradients are permitted within a stream; only in the blocks are the functions in the code that apply the processes being modeled according to which incoming streams and outgoing streams may differ. The blocks are the basic units of operations within which certain relationships between inputs and outputs must be maintained. Blocks can be coded to include such laws as conservation of total mass, conservation of individual atoms, and conservation of energy, which are applied to the streams coming in and out. A model of a boiler, for example, would have streams of water, heat, and steam, and a block called a boiler which maps incoming streams to outgoing streams (and vice versa). Additional blocks to represent a furnace and a steam turbine would represent a more involved industrial process.

End Caps are special blocks at which streams begin and terminate. Each stream has its own End Cap, which functions as the interface between the system being modeled and its surroundings. For example, a model of a boiler would contain End Caps for the water, steam, and heat. A complete model is referred to in the code as a Flowsheet:

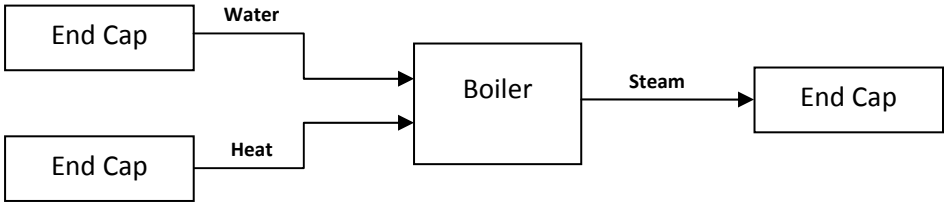

Figure 3.1: A sample flowsheet

End Caps can impose certain values onto the streams flowing in and out of them. Therefore the system can be constrained from either or both ends such that these constrained initial values do not vary, while any unconstrained streams' flow rates and properties may vary from the user's initial guesses in order to satisfy the operations and conservation laws written into the blocks.

The fuel synthesis network model approaches a solution in a fundamentally different way from one that would step through the system in time and space. The model instead takes an .xml input file delineating the components of the network and a set of guesses as to what select quantities and descriptive parameters of the flow should be. These parameters can be fixed or subject to change as necessary and revisited throughout the network in each successive iteration until the differences from one iteration to the next are sufficiently small (a tolerance for error also specified by the user.) In the final solution, then, the values for the streams flowing throughout the Flowsheet are internally consistent as defined by the relationships between inputs and outputs that each block has been coded to obey.

I.1. Flowsheet Blocks

One of the most important structural changes made to the code during the completion of this work was to write smoothly functioning and modular Flowsheet Blocks. There is a built-in

library of objects in the form of streams and blocks that the model is capable of assembling. For this research, for example, chemical and heat streams were written into the stream library and various chemical networking units described below were written into the block library to apply fuel synthesis reactions. A user-defined xml input sheet instructed the code to assemble these blocks and streams into a functional simulation. Flowsheet Blocks, however, enable something much more powerful, which is the ability of the user to write a Flowsheet within a Flowsheet. A Flowsheet is some assembly of blocks and streams. In writing a Flowsheet Block, the user may register that Flowsheet in the library to itself be used as a block within a larger macroscopic arrangement of blocks and streams. For example, the user may have a Flowsheet of a power plant containing a boiler block and a steam turbine block, but may subsequently write a more rigorous version of the steam turbine block containing its own internal Flowsheet. Moreover, that user could write a series of smaller blocks which represent more realistic and granular slices of the larger steam turbine. With the ability to register user-defined Flowsheets, the user may define that new Flowsheet representing the steam turbine as a Flowsheet Block, and then refer to it in the larger Flowsheet as a simple block. In the former case, the model would execute the simple steam turbine block algorithm during each of the reconciling iterations; in the latter case, the model will reconcile the entire rigorous multifaceted steam turbine Flowsheet *within* that block, and any Flowsheets within that Flowsheet, and then return to the above Flowsheet. Furthermore, the ability to refer within the Flowsheet Block to yet another, deeper Flowsheet within that Flowsheet Block was also enabled; as long as the user is referring to a Flowsheet Block already defined in the xml input sheet, the code can fetch it from the library and write it into the Flowsheet. By nesting Flowsheets within Flowsheets in this way, the code became truly

hierarchical, and the various aspects of fuel synthesis network modeling could be compartmentalized.

The ability to nest Flowsheets within Flowsheets is also critical to permitting more rapid convergence to a solution. A Flowsheet, with all contained blocks and streams visited successively at each iteration, can require a long processing time. Particularly in the early iterations of a simulation, the values that each unit is reconciling are not yet correct, as information has not yet percolated through the entire Flowsheet. The nested Flowsheet Blocks were coded to a gentler standard of convergence, as they are required only to get 90% more reconciled during a given iteration. For example, if incoming value a_{in} must by conservation be equal to a_{out}, the nested Flowsheet need only adjust these two values until they are 90% closer to one another than they were at the beginning of the iteration. In this way, the code does not take the time and iterations to reconcile underlying Flowsheets to values inherited from above that are themselves not yet correct. The error tolerance for the Flowsheet at large will still be respected, and a_{in} will end up within that tolerance of a_{in}, but the underlying Flowsheets will not arrive at that required tolerance until the surrounding units are themselves much closer to a solution. This flexibility, once written into the code, allowed for much more rapid convergence times and numbers of iterations required for a solution.

I.2. Variable Input Parameters (VIPs)

Blocks are coded with some set of input parameters that have default values but can be user-defined. Similarly, when a Flowsheet Block is defined and registered to the library, the user can specify default parameters that will be assumed when the Flowsheet Block is called and

inserted within an overlying Flowsheet. Additionally, the ability to redefine those parameters when the Flowsheet Block is called from the library was written into the code.

Consider as an example a network of chemical reactors with chemical streams flowing through various units. There must be intersections in this network to direct traffic, and these intersections could include an array of splitters which agnostically separate incoming chemicals, separators which preferentially separate incoming chemicals on a mass basis, and mergers which combine various streams. A Flowsheet containing these units could be written as a Flowsheet Block named “Intersection” and stored in the library with a set of default values for splitter ratios and mass-based separation means about which to separate. This Flowsheet would be called into the overlying Flowsheet as if it were simply a block of type “Intersection”; the overlying flowsheet doesn’t need to know what’s in it. When these Intersection blocks are inserted into the larger Flowsheet, the split ratios, separation means, and even guesses at the profile of the underlying chemical streams can be passed into the underlying Flowsheet Block as it is copied and constructed.

In addition to ability to modify the parameters of simple blocks and underlying Flowsheets, the user can also specify Variable Input Parameters (VIPs), along with an initial value for that VIP, a range of permissible values, and an increment of variation. This has two applications. One application is simply that if the code is unable to converge the user’s specifications to a solution, for example in the event that the user defined split ratios and stream values that do not conserve mass, then the code can adjust those values and try to reach a converged solution with the new parameters. Another application is to permit optimization. The

blocks and Flowsheets come equipped with penalty functions, which canvas the Flowsheet for any penalties for that particular solution. The user can optimize by varying a particular VIP across a range of values, calculating the penalty for the converged solution at each value, and report a summary of these results with the minimum penalty and the parameters used in the converged solution corresponding to that penalty. Underlying Flowsheets disguised as Flowsheet Blocks can also have VIPs that the user can characterize and permute from the top level down.

I.3. Constraints and Weighting

When a simulation is run, there are typically initial guesses at what the converged solution might be, as well as constraints on the system. For example, a Fischer-Tropsch fuel synthesis simulation might begin with a specified input of CO and H_2, which would determine the throughput throughout the network if the number of degrees of freedom is equal to the number of constraints. The algorithms arrive at a correct solution by continually reconciling inherited values at the block level, and any values observed by the constrained input block, in this case the syngas production unit, would not be averaged but rather be reset to those input constraints. The code performs much more effectively, however, if these constraints percolate throughout the system more rapidly.

I.3.1. Constraints and Propagation

The most elementary weighting scheme presently available in the code is “Propagate Constraint.” This scheme operates according to the principle that if there are as many degrees of certainty entering a calculation as there are degrees of freedom in the system being solved, then

all outgoing values are also certain. For example, if an End Cap is constrained, then the values entering the stream connecting it must be equal to the values exiting that stream, and those exiting values are now also constrained. Recall that a "stream" functions as a "dumb pipe" that must have equal properties entering and leaving it. If those values exiting the stream are entering a splitter which equally splits the stream, then whatever values the splitter may have initially encountered for its one inlet and two outlets, the two outlets must now each be one half of the constrained input, and those outlets must also now be constrained. In this way a constraint percolates through the rest of the Flowsheet one iteration at a time. In the absence of looping, this requires only as many iterations as there are blocks to reach the far corners of the Flowsheet and converge to a solution. A calculation that might otherwise have taken thousands of iterations may now only take 5-10 iterations to converge in a very small fraction of the time. Once a propagating constraint reaches a unit in which there are more degrees of freedom than degrees of certainty, however, the local reconcile takes over. While it will not alter the incoming constrained stream, that constraint cannot propagate to other outgoing streams as being constrained. Subsequently encountered blocks and stream revert to unweighted averaging.

I.3.2. Weighted Constraints and Propagation

Unless a Flowsheet is completely constrained, and even if it is constrained as an overall system, it will eventually encounter a block whose local degrees of freedom exceed the degrees of incoming certainty. In this case the constraint has hit a dead end, and downstream (or upstream) calculations will be unaware that it may be as close as one block away from a constrained answer. Such downstream unconstrained blocks will eventually arrive at the solution required by the nearby constraint that is out of computational earshot, as incorrect solutions will

be iteratively averaged upstream with a static constrained solution and thus will average their way to it within an epsilon, but this incurs computational cost. Furthermore, downstream solutions may wander into modes that evade convergence. A solution to this inefficiency is to impose propagated weighted constraints. A constrained solution, such as one that flows directly from a strictly defined End Cap, is assigned a weight of one over epsilon, while an unconstrained solution is assigned a weight of zero. Constrained solutions never change their weights, but when constrained solutions encounter unconstrained solutions, the results that propagate through unconstrained streams are assigned a numerical weight equal to the average of the stream weights that went into that reconcile. These unconstrained but now numerically weighted streams propagate downstream with greater confidence, and any completely unweighted solutions concede their values to weighted streams. There are now three categories of weight for a stream; constrained, unconstrained but weighted, and unconstrained and unweighted. In a reconcile with a stream that is unconstrained and unweighted, an unconstrained but weighted stream is effectively constrained. Subsequent iterations behave as if they were propagating constraint, however if unconstrained but weighted solutions encounter other unconstrained and weighted solutions, which must in turn be able to be traced back to a strictly defined End Cap, weighted averaging resolves the discrepancy. Use of this algorithm in the code permitted dramatically faster convergence of solutions, by orders of magnitude in iteration counts, and in many cases allowed a solution to be convergent in simulations which had theretofore wandered off into non-convergent wilderness.

I.3.3. Inflexibility Biases

Inflexibility bias is a capability written into the code by which inflexibility is rewarded. The closer a stream is to a constrained node, such as an End Cap that has rigidly defined flow and stream properties, the less the averaged values of that stream will vary, since the stream values are being averaged closer and closer to a constant number with every passing iteration. The code can therefore presume that encountered stream values that have not varied very much since the last time they were averaged are more closely connected to constrained nodes, and therefore should be weighted more highly. This weight *w* of value *x* of property *n* at a iteration *t* is expressed as

$$w_{n_t} = \frac{1}{\Delta n_t + \varepsilon} \tag{1}$$

$$\Delta n_t = \frac{x_t - x_{t-1}}{\sqrt{x_t^2 + x_{t-1}^2} + \varepsilon} \qquad x_t, x_{t-1} \neq 0 \tag{2}$$

in which the added epsilons insure an upper bound on the weight, especially in the case of values that have not varied and might therefore by logical extension of these ideas be weighted infinitely. This weighting scheme required additional considerations and modification without which coded simulations were victim of infant rigidity, meaning that if most of the unconstrained streams were initially unspecified and therefore unpopulated by chemicals, they would of course not vary at all until information from the constrained chemical-containing streams reached them. If an empty stream were 5 blocks away from a constrained and well-defined End Cap, it would have values set at zero for the first 5 iterations, and therefore under the above scheme be very heavily weighted as inflexible even though they in fact were informed by nothing at all. The inflexibility bias therefore was not triggered until later in the simulation. The weighted

propagation scheme described immediately above seemed to bear more fruit, however, in that solutions converged in fewer iterations, and in some cases converged where the inflexibility bias could not. It is very possible that the difference is due to the fact that the inflexibility bias is a liability very early in the iterations, whereas weighted propagation serves the important purpose of radiating immediately from the vicinity of a constrained stream before the streams have a chance to wander in an inappropriate numerical direction.

I.3.4. Stream Nullification

One crucial adjustment to the code that permitted simulations of network reactors to be truly looped instead of merely partially recycled was to code the ability of the user to instruct certain blocks to disregard certain streams entirely in search of convergent solution. Initial looping simulations had the unfortunate tendency to run away from a correct answer, either towards zero or diverging to infinity. This occurred even though the constraints and conservation laws of the system clearly pointed to a unique solution. For example, consider a simple system containing only a source of chemicals, a merger, a splitter that loops half of the throughput back to the merger, and a sink of chemicals:

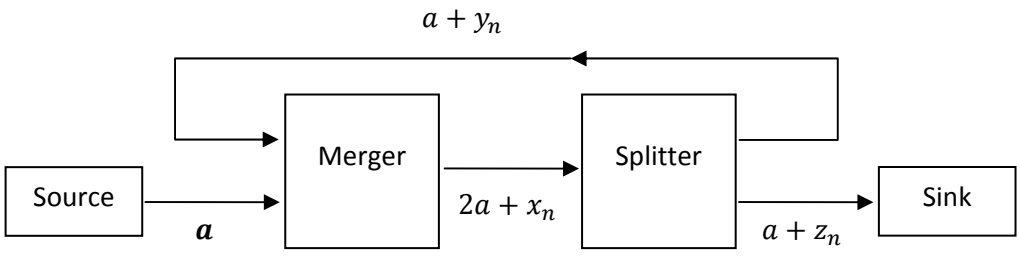

Figure 3.2: A simple looped simulation.

If the input is constrained in the amount *a* moles per second of a single chemical, then the output must be mass conservation also be *a* mol/s. If the splitter is set to split streams in an equal ratio, then that output of *a* mol/s demands that the other output also be *a* mol/s, and therefore that the input to the splitter be 2*a* mol/s, which puts the merger in perfect agreement with itself. In the figure these flows are indicated along with an error term for each one labeled x_n, y_n, and z_n, which must of course go to zero if the streams are to converge algorithmically to a correct answer.

To assist the model, a common assumption that is made is that any stream leading to an unconstrained End Cap (in this case the sink) is not permitted to influence the connecting block reconcile; it has no opinion. Thus the z_n term above may be neglected, as it will obey the outcome of the splitter reconcile.

Suppose the system begins the n^{th} iteration with the error vector in the state described above. The merger *M* currently observes an input in excess of the output in the amount $y_n - x_n$, and so subtracts half that amount from input and adds that amount to the output:

$$\begin{matrix} a + y_n \rightarrow \\ a \rightarrow \end{matrix}\left[\begin{matrix} \\ M \\ \\ \end{matrix}\right] \rightarrow a + x_n \quad \xrightarrow{reconcile} \quad a + \frac{x_n + y_n}{2} \rightarrow \left[\begin{matrix} \\ M \\ \\ \end{matrix}\right] \rightarrow 2a + \frac{x_n + y_n}{2} \qquad (1)$$

The splitter, *S*, at the same time, will receive the same streams as the merger, and since it is ignoring its output to the End Cap, it will equally consider x_n and $2y_n$ as two opinions on what the input to the splitter should be, settling on their average:

$$2a + x_n \rightarrow \left[\begin{array}{c} S \end{array}\right] \begin{array}{l} \rightarrow a + y_n \\ \rightarrow a + z_n \end{array} \xrightarrow{reconcile} 2a + \frac{x_n + 2y_n}{2} \rightarrow \left[\begin{array}{c} S \end{array}\right] \begin{array}{l} \rightarrow a + \frac{x_n + 2y_n}{4} \\ \rightarrow a + \frac{x_n + 2y_n}{4} \end{array} \quad (2)$$

Following the block reconcile is a stream reconcile, in which the streams receive contradictory inputs and average them:

$$2a + \frac{x_n + y_n}{2} \rightarrow [stream\ x\ ] \rightarrow 2a + \frac{x_n + 2y_n}{2} \xrightarrow{reconcile\ x} 2a + \frac{1}{2}x_n + \frac{3}{4}y_n \quad (3)$$

$$a + \frac{x_n + 2y_n}{4} \rightarrow [stream\ y\ ] \rightarrow a + \frac{x_n + y_n}{2} \xrightarrow{reconcile\ y} 2a + \frac{3}{8}x_n + \frac{1}{2}y_n \quad (4)$$

Therefore, over the course of the n^{th} iteration, the following mapping and implied matrix have been employed to transform the error:

$$\begin{bmatrix} x_{n+1} \\ y_{n+1} \end{bmatrix} = \begin{bmatrix} \frac{1}{2}x_n + \frac{3}{4}y_n \\ \frac{3}{8}x_n + \frac{1}{2}y_n \end{bmatrix} = A \begin{bmatrix} x_n \\ y_n \end{bmatrix} = \frac{1}{8}\begin{bmatrix} 4 & 6 \\ 3 & 4 \end{bmatrix}\begin{bmatrix} x_n \\ y_n \end{bmatrix} \quad (5)$$

Since the error vector $\begin{bmatrix} x_n \\ y_n \end{bmatrix}$ can be written as a linear combination of the eigenvectors of this matrix *A*, the only way the error can go to zero over repeated applications of *A* is if the eigenvectors of *A* are less than 1, i.e.

$$\overrightarrow{e_{n+N}} = A^N \overrightarrow{e_n} = \lambda^N \overrightarrow{e_n} = 0 \quad \leftrightarrow \quad |\lambda| < 1 \quad (6)$$

The eigenvalues of *A* satisfy the following relation in which one of them clearly exceeds 1:

$$\det(A-\lambda I)=\det\begin{pmatrix}\frac{1}{2}-\lambda & \frac{3}{4}\\ \frac{3}{8} & \frac{1}{2}-\lambda\end{pmatrix}=0 \quad \rightarrow \quad \lambda=\frac{1}{8}(4\pm 3\sqrt{2}) \tag{7}$$

This demonstrates a situation in which the algorithm contains an intrinsic instability which must be resolved if looped modeling with units such as these is to converge successfully. In this particular case, the resolution is to recognize that the looped stream is in effect being given too much weight, as its feedback is passed through the merger to the splitter and then right back to the merger [1]. If the splitter is modified to disregard the looped output, and let the merger adjudicate its value, this instability vanishes:

$$2a+x_n \rightarrow \left[\begin{array}{c} S \end{array}\right] \begin{array}{l}\rightarrow a+y_n \\ \rightarrow a+z_n\end{array} \quad \xrightarrow{reconcile} \quad 2a+x_n \rightarrow \left[\begin{array}{c} S \end{array}\right] \begin{array}{l}\rightarrow a+\frac{x_n}{2} \\ \rightarrow a+\frac{x_n}{2}\end{array} \tag{8}$$

$$2a+x_n \rightarrow [stream\ x\ ] \rightarrow 2a+\frac{x_n+2y_n}{2} \quad \xrightarrow{reconcile\ x} \quad 2a+\frac{3}{4}x_n+\frac{1}{2}y_n \tag{9}$$

$$a+\frac{x_n}{2} \rightarrow [stream\ y\ ] \rightarrow a+\frac{x_n+y_n}{2} \quad \xrightarrow{reconcile\ y} \quad 2a+\frac{1}{2}x_n+\frac{1}{4}y_n \tag{10}$$

$$\begin{bmatrix}x_{n+1}\\ y_{n+1}\end{bmatrix} = \begin{bmatrix}\frac{3}{4}x_n+\frac{1}{2}y_n\\ \frac{1}{2}x_n+\frac{1}{4}y_n\end{bmatrix} = A\begin{bmatrix}x_n\\ y_n\end{bmatrix} = \frac{1}{4}\begin{bmatrix}3 & 2\\ 2 & 1\end{bmatrix}\begin{bmatrix}x_n\\ y_n\end{bmatrix} \tag{11}$$

$$\det(A-\lambda I)=\det\begin{pmatrix}\frac{3}{4}-\lambda & \frac{1}{2}\\ \frac{1}{2} & \frac{1}{4}-\lambda\end{pmatrix}=0 \quad \rightarrow \quad -1<\lambda=\frac{1}{8}\left(2\pm\sqrt{5}\right)<1 \tag{12}$$

The new eigenvalues are demonstrably less than one, and in practice simulations of this form, even with greater numbers of Flowsheet Blocks in series, successfully converged. This ability to instruct a block to disregard one of the streams it was reconciling, while still propagating information through that stream such that the block on the other end might receive information from it, proved invaluable.

II. The Network Modules

II.1. The Reconcile

The reconcile algorithm for the streams flowing within the network is a straightforward averaging of all pertinent variables, as the streams serve as “dumb pipes” connecting the more functionally interesting blocks. Since no substantive changes are permitted within a stream, all that is needed to reconcile one is a conservation of the overall flow rate, which is an extensive variable, and a conservation of the relevant intensive parameters. These are accomplished by a literal averaging of the inflow and outflow values. Each stream has its own means of averaging its properties, and the calling function does not need to know what sort of stream it is calling to be reconciled.

In the case of a stream of chemicals, the flow rate is measured in moles per second while the intensive properties being tracked at this stage of the research are the temperature of the stream as a whole and the mole fraction of each constituent compound of the chemical spectrum.

Heat is not exchanged within the streams; all physical and chemical changes take place within blocks.

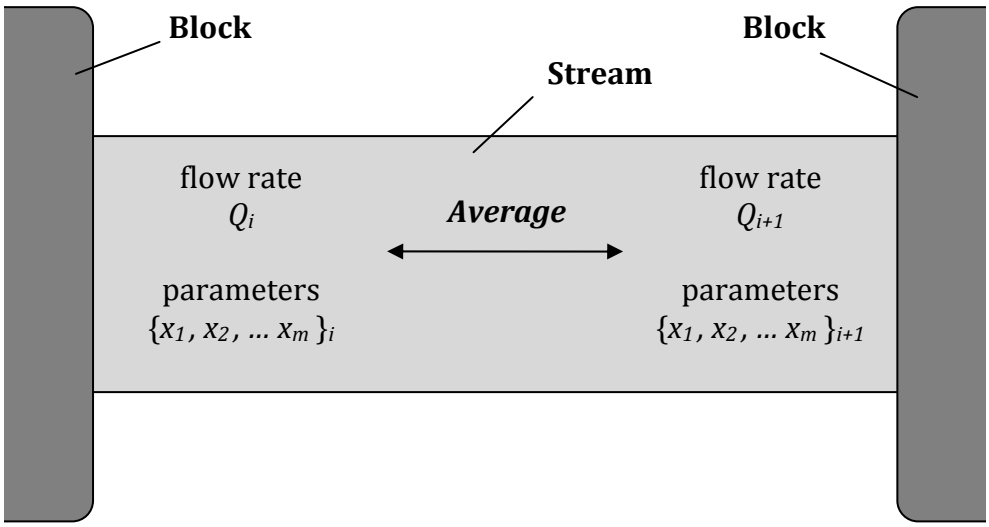

Figure 3.3: Schematic of stream reconciliation.

The reconcile algorithm within the various units, referred to in the code as blocks, calculates the mapping of input streams into physically and chemically different output streams that must obey all relevant conservation laws $f_i(x_1, x_2, x_3, \ldots x_N)$. If there are *n* conservation laws for *m* variables, they can be expressed as a series of equations of the form

$$f_1(x_1, x_2, x_3, \ldots x_N) = 0 \qquad (3)$$
$$\vdots$$
$$f_n(x_1, x_2, x_3, \ldots x_N) = 0$$

These equations ensure the validity of the results of the simulation. Additional functional equations $g_i(x_1, x_2, x_3, \dots x_N)$ are required to express the purpose of the unit, and can be written in the form

$$g_1(x_1, x_2, x_3, \dots x_N) = 0 \qquad (4)$$
$$\vdots$$
$$g_m(x_1, x_2, x_3, \dots x_N) = 0$$

There are therefore $n + m$ equations to reconcile *N* unknowns, but there is no guarantee that $n + m = N$. In order to complete the system of equations, artificial "conservation" equations $h_i(x_1, x_2, x_3, \dots x_N)$ can be introduced that function. These are not dictated by intrinsic physical laws or by the specific functionality of the unit, but rather serve to wrap up the current iteration and move on to the next unit. These additional equations are contrived to maintain numerical stability, conserving the sum of the magnitudes all initial flows in and out, for example, or constraining the multiplying factors by which new flows exceed old flows in order to minimize how drastically a given iteration can alter the streams. The user can choose to specify these extra constraints as minimize certain parameters or certain deviations of parameters. In this work, the additional constraints that were not intrinsically required by physical laws or process necessities were imposed by the method of Lagrange multipliers to minimize deviations. If an extra constraint were required, the weighted sum of the squared differences between the parameter values inherited by the block and those reconciled by the block was assumed to be minimized. This is explained in greater detail below.

II.1.1. Splitter Unit

As a simple example, consider a Splitter, which takes one input stream of chemicals and maps it into two output streams with no bias whatsoever except for a split ratio selected by the user via the xml input file. For example, a 2:1 split of a 300 mol/s chemical flow would produce a 100 mol/s output stream and a 200 mol/s output stream that are chemically identical but are then physically piped to two distinct units. One can imagine a simple divider that slides back and forth across the unit to accomplish this split ratio.

Each time the model runs the reconcile for this block, it observes one input stream and two output streams that were produced by the most recent reconcile of the adjoining streams but which may not be consistent. Most units in the this fuel synthesis network must convert intensive variables to extensive variables to operate properly, since chemical reactions to not conserve the total number of moles and mole fractions cannot be conserved, but since the Splitter does not alter any intensive properties, the reconcile performs a numerical average in the same way that a stream would. To reconcile flow rates, assuming no heat is exchanged since temperature is conserved, the mass conservation equation can be written

$$f_1(Q_{in}, Q_{out1}, Q_{out2}) = Q_{in} - Q_{out1} - Q_{out2} = 0 \quad (5)$$

The functional equation expressing the purpose of the unit to produce a split ratio such that fractions a and β of the incoming flow are sent through the outputs are

$$g_1(Q_{in}, Q_{out1}, Q_{out2}) = \alpha Q_{in} - Q_{out1} = 0 \quad (6)$$

$$g_2(Q_{in}, Q_{out1}, Q_{out2}) = \beta Q_{in} - Q_{out1} = 0 \quad (7)$$

Though since $a + \beta = 1$, this last equation is redundant with the previous two. Since the ratio of the split is user-defined, this unit has only 1 degree of freedom; if any stream is known then the previous two equations resolve the other two. The Splitter algorithm therefore resolves the reconciled value of the incoming stream according to the weighted average

$$Q_{in} = \frac{w_{in} \cdot Q_{in_{previous}} + w_{out1} \cdot \frac{Q_{out1_{previous}}}{\alpha} + w_{out2} \cdot \frac{Q_{out2_{previous}}}{\beta}}{w_{in} + w_{out1} + w_{out2}} \quad (8)$$

Thus the incoming and outgoing streams received by the block from the previous iteration are considered to be three weighted opinions as to the correct incoming flow, which is a weighted average of the three.

II.1.2. Separator Unit

More critical for the fuel synthesis network model than the Splitter is the Separator, which does apply a weight bias since the carbon spectrum can be usefully differentiated by mass and phase. A Separator with one input and two outputs requires the same conservation equations as the Splitter, except that since the Separator is diverting different chemicals differently, it requires a separate variable for each flow of each species and not simply one overall flow variable as in the Splitter, e.g.

$$f_1(H_{2_{in}}, H_{2_{out1}}, H_{2_{out2}}) = H_{2_{in}} - H_{2_{out1}} - H_{2_{out2}} = 0 \quad (9)$$

$$\vdots$$

$$f_n\left(C_{16}H_{34_{in}}, C_{16}H_{34_{out1}}, C_{16}H_{34_{out2}}\right) = C_{16}H_{34_{in}} - C_{16}H_{34_{out1}} - C_{16}H_{34_{out2}} = 0$$

If a set of dimensionless bias coefficients $\{b_1, b_2, \ldots b_n\}$ is developed to express a specific split ratio for each chemical species, and which can be interpreted as a probability of a given chemical being directed to one output over the other one, the resulting constraints are

$$g_1\left(Q_{1_{in}}, Q_{1_{out1}}, Q_{1_{out1}}\right) = Q_{1_{out1}} - b_1 * Q_{1_{out1}} = 0$$

$$\vdots$$

$$g_n\left(Q_{n_{in}}, Q_{n_{out1}}, Q_{n_{out1}}\right) = Q_{n_{out1}} - b_n * Q_{n_{out1}} = 0 \tag{10}$$

These bias coefficients are derived from the transformed Gaussian error function defined by

$$\text{erf}\,(x) = \frac{2}{\sqrt{\pi}} \int_0^x e^{-t^2}\, dt$$

$$b_n = \frac{1}{2}(1 + \text{erf}\,(x_n - x_0)) = \frac{1}{2}\left(1 + \frac{2}{\sqrt{\pi}} \int_0^{x_n - x_0} e^{-t^2}\, dt\right) \tag{11}$$

The linear transformation ensures that the bias coefficients will range from 0 to 1 and that the species of the exact center of the distribution x_0 will be split equally into each outflow. The independent variable x_n is a dimensionless function of the mass of component n.

Like the Splitter, the Separator has only 1 degree of freedom per species, since each species is conserved and distributed according to the ratio reflected by the bias coefficients. There are n species, however, and these bias coefficients depend on the characteristic mass of each species and the center of the separation, x_0. In the most agnostic mode of the Separator, the

center of the separation is taken to be the center of the distribution of A_i incoming moles of each species i with molar mass M_i according to

$$mean\ mass = m_0(A) = \frac{\sum_{i=1}^{i=n_{max}} M_i \cdot A_i}{\sum_{i=1}^{i=n_{max}} A_i} \tag{12}$$

The bias coefficient for a chemical of mass M_n is thus

$$b_n(m_0, M_n) = \frac{1}{2}(1 + \ \mathrm{erf}\,(M_n - m_0)) \tag{13}$$

The heavy output (H) is fraction b_n of the incoming chemicals (A) and the light output (L) is fraction $1 - b_n$.

$$\begin{aligned} H_n &= b_n \cdot A_n \\ L_n &= (1 - b_n) \cdot A_n \end{aligned} \tag{14}$$

Thus the mean masses of the incoming distribution implied by the heavy and light streams returned by the previous stream reconcile are

$$\begin{aligned} m_0(H) &= \frac{\sum_{i=1}^{i=n_{max}} M_i \cdot A_i}{\sum_{i=1}^{i=n_{max}} A_i} = \frac{\sum_{i=1}^{i=n_{max}} M_i \cdot \frac{H_i}{b_i}}{\sum_{i=1}^{i=n_{max}} \frac{H_i}{b_i}} \\ m_0(L) &= \frac{\sum_{i=1}^{i=n_{max}} M_i \cdot A_i}{\sum_{i=1}^{i=n_{max}} A_i} = \frac{\sum_{i=1}^{i=n_{max}} M_i \cdot \frac{L_i}{1 - b_i}}{\sum_{i=1}^{i=n_{max}} \frac{L_i}{1 - b_i}} \end{aligned} \tag{15}$$

Since the bias coefficients in these relations are themselves a function of m_0, these relations must be iteratively repeated until the mean central mass on the left hand side is consistent with the bias coefficients on the right hand side. It is in this way that the mean center of the distribution

implied by the incoming, heavy outgoing, and light outgoing flows is calculated, and therefore the reconciled input stream Q_{in} for component i as suggested by the incoming and outgoing streams are

$$Q_{in_i}(A) = A_i$$

$$Q_{in_i}(H) = \frac{H_i}{b_i(m_0(H), M_i)}$$

$$Q_{in_i}(L) = \frac{L_i}{1 - b_i(m_0(L), M_i)} \tag{16}$$

and as with the Splitter, a weighted average resolves the reconciled input stream.

$$Q_{in_i} = \frac{w_A \cdot A_i + w_H \cdot Q_{in_i}(H) + w_L \cdot Q_{in_i}(L)}{w_A + w_H + w_L} \tag{17}$$

This newly reconciled input stream has its own mean which can be calculated as above to produce bias coefficients and therefore the outgoing heavy and light reconciled streams.

It is substantially computationally simpler when the Separator operates with a user-specified separation mean, wherein the user selects a mass such that chemicals heavier than that mass bias one way and chemicals lighter than that mass bias the other way. In this case the bias coefficients can be immediately calculated as in the final steps above, and the weighted average produces the reconciled streams.

Another version of the Separator employed to simulate the focusing of a product stream down to a particular chemical is the Gaussian separator, which instead of separating left and right of a central mean instead produces a Gaussian peak through one output and the remainder of the

stream through the other output. This represents a first approximation of what would ideally converge to a Delta separator (named for the Dirac delta function), which would perfectly select a specified chemical to pass through one outlet and the remaining chemicals would be passed through the other outlet. In all cases the mapping function is operating with molar mass as the input variable. The Gaussian mapping function was written to be 70-80% effective at passing the mass in question through the selector output, with a standard deviation equal to at least the mass of a CH_2 monomer (14 grams) in either direction. Typically this value was conservatively set at 20 grams. For a specified mass filter with a peak centered at μ and an incoming chemical of mass m, the probability of the Gaussian selector passing that chemical through the selection outlet is therefore given by

$$P(m) = 0.75 \cdot e^{-\left(\frac{m-\mu}{20}\right)^2} \tag{18}$$

The function was limited to a minimum probability of 1%, meaning that it is assumed never to be better than 99% effective at filtering out unwanted chemicals no matter their mass, and therefore is actually coded as

$$P(m) = \max\left(0.75 \cdot e^{-\left(\frac{m-\mu}{20}\right)^2}, 0.01\right) \tag{19}$$

Replacing the bias coefficients above with the likelihood of a particular chemical flowing out of the selected port, these probabilities are used in the same weighting procedure to reconcile incoming and outgoing streams. The existence of only one degree of freedom is confirmed by observing that if the probability of a chemical flowing out of the selected port is, say, 20%, then

a given outflow implies five times as much must have flowed in and four times as much must have flowed out of the other port, thereby resolving all three ports of the Separator.

II.1.3. Merger Unit

The Merger follows similar principles as outlined above, with the added complication that reconciling the intensive variables must account for the fact that they may change. While an unbiased Separator will not alter the temperatures and mole fractions of each of the *n* species in the chemical spectra, a Merger may well inherit two streams whose values differ. Mole fractions are no longer a convenient parameter, and so the reconcile must consider *n* actual flow rates in each stream. Considering two inputs and one output for each species, along with temperatures for the assumed isothermal two inputs and one output, would lead to $3n + 3$ variables to reconcile. Note that energy need not necessarily be conserved by the Merger within a given species, since the flow of species *i* may have been heated by flow of species *j*.

Since simple mass conservation is not enough to constrain the system, a variety of algorithms are employed to reconcile the unit. In the unconstrained and unweighted case of three equally valid inputs, the method of Lagrange multipliers minimized deviation from the previous iteration by minimizing

$$f(a,b,c) = (A-a)^2 + (B-b)^2 + (C-c)^2 \tag{20}$$

subject to the constraint

$$g(a,b,c) = a + b - c = 0 \tag{21}$$

where *A*, *B*, merge to *C* in before the reconcile, and *a*, *b*, and *c* do so afterwards. The result of the Lagrange calculation is that the incoming flows are corrected by

$$\begin{aligned} a &= A + \frac{1}{3}(C - A - B) \\ b &= B + \frac{1}{3}(C - A - B) \\ c &= C - \frac{1}{3}(C - A - B) \end{aligned} \tag{22}$$

Thus if the output exceeds the input then the inputs are increased and the output decreased accordingly. An additional positivity constrained is included in the event that any of the above quantities become negative, in which case *a* and *b* are modified while preserving *a* + *b* and not changing *c* (which cannot in the above formulation have been negative)

If the inputs are weighted, then the quantity to be minimized is

$$f(a,b,c) = w_a(A-a)^2 + w_b(B-b)^2 + w_c(C-c)^2 \tag{23}$$

subject to the same constraint. In this more complicated case, however, the method of Lagrange multipliers yields

$$a = A - \frac{\omega}{w_a}(A + B - C)$$

$$\mathrm{b} = \mathrm{B} - \frac{\omega}{w_b}(\mathrm{A} + \mathrm{B} - \mathrm{C})$$

$$c = C + \frac{\omega}{w_c}(A + B - C)$$

$$\frac{1}{\omega} = \frac{1}{w_a} + \frac{1}{w_b} + \frac{1}{w_c} \tag{24}$$

If one of the streams is constrained while the other two are merely weighted, the Lagrange multipliers are re-derived for those cases. In fact, considering that each of three streams may be constrained, numerically weighted, or unweighted, there are 27 possible scenarios of constraints, weights, & free streams for which the merging unit must assign the appropriate algorithm with which to reconcile them.

II.1.4. Fuel Synthesis Reactor Unit

The Synthesizer is a unit that will initially be modeled to approximate a Fischer-Tropsch reaction chamber, although the nature of the catalytic process can be specified and altered by choices of input files. Since the structure of the code is not simply to step forward from input to output but rather to reconcile inputs and outputs, existing model equations for well-known Fischer-Tropsch reaction behavior are incorporated into this way of doing things. As a first approximation, the ASF distribution detailed above is adapted as follows:

1. Input stream conditions are projected forwards to an implied output.
2. The implied output is averaged with the existing output.
3. The averaged output is projected *backwards* to an implied input.

4. The implied input and the averaged output represent reconciled solutions that are returned to the Flowsheet.

The equations deployed for this purpose in the first iteration of the reconcile are a flow balance as per the above methods of reconciling overall mole flow and then corrections followed by the above chain growth relation, modified to recognize the chain-length dependence of growth, namely

$$x_n = (1 - \alpha_n) \cdot \alpha_n{}^{(n-1)} \tag{25}$$

The chain growth probability α is a property of the reactor itself, subscripted above to reflect the dependence that may be determined from the Botes equation

$$\alpha_n = \frac{1}{1 + \tau_P + \tau_O \cdot \mathrm{e}^{-k \cdot n}} \tag{26}$$

The reactor algorithm is described in much greater detail in Chapter 4.

II.1.5. Cracker Unit

The Cracker is a unit that in a large-scale Fischer-Tropsch facility would be external to syncrude production but which presently will be integrated into the production network itself. Generally, the purpose of the cracker is to give undesirable hydrocarbons another crack at synthesis into a specified product. The unit is designed to follow the Schulz & Weitkamp “ideal hydrocracking” guidelines that the largest molecules are cracked selectively and that no secondary cracking occurs. Mathematically, the Cracker maps an incoming chemical spectrum into a spectrum of lighter constituent parts. In detailed practice this process is a function of

individual bond energies, but in the first iteration the reconcile will assign probabilities to individual bonds based on the nature and size of the hydrocarbons comprising the incoming stream, introducing biases for example towards the ends of a carbon chain. The output chemical flow is then fed into a separator that biases the new spectrum back to other units. The cracker algorithm is described in much greater detail in Chapter 4.

II.1.6. Refiner Unit

A Refiner is a unit that would have increasing variety as chemical production options in the network are expanded. As a refinery is not a uniform reaction chamber but rather a host of sub-processes specific to the feed and product, it is perfectly adaptable to a modular network of specific units. Units in the modular network would need to simulate those processes most useful for fuel synthesis, namely olefin dimerization and oligomerization, aromatic alkylation, pentene skeletal isomerization with etherification, hydrotreating, hydroisomerization, hydrocracking, nonacidic Pt/L-zeolite reforming and alcohol dehydration [2]. The recent work of de Kerk has characterized in detail these process as best applied to Fischer-Tropsch, but rather than model chemical reactions on a bond-level of detail, the numerical simulation can instead be informed by mass percentage and operating condition characterizations of the input and output streams to inform a mapping of an input stream onto an output stream in the same way as was described above for the fuel synthesis units [3]. The completed work found product sharpening that was possible down to a single user-specified molecule using processes of thermal cracking of alkenes and alkanes, steam reforming of methane, and hydrocracking of alkenes into alkanes. The other

refining options referred to here and elsewhere remain available and potentially adaptable to small-scale networks and this code, but proved not be necessary in the present work, since the network was demonstrated to be capable of perfect specificity of output without any more exotic flavors of unit than reactors and crackers.

II.2. Networking Flowsheets

A great advantage of modeling the fuel synthesis network with this particular code is that the structure of Flowsheets is much more conducive to convergence within a reasonable amount of processing time. Rather than treating the network of units and pipes as being a large set of discrete units of undifferentiated standing, the completed work assembles these units in Flowsheets as described above, and each Flowsheet is internally reconciled before the Flowsheets are interconnected in the greater network. Streams flowing through the incoming and outgoing open ports of a Flowsheet Block are routed into the simple blocks within the Flowsheet actually represented by that Flowsheet Block. Observing the properties of the network within a given Flowsheet and then within a collection of Flowsheets informed how the greater network was constructed and how to code decision-making for directing the various streams as an automated system would.

The structure of the code as described thus far is Eulerian in nature, in that the code is visiting each block and each stream to be reconciled one by one. However there is also a Lagrangian analysis that is important to assessing the effectiveness of the network, i.e. how much time does each carbon atom spend before emerging as an economically and energetically

viable fuel? Various fractions of a given spectrum of carbon will emerge victorious from the network sooner than others, and so time spent, or rather number of blocks visited, will be incorporated into assessing and therefore minimizing a penalty similar to the distance measurement that reconcile functions assess. The difference is that one set of fully reconciled Flowsheets may not be as valuable as the next.

II.3. Penalties

The penalty calculations became relevant once a configured network, that meets practical design specifications to produce a plausible and economically viable suite of hydrocarbon products, was numerically converging. Optimization of such a network required a formalization of how one path is favored over another, which was accomplished by assigning penalties to the network. Producing sub-optimal byproducts to the specified hydrocarbon must be discriminated against, so deviations from the desired spectrum must be penalized. Furthermore, even a network that produces a 100% pure output of a single specified chemical has incurred a cost as a function of how looping was required to process it. Through how many units must a single carbon atom pass before it emerges as part of an economically viable user-specified product? Time spent in the system must be penalized in the form of either residence time or path length. Since a steady-state solution is desirable, a Lagrangian tracing of the path length of each carbon atom is approximated as an Eulerian characterization of the throughput in a given unit. To accomplish this, each stream may emerge from a unit with an “age” that is been incremented depending on the cost of the unit. A Synthesis unit ages a stream more than a Separator, which in turn may age

a unit more than a simple Splitter. Since chemical flows are separated and merged throughout the system, these junctions will average the "age" of the constituents as weighted by molecular mass. This "age" is a penalty. Spectrum accuracy and stream age will in turn have weight coefficients so that the model has flexibility in favoring one over the other. This approach quantifies the trade-off between spectrum sharpness and the weighted average length of the chain of units through which that spectrum passed.

II.4. Modeling Strategy

The bulk of the completed dissertation work was to code and simulate reactor configurations in order to develop scaling laws and demonstrate the tune-ability and flexibility of the network. Rules of the thumb were observed in order to ensure the convergent stability of the system, since the greater the number of reactors (Flowsheets) built into the model, the greater the complexity of the reconcile. The closer the input files were to initial values that are real, the better the chance of convergence. The code produces results that are not necessarily unique given the operating parameters, but which would physically result from unit inputs, so previous results could inform the context of successive investigations.

Two fundamental types of network configurations were considered and modeled in the completed work, namely unidirectional and closed loop recycling. The unidirectional work was undertaken to demonstrate how the chemical spectrum sharpens from unit to unit in a series of small scale applications of the process versus single large scale applications of the process. This is a more forgiving undertaking since looped steady state convergence is not necessary; the

system is fully and clearly constrained by inputs which are simply and rapidly propagated forward. With the assistance of the weight propagation and eigenvalues reduction techniques discussed above, however, more aggressive configurations and constraints can be imposed to create a closed loop recycling configuration that only permits specific chemicals to leave the system. These configurations also converged and were studied under various permutations of sizes and parameter values to show how the network sharpens the outputs. Important characteristics to vary included type, distribution, and size of reactor units, distribution of high and low temperature units, type of catalyst used throughout the network as expressed in the reactions permitted and growth probabilities achieved in the unit, and the number of passes per carbon atom required in order to achieve a particular chemical output.

III. References

1. Lackner, K., *Conversations with Professor Klaus Lackner.* 2013.
2. de Klerk, A., *Fischer-Tropsch refining: technology selection to match molecules.* Green Chemistry, 2008. **10**(12): p. 1249-1279.
3. de Klerk, A., *Fischer-Tropsch fuels refinery design.* Energy & Environmental Science, 2011. **4**(4): p. 1177-1205.

Chapter 4

Justification of the Maps for Fuel Synthesis and Thermal Cracking

I. Fischer-Tropsch Reactor Unit

The Synthesizer is a unit that was modeled as a simplified catalysis process based on a Fischer-Tropsch reaction chamber, although the nature of that catalytic process can be specified and altered by choices of input files. The specific identity of the process exists solely in the mapping matrix that is constructed according to the instructions provided by the incoming xml parameters. Since the structure of the code is not to simply step forward from input to output but rather to reconcile inputs and outputs, existing model equations for well-known Fischer-Tropsch reaction behavior are studied to simulate a representative fuel synthesis that is numerically adapted to this way of doing things. Essentially, the ASF distribution detailed above is adapted as follows:

1. Input stream conditions are projected forwards to an implied output.
2. The implied output is averaged with the existing output.

3. The averaged output is projected *backwards* to an implied input.
4. The implied input and the averaged output represent reconciled solutions that are returned to the Flowsheet.

The Flowsheet takes these returned solutions to streams and reconciles them, as described above. They may not be fully reconciled at this point if the Flowsheet is actually a Flowsheet Block within a larger Flowsheet, but when the model converges to a solution the inputs and outputs to the reactor unit will obey the coded ASF relationship between incoming and outgoing hydrocarbons.

I.1. Chain Growth

The equations deployed for this purpose represent a flow balance as per the above methods of reconciling overall mole flow and then corrections followed by the above chain growth relation, modified to recognize the chain-length dependence of growth, namely [1]

$$y_n = (1 - \alpha_n) \cdot {\alpha_n}^{(n-1)} \tag{1}$$

in which y_n represents the mole fraction in the output stream of hydrocarbons containing n carbon atoms, and the chain growth probability α_n is a property of the reactor itself determined from the above Botes equation [2]

$$\alpha_n = \frac{1}{1 + \tau_P + \tau_O \cdot \mathrm{e}^{-k \cdot n}} \tag{2}$$

This chain growth probability is a relatively mathematically trivial representation of underlying processes that are decidedly not trivial, and precisely modeling α, it should be noted, is not the

aim of this research. This variation as a function of chain-length is subtle and often simplified in the experimental literature to a single value, and this practice is followed here as well. Typical reported values for chain growth go as high as 90%, but the values used here were in the range of 70-80% to compensate for the computational simplification of the lengths of chains modeled. As described below, this mathematical formulation only conserves carbon if very long chains are grown; this is the difference between considering the exponential equation above to be an infinite geometric series or a finite geometric series. Capping the permissible length of carbon chains for modeling purposes makes this decidedly a finite geometric series, the higher order terms, which actually represent the fraction of carbon that would have been converted to longer chains than those considered here, must allocate their carbon to chains that are considered. The simulations performed here modeled carbon chains growing as long as 16 carbons, which imply 16 alkanes (C_1-C_{16}) and 15 alkenes (C_2-C_{16}) produced. Oxygenates and alkynes were not considered in the present work, since the benefits of networking need only demonstrate improvements to a complex process compared to the non-networked version. This comparison is valid provided that the scope of the networked process and the scope of the non-networked process are the same.

The probability constraint

$$\sum_{n=1}^{n_{max}} y_n = \sum_{n=1}^{n_{max}} (1-\alpha)\cdot\alpha^{n-1} = 1 \tag{3}$$

would have been satisfied automatically as $n_{max} \to \infty$, but must be corrected here by assuming that all chains longer than n_{max} are instead parking their carbons in C_{max}. This correction is the infinite sum

$$\sum_{n=n_{max}+1}^{\infty} y_n = \sum_{n=n_{max}+1}^{\infty} (1-\alpha)\cdot\alpha^{n-1} = \frac{(1-\alpha)\cdot\alpha^{n_{max}}}{1-\alpha} = \alpha^{n_{max}} \quad (4)$$

For $\alpha = 0.9$ and $n_{max} = 16$, this correction is a whopping 18.5% increased likelihood of forming the heaviest carbon chain if the carbons of all heavier chains are allocated there, whereas for $\alpha = 0.8$ and $n_{max} = 16$, this correction is merely 2.9%, and for $\alpha = 0.7$ and $n_{max} = 16$, this correction is merely 0.33%. The modeled reactor network can live with this as long as it is understood that results pertaining to the heaviest carbon chain are slightly exaggerated, while the shorter carbon chains are still containing only those carbons they would have contained anyway if the longer chains had been considered.

The reactor network is modeled as a steady state conversion of carbon molecules, as per typical assumptions about the rate of flow of incoming hydrocarbons and the residence time of these species. The assumption of first order kinetics is considered valid [3].

I.2. Secondary Reactions

As previously noted, deviations from the primary distribution predicted by the ASF model and patterns in the relative concentrations of olefins and paraffins as a function of chain length are due in part to secondary reactions of primary products. Without such secondary reactions, for example, primary selectivity of α-olefins over Fe/Mn has been reported as high as 70-90% by mole [4]. Although there has been some debate as to whether the chain length dependence of these secondary reactions and deviations are most influenced by physisorption,

solubility, or diffusivity [4-7], it is clear that secondary reactions of hydrogenation, isomerization, resinsertion, and hydrogenolysis influence the outgoing product distribution, and that whatever the underlying cause, the olefin fraction of the total product decreases with increasing carbon number.

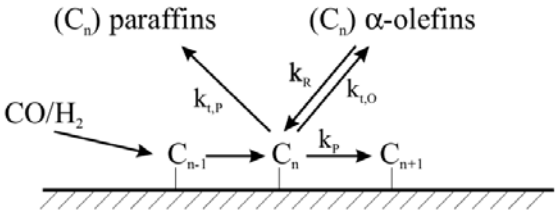

Figure 4.1: Illustration of chain growth and termination [8]

Secondary reactions occur in greater frequency in Fe, Ru, and Co catalysts, respectively [1]. Both ethene and propene have been observed to readsorb more readily than other olefins [9], though in general olefins readsorb better at higher carbon numbers due to decreased mobility [10]. The important conclusion from these observations of Fischer-Tropsch behavior is that the process is more complicated than simply a consumption of CO and production of longer hydrocarbons, and that consumption of other molecules is precisely the way a network can change the output spectrum by adjusting the input spectrum. Since the simulated fuel synthesis network aims to represent actually occurring processes in an attempt to sharpen the ultimate distribution of products, readsorption of hydrocarbons produced via primary synthesis was written into the matrices, mapping an approximated Fischer-Tropsch reactor's incoming chemical flows of syngas and synthesized hydrocarbons to reactor outputs. The parameters informing this mapping were derived from studies of co-fed olefins, including isotopic tracing,

so that modeled behavior of co-fed olefins would more closely match what has been observed in real reactors.

Secondary reactions are very sensitive to conditions of temperature, partial pressures of H_2, CO_2, and H_2O, and residence time [4]. Naturally the extent of secondary reactions will be greater with longer residence times, as primary products linger longer near potential readsorption sites. It is a consistent observation in the literature that propene is the olefin least secondarily reacted, and that ethene is consumed in this manner with 10-40 times greater reactivity than longer olefins. Hydrogenation of α-olefins to paraffins of the same length is the dominant reaction. Incorporation of primary olefins into further chain growth was long observed to be less prevalent, but took place at molar conversion rates of up to 30% over cobalt and up to 12% over iron in the work of Schulz et al. [11]. Ethene is a particularly strong chain initiator at lower temperatures and at lower ratios of H_2:CO [4], and co-fed ethene has been shown to cut methane selectivity in half in favor of greater CO conversion and longer-chain olefin production [12]. Competitive absorption of CO and olefins explains the increases in olefin reactions with decreasing CO partial pressure observed by Boelee et al. [13] and with higher CO conversion rates as well as lower CO partial pressure observed by Hanlon and Satterfield [4]. Additional research by Iglesia et al. [14] under what they considered more industrially realistic conditions examined the role of H_2O demonstrated that olefin hydrogenation was prevalent in the hydrogenation of olefins over cobalt, at the expense of minimal reincorporation, whereas high water concentrations produced greater incorporation of olefins and much less prevalent hydrogenation and isomerization. It was in this context that Iglesia et al. argued their diffusion-

based model for deviations from the Schulz-Flory distribution towards more paraffins at high carbon numbers. Strong cases have been made elsewhere [15] for physisorption and solubility effects being as critical if not more determinant, but the murky underlying mechanisms for intra-catalyst processes are less important than writing a realistic mapping of reactants to products based on observed industrial and experimental results.

These observations from the literature as to the behavior of co-fed olefins under Fischer-Tropsch synthesis suggest important modifications to the mapping matrix of the reactor, and illustrate the opportunity for tweaking the outgoing distribution based on reactor inputs. In an attempt to strike a balance between representing a realistic and industrially relevant chemical process and performing computational research of reasonable complexity and convergence time, isomerization, double-bond-shifting and production of oxygenates were neglected. They are not overly dominant in practice and not critical to studying the effects of automated throughput redirection on a networked chemical system, as was the stated goal of this work. Hydrogenation and incorporation of co-fed olefins was written into the matrix mapping the reactor operation using the values based on those reported by Schulz & Claeys [4] while conforming to the above assumptions and subject to change depending on the availability of the relevant reactants in the incoming chemical stream:

Cn	O(n)	Xol(n)	Yinc(n)	Yhyd(n)
2	0.37	0.82	0.38	0.44
3	0.65	0.12	0.04	0.08
4	0.60	0.25	0.10	0.15
5	0.55	0.40	0.18	0.36
6	0.50	0.54	0.24	0.56
7	0.46	0.68	0.30	0.38
8	0.43	0.78	0.35	0.43
9	0.39	0.82	0.40	0.42
10	0.36	0.86	0.42	0.44
11	0.33	0.90	0.45	0.45

O(n) = *probability of chain termination as an olefin in primary production*

Xol(n) = *probability of an incoming olefin readsorbing and reacting*

Yhyd(n) = *probability of a readsorbed olefin simply saturating with hydrogen*

Yinc(n) = *probability of a readsorbed olefin reinitiating chain growth*

Table 4.1: Default reactor parameters

I.3. Primary Production Maps

To build the forward projection matrix, first consider the synthesis of incoming CO producing a total number of moles N of primary hydrocarbons each containing n carbons, which can be written as

$$\mathrm{C}_n = y_n(\alpha, n) \cdot N \tag{5}$$

where N is the total number of moles of newly produced carbon chemicals, y_n is the fraction of those chemicals containing n carbon atoms. Therefore,

$$N = \sum_{k=1}^{n_{max}} \mathrm{C}_n \tag{6}$$

$$\mathrm{C}_n = y_n \cdot \left(\sum_{n=1}^{n_{max}} \mathrm{C}_n \right) = y_n \cdot N \tag{7}$$

$$\mathrm{CO}_i \cdot X_{\mathrm{CO}} = \sum_{k=1}^{n_{max}} k \cdot \mathrm{C}_k = \text{total reacted carbon} \tag{8}$$

$$\mathrm{CO}_i \cdot X_{\mathrm{CO}} = \mathrm{C}_1 \cdot 1 + \mathrm{C}_2 \cdot 2 + \cdots + \mathrm{C}_{n_{max}} \cdot n_{max} \tag{9}$$

Substituting only the converted carbon for each type,

$$\mathrm{CO}_i \cdot X_{\mathrm{CO}} = y_1 \cdot N \cdot 1 + y_2 \cdot N \cdot 2 + \cdots + y_{n_{max}} \cdot N \cdot n_{max} = N \cdot \left(\sum_{n=1}^{n_{max}} n \cdot y_n \right) \tag{10}$$

$$\Sigma_{ny} \equiv \sum_{n=1}^{n_{max}} n \cdot y_n \tag{11}$$

$$N = \frac{\mathrm{CO}_i \cdot X_{\mathrm{CO}}}{\sum_{n=1}^{n_{max}} n \cdot y_n} = \frac{\mathrm{CO}_i \cdot X_{\mathrm{CO}}}{\Sigma_{ny}} = \frac{X_{\mathrm{CO}}}{\Sigma_{ny}} \cdot \mathrm{CO}_i \tag{12}$$

$$\mathrm{C}_n = y_n \cdot N = y_n \cdot \frac{X_{\mathrm{CO}}}{\Sigma_{ny}} \cdot \mathrm{CO}_i \tag{13}$$

I.4. Methane Correction

Suppose a given %CH_4 of the converted carbon:

$$\mathrm{CO}_i \cdot X_{\mathrm{CO}} = \%\mathrm{CH}_4 \cdot N + y_2 \cdot N \cdot 2 + \cdots = N \cdot \left(\%\mathrm{CH}_4 + \sum_{n=2}^{n_{max}} n \cdot y_n \right) \tag{14}$$

$$\Sigma_{ny_{corr}} \equiv \%\mathrm{CH_4} + \sum_{n=2}^{n_{max}} n \cdot y_n \tag{15}$$

$$N_{corr} = \frac{X_{\mathrm{CO}}}{\Sigma_{ny_{corr}}} \cdot \mathrm{CO}_i \tag{16}$$

$$\mathrm{C_1} = \%\mathrm{CH_4} \cdot N_{corr} = \frac{\%\mathrm{CH_4} \cdot X_{\mathrm{CO}}}{\Sigma_{ny_{corr}}} \cdot \mathrm{CO}_i \tag{17}$$

$$\mathrm{C_{2+}} = y_n \cdot N_{corr} = y_n \cdot \frac{X_{\mathrm{CO}}}{\Sigma_{ny_{corr}}} \cdot \mathrm{CO}_i \tag{18}$$

Note that the uncorrected methane fraction is simply (1 – α). For lower alpha value simulations, in which methane would be predicted to be produced in a much higher fraction of the output, this correction is not useful to apply, as it too dramatically interferes with the geometric series summation that follows for other carbon numbers.

I.5. Secondary Production Maps

This last result for C_n represents only the number of moles of hydrocarbons of length *n* produced by primary synthesis. What about reincorporated olefins? They may simply hydrogenate, or they may re-initiate chain growth. If they re-initiate chain growth, a similar calculation follows, however since not as much chain growth is required for a chain already of length *n* to produce a hydrocarbon of length n_{o} , we have for example the following expression for the number of moles of butane and butene produced from incoming moles of olefins, $C_{n_{in}}$, which have a probability $P_{inc,n}$ of reincorporating and initiating chain growth:

$$C_4 = C_{2_{in}} \cdot P_{inc,2} \cdot \alpha^2 + C_{3_{in}} \cdot P_{inc,3} \cdot \alpha \tag{19}$$

In general, for a readsorbed olefin chain of length *k*,

$$y_{n,k} = (1 - \alpha_n) \cdot \alpha_n^{n-k} \tag{20}$$

$$C_{n>2} = \sum_{k=2}^{n-1} P_{inc,k} \cdot y_{n,k} \cdot C_{k_i} \tag{21}$$

The resulting secondary products are apportioned between paraffins and olefins as before. Experimental data reported in the literature represent probabilities that incoming olefins are successfully incorporated into growing chains. Thus conservation of mass requires that while nothing actually happens to an olefin that readsorbs and then departs the catalyst, the fraction of that olefin that grows must be related carefully to reported values, $P_{exp,k}$. For example,

$$C_4 = \cdots + C_{3_i} \cdot P_{inc,3} \cdot (1 - \alpha) \cdot \alpha$$

$$C_5 = \cdots + C_{3_i} \cdot P_{inc,3} \cdot (1 - \alpha) \cdot \alpha^2$$

$$\vdots$$

$$C_{max} = \cdots + C_{3_i} \cdot P_{inc,3} \cdot (1 - \alpha) \cdot \alpha^{max-3}$$

All of the readsorbed and reincorporated propene must obey

$$P_{inc,3} \cdot (1 - \alpha) \cdot (\alpha + \alpha^2 + \cdots + \alpha^{max-3}) = P_{exp,3}$$

Since this is a finite geometric series,

$$\alpha + \alpha^2 + \cdots + \alpha^{max-3} = \frac{\alpha \cdot (1 - \alpha^{max-3})}{1 - \alpha}$$

$$P_{inc,3} \cdot (1 - \alpha) \cdot \frac{\alpha \cdot (1 - \alpha^{max-3})}{1 - \alpha} = P_{exp,3}$$

$$P_{inc,3} \cdot \alpha \cdot (1 - \alpha^{max-3}) = P_{exp,3}$$

And in general, for secondary chain growth initiation by olefins of length *k*, the incorporation probabilities must be related to the experimental observations by

$$P_{inc,k<max} = \frac{P_{exp,k}}{\alpha \cdot (1 - \alpha^{max-k})} \tag{22}$$

A critically important adjustment was made due to secondary synthesis, which is that the CO conversion, X_{CO}, represents the fraction of CO molecules adsorbing onto the catalyst surface. If secondary synthesis is taking place, then that CO is being shared by primary and secondary chains, and the amount available to grow paraffins and olefins via primary synthesis is reduced accordingly. This correction is addressed by consideration of CO conservation. The uncorrected consumption of CO is given by

Incoming CO: CO_i

Primary olefins: $-\sum_{n=1}^{n_{max}} n \cdot P_{\mathrm{O},n} \cdot \left(y_n \cdot \frac{X_{\mathrm{CO}}}{\Sigma_{ny}}\right) \cdot \mathrm{CO}_i$

Primary paraffins: $-\sum_{n=1}^{n_{max}} n \cdot P_{\mathrm{P},n} \cdot \left(y_n \cdot \frac{X_{\mathrm{CO}}}{\Sigma_{ny}}\right) \cdot \mathrm{CO}_i$

Secondary hydrogenation: -0

Secondary olefins: $-\sum_{k=2}^{n_{max}}\sum_{n=k}^{n_{max}}(n-k)\cdot P_{\mathrm{O},n}\cdot \mathrm{C}_k\mathrm{H}_{2k_i}\cdot P_{inc,k}\cdot y_{n,k}$

Secondary paraffins: $-\sum_{k=2}^{n_{max}}\sum_{n=k}^{n_{max}}(n-k)\cdot P_{\mathrm{P},n}\cdot \mathrm{C}_k\mathrm{H}_{2k_i}\cdot P_{inc,k}\cdot y_{n,k}$

$$= \mathrm{CO} \tag{23}$$

Since $P_{\mathrm{P},n} + P_{\mathrm{O},n} = 1$, the primary terms' CO_i coefficients satisfy

$$\sum_{n=1}^{n_{max}} n\cdot P_{\mathrm{O},n}\cdot\left(y_n\cdot\frac{X_{\mathrm{CO}}}{\Sigma_{ny}}\right)+\sum_{n=1}^{n_{max}} n\cdot P_{\mathrm{P},n}\cdot\left(y_n\cdot\frac{X_{\mathrm{CO}}}{\Sigma_{ny}}\right)=\sum_{n=1}^{n_{max}} n\cdot\left(y_n\cdot\frac{X_{\mathrm{CO}}}{\Sigma_{ny}}\right)=X_{\mathrm{CO}} \tag{24}$$

This is the same X_{CO} that was used to calculate primary production, but that X_{CO} had to be reduced by the proportion consumed by secondary production, $X_{CO,s}$, in order to accurately describe the proportion $X_{CO,p}$ consumed by primary production:

$$\mathrm{C}_{n,primary} = y_n\cdot N=\frac{y_n}{\Sigma_{ny}}\cdot\left(X_{\mathrm{CO,p}}\cdot\mathrm{CO}_i\right)=\frac{y_n}{\Sigma_{ny}}\cdot\left(X_{\mathrm{CO}}\cdot\mathrm{CO}_i - X_{\mathrm{CO,s}}\cdot\mathrm{CO}_i\right) \tag{25}$$

It was already shown above that the CO consumed by secondary production of paraffins and olefins is

$$\sum_{k=2}^{n_{max}}\sum_{n=k}^{n_{max}}(n-k)\cdot P_{\mathrm{O},n}\cdot \mathrm{C}_k\mathrm{H}_{2k_i}\cdot P_{inc,k}\cdot y_{n,k}+\sum_{k=2}^{n_{max}}\sum_{n=k}^{n_{max}}(n-k)\cdot P_{\mathrm{P},n}\cdot \mathrm{C}_k\mathrm{H}_{2k_i}\cdot P_{inc,k}\cdot y_{n,k} \tag{26}$$

so

$$X_{\mathrm{CO,s}}\cdot\mathrm{CO}_i=\sum_{k=2}^{n_{max}}\sum_{n=k}^{n_{max}}(n-k)\cdot \mathrm{C}_k\mathrm{H}_{2k_i}\cdot P_{inc,k}\cdot y_{n,k} \tag{27}$$

and

$$\mathrm{C}_{n,P,primary} = P_{P.n} \cdot \frac{y_n}{\Sigma_{ny}} \cdot X_{\mathrm{CO}} \cdot \mathrm{CO}_i - P_{P.n} \cdot \frac{y_n}{\Sigma_{ny}} \sum_{k=2}^{n_{max}} \sum_{n=k}^{n_{max}} (n-k) \cdot \mathrm{C}_k\mathrm{H}_{2k_i} \cdot P_{inc,k} \cdot y_{n,k} \tag{28}$$

$$\mathrm{C}_{n,O,primary} = P_{O.n} \cdot \frac{y_n}{\Sigma_{ny}} \cdot X_{\mathrm{CO}} \cdot \mathrm{CO}_i - P_{O.n} \cdot \frac{y_n}{\Sigma_{ny}} \sum_{k=2}^{n_{max}} \sum_{n=k}^{n_{max}} (n-k) \cdot \mathrm{C}_k\mathrm{H}_{2k_i} \cdot P_{inc,k} \cdot y_{n,k} \tag{29}$$

As a concrete example, suppose that incorporated butane (k = 4) is poaching CO from primary hexane. Hexane production would have been

$$\mathrm{C}_{6,P,primary} = P_{P.6} \cdot \frac{y_6}{\Sigma_{ny}} \cdot X_{\mathrm{CO}} \cdot \mathrm{CO}_i = P_{P.6} \cdot \frac{(1-\alpha)\alpha^5}{\Sigma_{ny}} \cdot X_{\mathrm{CO}} \cdot \mathrm{CO}_i \tag{30}$$

However the incorporated butene can consume

$$CO_{unavailable} = \sum_{n=2}^{n_{max}} (n-4) \cdot \mathrm{C}_4\mathrm{H}_{8_i} \cdot P_{inc,4} \cdot y_{n,4} \tag{31}$$

and so the actual amount of hexane produced by primary product would be

$$\mathrm{C}_{6,P,primary} = P_{P.6} \cdot \frac{y_6}{\Sigma_{ny}} \cdot (X_{\mathrm{CO}} \cdot \mathrm{CO}_i - CO_{unavailable})$$

$$\mathrm{C}_{6,P,primary} = P_{P.6} \cdot \frac{y_6}{\Sigma_{ny}} \cdot \left(X_{\mathrm{CO}} \cdot \mathrm{CO}_i - \left(\sum_{n=2}^{n_{max}} (n-4) \cdot \mathrm{C}_4\mathrm{H}_{8_i} \cdot P_{inc,4} \cdot y_{n,4} \right) \right)$$

$$\mathrm{C}_{6,P,primary} = \left(P_{P.6} \cdot \frac{y_6}{\Sigma_{ny}} \cdot X_{\mathrm{CO}} \right) \cdot \mathrm{CO}_i - \left(P_{P.6} \cdot \frac{y_6}{\Sigma_{ny}} \sum_{n=2}^{n_{max}} (n-4) \cdot P_{inc,4} \cdot y_{n,4} \right) \cdot \mathrm{C}_4\mathrm{H}_{8_i} \tag{32}$$

Thus, the primary production of paraffins and olefins is a linear combination of inputs provided that the incorporation probabilities $P_{inc,k}$ are known. Now these incorporation probabilities are

also a function of CO, since at higher partial pressures of CO there is a reduced probability of incoming alkenes to adsorb on the catalyst surface, but the model accounts for this by performing the following algorithm to reconcile the streams:

1. Since X_{CO} is a property of the reactor, and since no CO can be produced, the incoming CO implies an outgoing CO and vice versa according to $\mathrm{CO}_f = X_{\mathrm{CO}} \cdot \mathrm{CO}_i$, and so these are averaged first.
2. Once the CO concentrations are known, the probabilities of olefin incorporation are known, and so the matrix maps with those values, and a simple X_{CO} mapping of the now reconciled incoming CO.

Note that this is only a logical correction if

$$X_{\mathrm{CO},s} = \sum_{k=2}^{n_{max}} \sum_{n=k}^{n_{max}} (n-k) \cdot y_{n,k} \cdot \left(\frac{P_{inc,k} \cdot \mathrm{C}_k\mathrm{H}_{2k_i}}{\mathrm{CO}_i} \right) < X_{\mathrm{CO}} \tag{33}$$

This imposes a constraint on the parenthetical term, violation of which implies either insufficient CO relative to the incoming olefins or an overstated probability of olefin adsorption.

I.6. Total Hydrocarbon Output

The total output of paraffins and olefins is a sum of primary and secondary synthesis subject to hydrogenation. As previously discussed, there is a great deal of varied research into the ratio of olefins to paraffins as a function of chain length, as well as to the explanations for these patterns. As a first approximation, the data from Schulz & Claeys [4] for the fractions of

olefins to paraffins, the probability of hydrogenation, and the probability of reinitiating chain growth are used, linearly interpolating the data for all chain lengths since that work produced fitted curves for chain lengths 2, 3, 5, 8, and 11. The correction factor derived immediately above can be quite large for high chain growth probabilities, but the data used to model the first iteration of this work demonstrated an α-value of 0.32, in which case the correction derived above is less than epsilon for chain lengths greater than 8. This is convenient since it is computationally more efficient to first study the behavior of a smaller range of hydrocarbons.

In summary, the total *production* of chemicals of carbon chain length *n* will come from primary synthesis of CO, secondary synthesis of adsorbed olefins, and non-reaction.

$$\mathrm{C}_n = \left(y_n \cdot \frac{X_{\mathrm{CO,P}}}{\Sigma_{ny}} \cdot \mathrm{CO}_i \right) + \left(\sum_{k=2}^{n} P_{inc,k} \cdot y_{n,k} \cdot C_{k_i} \right) + \left(\mathrm{C}_{n_i} \right) \tag{34}$$

It is important however to distinguish between paraffin output and olefin output; this distinction in applied to two ways. One is that a certain probability of incoming olefins of a given chain length will be hydrogenated. The other is that a certain fraction of primary and secondary synthesis products will be paraffin or olefin, and probability of being an olefin at chain length *n*, $P_{\mathrm{O},n}$, must be applied to the preceding equation:

$$\mathrm{C}_{n,O} = P_{O,n} \cdot \left(y_n \cdot \frac{X_{\mathrm{CO}}}{\Sigma_{ny}} \cdot \mathrm{CO}_i + \sum_{k=2}^{n} C_{k_{i,O}} \cdot P_{inc,k} \cdot y_{n,k} \right) + P_{NR,n} \cdot \mathrm{C}_{n_{i,O}} \tag{35}$$

where $P_{NR,n}$ is the probability of an incoming olefin not reacting. If we account for the probability of an incoming olefin hydrogenating to a paraffin, we have

$$P_{O,n} + P_{P,n} = 1$$

$$P_{inc,n} + P_{hyd,n} + P_{NR,n} = 1 \tag{36}$$

and outgoing paraffins are given by

$$\mathrm{C}_{n,P} = P_{P,n} \cdot \left(y_n \cdot \frac{X_{\mathrm{CO,P}}}{\Sigma_{ny}} \cdot \mathrm{CO}_i + \sum_{k=2}^{n} C_{k_{i,O}} \cdot P_{inc,k} \cdot y_{n,k} \right) + P_{hyd,n} \cdot \mathrm{C}_{n_{i,O}} + \mathrm{C}_{n_{i,P}} \tag{37}$$

For each carbon number, these equations conserve incoming olefins.

I.7. Hydrogen and CO Conservation

To balance the hydrogen coming in and out of the reactor is a matter of correcting incoming and outgoing H_2 and H_2O. The following stoichiometric relations hold, respectively, for primary synthesis of olefins, primary synthesis of paraffins, secondary hydrogenation of olefins, secondary synthesis of olefins and secondary synthesis of paraffins:

$$n\mathrm{CO} + 2n\mathrm{H}_2 \rightarrow \mathrm{C}_n\mathrm{H}_{2n} + n\mathrm{H}_2\mathrm{O} \tag{38}$$

$$n\mathrm{CO} + (2n+1)\mathrm{H}_2 \rightarrow \mathrm{C}_n\mathrm{H}_{2n+2} + n\mathrm{H}_2\mathrm{O} \tag{39}$$

$$\mathrm{C}_n\mathrm{H}_{2n} + \mathrm{H}_2 \rightarrow \mathrm{C}_n\mathrm{H}_{2n+2} \tag{40}$$

$$\mathrm{C}_k\mathrm{H}_{2k} + (n-k)\mathrm{CO} + 2(n-k)\mathrm{H}_2 \rightarrow \mathrm{C}_n\mathrm{H}_{2n} + (n-k)\mathrm{H}_2\mathrm{O} \tag{41}$$

$$\mathrm{C}_k\mathrm{H}_{2k} + (n-k)\mathrm{CO} + (2(n-k)+1)\mathrm{H}_2 \rightarrow \mathrm{C}_n\mathrm{H}_{2n+2} + (n-k)\mathrm{H}_2\mathrm{O} \tag{42}$$

The amount of H_2 output from the reactor is given by

Incoming hydrogen: H_{2_i}

Primary olefins: $-\sum_{n=1}^{n_{max}} 2n \cdot P_{\mathrm{O},n} \cdot \left(y_n \cdot \frac{X_{\mathrm{CO,P}}}{\Sigma_{ny}}\right) \cdot \mathrm{CO}_i$

Primary paraffins: $-\sum_{n=1}^{n_{max}} (2n+1) \cdot P_{\mathrm{P},n} \cdot \left(y_n \cdot \frac{X_{\mathrm{CO,P}}}{\Sigma_{ny}}\right) \cdot \mathrm{CO}_i$

Secondary hydrogenation: $-\sum_{n=1}^{n_{max}} P_{hyd,n} \cdot \mathrm{C}_n\mathrm{H}_{2n_i}$

Secondary olefins: $-\sum_{n=2}^{n_{max}} \sum_{k=2}^{n} 2(n-k) \cdot P_{\mathrm{O},n} \cdot \mathrm{C}_k\mathrm{H}_{2k_i} \cdot P_{inc,k} \cdot y_{n,k}$

Secondary paraffins: $-\sum_{n=2}^{n_{max}} \sum_{k=2}^{n} (2(n-k)+1) \cdot P_{\mathrm{P},n} \cdot \mathrm{C}_k\mathrm{H}_{2k_i} \cdot P_{inc,k} \cdot y_{n,k}$

$$= \mathrm{H}_2 \tag{43}$$

As per the preceding discussion of secondary synthesis adjustments, the moles of H_2 purported to be consumed by primary synthesis must be similarly adjusted by the same correction to X_{CO} described above, replacing

$$X_{\mathrm{CO,P}} \cdot \mathrm{CO}_i = X_{\mathrm{CO}} \cdot \mathrm{CO}_i - \sum_{n=2}^{n_{max}} \sum_{k=2}^{n} (n-k) \cdot \mathrm{C}_k\mathrm{H}_{2k_i} \cdot P_{inc,k} \cdot y_{n,k} \tag{44}$$

The production of H_2O follows simply and directly from the requirement that the reactor build hydrocarbons out of X_{CO} of the incoming CO, since that is the only source of oxygen in this reactor. The number moles of CO consumed is precisely the amount of water produced.

$$\mathrm{H}_2\mathrm{O} = X_{\mathrm{CO}} \cdot \mathrm{CO}_i + \mathrm{H}_2\mathrm{O}_i \tag{45}$$

All of the above derivations produce linear equations relating inputs to outputs, and these can be expressed in the form of a matrix that maps reactants to products based on the derived functions (all of which are subject to a positivity constraint).

$$FT_{matrix} \cdot \begin{bmatrix} \mathrm{CO} \\ \mathrm{CH_4} \\ \vdots \\ \mathrm{C_nH_{2n+2}} \\ \vdots \\ \mathrm{C_2H_4} \\ \vdots \\ \mathrm{C_nH_{2n}} \\ \vdots \\ \mathrm{CO_2} \\ \mathrm{H_2} \\ \mathrm{H_2O} \end{bmatrix}_{inputs} = \begin{bmatrix} \mathrm{CO} \\ \mathrm{CH_4} \\ \vdots \\ \mathrm{C_nH_{2n+2}} \\ \vdots \\ \mathrm{C_2H_4} \\ \vdots \\ \mathrm{C_nH_{2n}} \\ \vdots \\ \mathrm{CO_2} \\ \mathrm{H_2} \\ \mathrm{H_2O} \end{bmatrix}_{outputs}$$

$$\mathrm{CO} = f(\{\mathrm{CO}, \mathrm{H_2}, \mathrm{C_nH_{2n}}\}_i)$$

$$\mathrm{H_2} = g(\{\mathrm{CO}, \mathrm{H_2}, \mathrm{C_nH_{2n}}\}_i)$$

$$\mathrm{H_2O} = h(\{\mathrm{CO}, \mathrm{H_2}, \mathrm{H_2O}, \mathrm{C_nH_{2n}}\}_i)$$

$$\mathrm{C_nH_{2n}} = O(\{\mathrm{CO}, \mathrm{H_2}, \mathrm{C_nH_{2n}}\}_i)$$

$$\mathrm{C_nH_{2n+2}} = P(\{\mathrm{CO}, \mathrm{H_2}, \mathrm{C_nH_{2n}}, \mathrm{C_nH_{2n+2}}\}_i) \tag{46}$$

For concision, define

$$y_{n,k} = (1 - \alpha_n) \cdot \alpha_n^{n-k} \tag{47}$$

$$P_{y_{n,k}} = P_{inc,k} \cdot y_{n,k} \tag{48}$$

The CO relation can be shown more clearly as a linear combination of olefins as follows:

$$\sum_{n=2}^{n_{max}} \sum_{k=2}^{n} (n-k) \cdot \mathrm{C}_k\mathrm{H}_{2k_i} \cdot P_{y_{n,k}} \tag{49}$$

$$= \sum_{n=2}^{n_{max}} (n-2) \cdot \mathrm{C}_2\mathrm{H}_{4_i} \cdot P_{y_{n,2}} + (n-3) \cdot \mathrm{C}_3\mathrm{H}_{6_i} \cdot P_{y_{n,3}} + \cdots + (n-n_{max}) \cdot \mathrm{C}_{n_{max}}\mathrm{H}_{2n_{max}i} \cdot P_{y_{n,n_{max}}}$$

$$= 0$$

$$+1 \cdot \mathrm{C}_2\mathrm{H}_{4_i} \cdot P_{y_{3,2}}$$

$$+2 \cdot \mathrm{C}_2\mathrm{H}_{4_i} \cdot P_{y_{4,2}} + 1 \cdot \mathrm{C}_3\mathrm{H}_{6_i} \cdot P_{y_{4,3}}$$

$$+3 \cdot \mathrm{C}_2\mathrm{H}_{4_i} \cdot P_{y_{5,2}} + 2 \cdot \mathrm{C}_3\mathrm{H}_{6_i} \cdot P_{y_{5,3}} + 1 \cdot \mathrm{C}_4\mathrm{H}_{8_i} \cdot P_{y_{5,4}}$$

$$+4 \cdot \mathrm{C}_2\mathrm{H}_{4_i} \cdot P_{y_{6,2}} + 3 \cdot \mathrm{C}_3\mathrm{H}_{6_i} \cdot P_{y_{6,3}} + 2 \cdot \mathrm{C}_4\mathrm{H}_{8_i} \cdot P_{y_{6,4}} + 1 \cdot \mathrm{C}_5\mathrm{H}_{10_i} \cdot P_{y_{6,5}}$$

$$+ \cdots$$

$$= \left(\sum_{n=2}^{n_{max}} (n-2) \cdot P_{y_{n,2}} \right) \mathrm{C}_2\mathrm{H}_{4_i} + \left(\sum_{n=3}^{n_{max}} (n-3) \cdot P_{y_{n,2}} \right) \mathrm{C}_3\mathrm{H}_{6_i} + \left(\sum_{n=4}^{n_{max}} (n-4) \cdot P_{y_{n,2}} \right) \mathrm{C}_4\mathrm{H}_{8_i} + \cdots$$

A rough representation of the reactor matrix is therefore

$$\begin{bmatrix} \mathrm{CO} & \cdots & \mathrm{C}_k\mathrm{H}_{2k+2} & \cdots & \cdots & \mathrm{C}_k\mathrm{H}_{2k} & \cdots & \mathrm{H}_2 & \mathrm{H}_2\mathrm{O} \\ 1-X_{\mathrm{CO}} & 0 & 0 & 0 & \cdots & -\left(\sum_{n=2}^{n_{max}}(n-k)\cdot P_{y_{n,k}}\right) & \cdots & 0 & 0 \\ \vdots & \vdots & \vdots & \vdots & \cdots & \cdots & \cdots & \vdots & \vdots \\ P_{P,n}y_n\dfrac{X_{\mathrm{CO}}}{\Sigma_{ny}} & 0 & 1 & 0 & \cdots & P_{hyd,k}\delta_{nk}+P_{P,n}P_{inc,k}y_{n,k}\delta_{n\geq k} & \cdots & 0 & 0 \\ \vdots & \vdots & \vdots & \vdots & \cdots & \cdots & \cdots & \vdots & \vdots \\ \vdots & \vdots & \vdots & \vdots & \cdots & \cdots & \cdots & \vdots & \vdots \\ P_{O,n}y_n\dfrac{X_{\mathrm{CO}}}{\Sigma_{ny}} & \vdots & \vdots & \vdots & \cdots & P_{O,n}P_{inc,k}y_{n,k}\delta_{n\geq k}+P_{NR,n}\delta_{nk} & \cdots & 0 & 0 \\ \vdots & \vdots & \vdots & \vdots & \cdots & \cdots & \cdots & \vdots & \vdots \end{bmatrix} \quad (50)$$

II. Cracker Unit

The cracker is a unit that in a large-scale commercial Fischer-Tropsch facility would be external to primary production but which presently will be integrated into the production network itself. Generally, the purpose of the cracker is to give undesirable hydrocarbons another crack at synthesis into a specified product. Mathematically, the cracker maps an incoming chemical spectrum into a spectrum of lighter constituent parts. In detailed practice this process is a function of individual bond energies, but in the first iteration the reconcile will assign breakage probabilities to individual bonds based on the nature and size of the hydrocarbons comprising the incoming stream and the strength of those bonds, introducing biases for example towards the ends of a carbon chain. The output chemical flow is then fed into a separator that biases the new spectrum back to other units.

The rate constant for thermal cracking derived empirically by Voge and Good [16] for paraffins of chain length *n* was

$$k_n = (n-1) \cdot (1.57 \cdot n - 3.9) \cdot 10^{-5} \quad (51)$$

The relation bears out the industrial observation that heavier products, with their longer chains and greater number of bonds exposed to the conditions of the cracker, are more likely to be converted into lighter products. As a simplifying assumption for the modeled cracker, the probability of a given molecule cracking was assumed to be the same for all incoming molecules regardless of length. This is if anything a conservative assumption with respect to a network of reactors and crackers, in which the greater the ability to crack and re-grow, the greater opportunity there is for specificity of output. Rather than an analytical framework for the products of alkane cracking, empirical results from the literature were used, as described below.

Thermal cracking is assumed in the literature to follow the radical hypothesis of thermal decomposition, explained by Rice and Kossiakoff [17] , that chain reactions propagate in cycles that may be several hundred links long, and that the products of these propagation reactions dominate the products of initiation and termination if the cycles are long. For example, consider the thermal decomposition of ethane as described by Rice [18] with primary and secondary reactions

$$CH_3CH_3 \rightarrow 2\,\dot{C}H_3 \quad (52)$$

$$CH_3CH_3 + \dot{C}H_3 \rightarrow CH_4 + CH_3\dot{C}H_2 \quad (53)$$

$$CH_3\dot{C}H_2 \rightarrow CH_2 = CH_2 + \dot{H} \quad (54)$$

These are equivalent to

$$3\ CH_3CH_3 \ \rightarrow \ 2\ CH_4 + \ 2\ CH_2 = CH_2 + 2\ H \qquad (55)$$

Thus there is a 1:1 ratio of methane to hydrogen atoms resulting from primary and secondary decomposition. Meanwhile, the propagation reaction is

$$CH_3CH_3 + \mathbf{H} \ \rightarrow \ H_2 + CH_3\dot{C}H_2 \ \rightarrow \ H_2 + CH_2 = CH_2 + \mathbf{H} \qquad (56)$$

in which it is clear that the hydrogen atom is a carrier of the propagation, and each cycle produces one hydrogen molecule and one ethene, and therefore that the number of times this occurs per hydrogen atom primarily produced is therefore the number of cycles per decomposition, which is observed as the ratio of H_2 : CH_4 in the product distribution. If there are a great many cycles, the ratio of the concentrations of hydrogen to ethene produced should approach 1:1.

In general, elementary unimolecular thermal decomposition results from bond rupture into two free radical species; decomposition of large free radicals into unsaturated compounds, and a smaller free radical or hydrogen atom; and reactions between the free radicals and un-decomposed hydrocarbons [19]. These reaction chains become rapidly unwieldy at higher carbon numbers, and indeed even thorough modeling of the kinetics of ethane cracking alone can take 49 reactions into account, and 66 reactions for ethene [20], so appropriate simplifications were made to construct a cracker map that is reasonably true to real pyrolysis, and important complications specific to Fischer-Tropsch throughput are accounted for while enabling timely computational simulation. It is important to consider that [17], [21]

1. At low pressures and high temperatures, unimolecular decomposition is favored over bimolecular reactions, whereas the units simulated here will tend to have high pressures.

2. The activation energy for hydrogen scavenging of hydrocarbons by radicals decreases linearly with the number of parent carbons; long chains are more susceptible.
3. Resonance stabilizes carbons of olefin radicals as far as the β position to the double bond.
4. Scission of any radical most likely takes place at the β position to the radical.
5. The particular decomposition of radicals is not equally likely across multiple possibilities, but will be approximated as such here.
6. Although isomerization clearly plays an important role in the product distribution of thermal crackers, these simulations are limited to those paraffins and α-olefins permitted to react and form in the reactor units.

Simple comparisons of activation energies explain the observations that: [18]

1. C – C bonds are overwhelmingly more like to rupture than C = C or C – H.
2. Methyl radicals will scavenge an H atom, and are 5-10 times more likely to form CH_4 and a hydrocarbon radical than the reverse reaction.
3. Ethyl radicals will either scavenge an H atom and to form ethane and a hydrocarbon radical or decompose into ethene and an H atom.
4. Higher carbon radicals may either decompose into an alkene and a smaller radical or decompose into an alkene and an H atom.

Theoretically, if a higher carbon radical reacts with a hydrocarbon, that radical can decompose into an alkene and an H atom that will scavenge an H atom from the hydrocarbon to form H_2 and

a new hydrocarbon radical, or it can scavenge an H atom from the hydrocarbon to form an alkane and leave a new hydrocarbon radical:

$$C_nH^{\cdot}_{2n+1} + C_mH_{2m+2} \rightarrow C_nH_{2n} + C_mH^{\cdot}_{2m+1} + H_2 \quad (57)$$

$$C_nH^{\cdot}_{2n+1} + C_mH_{2m+2} \rightarrow C_nH_{2n+2} + C_mH^{\cdot}_{2m+1} \quad (58)$$

As per the above assumptions regarding the decomposition of radicals via β-scission to form an olefin and a smaller radical, however, the dominant behavior pursuant to the Rice-Herzfeld theory is that such scissioning takes place until there is no longer a C–C bond β to the double bond, and therefore unimolecular decomposition reactions do not appreciably produce any daughter paraffins longer than ethane, [22] an observation that is reflected in the thermal cracking map and which explains the relative reluctance of the simulated network to produce alkanes in favor of alkenes. This is not problematic with respect to output sharpening since simple hydrotreating can saturate the favored alkenes into desired alkanes.

The simultaneous occurrence of all of the thermal decomposition reactions described here clearly points to competition among hydrocarbons for available radicals, which one can read as mutual inhibition. Indeed, for example, the inhibiting effects of ethene and propene on the thermal decomposition of propane and the resulting reaction rates within the mechanism have been studied in detail, and this inhibition will be taken into account [23, 24]. As to the overlapping of individually studied decomposition pathways, cracking of mixtures has been studied as well [25-27], and the superposition of individual decompositions mapped sufficiently well to the mixture decompositions for those individual results to inform the cracker modeling of

this work. Notably, the effect of the mixtures is to increase the pressure on the system, and higher pressure results from the literature were the ones used here to construct the cracking map.

II.1. Mapping Alkane Cracking

Thermal decomposition of alkanes C_2-C_5 was thoroughly characterized by Rice [18]. Assuming long propagation chains as per the preceding discussion, and that C–H scission is dramatically more likely than C=C scission, ethane decomposition is assumed to be strictly

$$C_2H_6 \rightarrow C_2H_4 + H_2 \tag{59}$$

The decomposition of propane produces equal parts (CH_4 + H_2) and (CH_2=CH_2 + CH_3CH=CH_2), with the ratio of CH_4: H_2 and CH_2=CH_2: CH_3CH=CH_2 being roughly equal, mildly dependent on temperature and the relative rates of the two chain propagation mechanisms, and assumed here in each case to be 3:2: [18]

$$C_3H_8 \rightarrow 0.6\ (CH_4 + C_2H_4) + 0.4\ (C_3H_6 + H_2) \tag{60}$$

Similar mechanistic studies of butane decomposition explain the experimental results that lead to the model assumption used that

$$C_4H_{10} \rightarrow 0.56\ (CH_4 + C_3H_6) + 0.44\ (2\ C_2H_4 + H_2) \tag{61}$$

Pentane decomposition is assumed to follow [28, 29], with slight adjustments made to hydrogen and introducing a modest amount of propane in the reported results in order to precisely conserve mass:

$$C_5H_{12} \rightarrow 0.24\ H_2 + 0.45\ CH_4 + 0.67\ C_2H_4$$

$$+0.30\ C_2H_6 + 0.59\ C_3H_6 + 0.01\ C_3H_8 + 0.2025\ C_4H_8 \quad (62)$$

Predictably, these balances get more complicated, but the C_{6+} alkane decompositions were modeled from the same data and corrections as pentane. The assumed coefficients for the cracked products of the remaining alkanes appear tabulated below. These coefficients conform to the assumptions discussed above and are verified to conserve hydrogen and carbon.

	C_2H_6	C_3H_8	C_4H_{10}	C_5H_{12}	C_6H_{14}	C_7H_{16}	C_8H_{18}	C_9H_{20}	$C_{10}H_{22}$	$C_{11}H_{24}$	$C_{12}H_{26}$	$C_{13}H_{28}$	$C_{14}H_{30}$	$C_{15}H_{32}$	$C_{16}H_{34}$
	↓	↓	↓	↓	↓	↓	↓	↓	↓	↓	↓	↓	↓	↓	↓
H_2	1	0.40	0.44	0.24	0.24	0.24	0.24	0.24	0.24	0.31	0.46	0.46	0.52	0.79	0.89
CH_4	0	0.6	0.56	0.45	0.45	0.45	0.45	0.45	0.45	0.45	0.45	0.45	0.45	0.45	0.45
C_2H_6	0	0	0	0.3	0.3	0.3	0.3	0.3	0.3	0.3	0.3	0.3	0.3	0.3	0.3
C_3H_8	0	0	0	0.01	0.01	0.01	0.01	0.01	0.01	0.01	0.01	0.01	0.01	0.01	0.01
C_2H_4	1	0.60	0.88	0.67	1	1	1	1	1	1	1	1	1	1	1
C_3H_6	0	0.4	0.56	0.59	0.4	0.4	0.4	0.4	0.4	0.4	0.4	0.4	0.4	0.4	0.4
C_4H_8	0	0	0	0.2025	0.255	0.24	0.24	0.24	0.24	0.24	0.24	0.24	0.24	0.24	0.24
C_5H_{10}	0	0	0	0	0.14	0.192	0.192	0.192	0.192	0.192	0.192	0.192	0.192	0.192	0.192
C_6H_{12}	0	0	0	0	0	0.133	0.192	0.192	0.192	0.192	0.192	0.192	0.192	0.192	0.192
C_7H_{14}	0	0	0	0	0	0	0.0926	0.1536	0.1536	0.1536	0.1536	0.1536	0.1536	0.1536	0.1536
C_8H_{16}	0	0	0	0	0	0	0	0.0716	0.138	0.138	0.138	0.138	0.138	0.138	0.138
C_9H_{18}	0	0	0	0	0	0	0	0	0.0519	0.124	0.124	0.124	0.124	0.124	0.124
$C_{10}H_{20}$	0	0	0	0	0	0	0	0	0	0.035	0.112	0.112	0.112	0.112	0.112
$C_{11}H_{22}$	0	0	0	0	0	0	0	0	0	0	0.0207	0.0896	0.0896	0.0896	0.0896
$C_{12}H_{24}$	0	0	0	0	0	0	0	0	0	0	0	0.0202	0.0896	0.0896	0.0896
$C_{13}H_{26}$	0	0	0	0	0	0	0	0	0	0	0	0	0.0129	0.0717	0.0717
$C_{14}H_{28}$	0	0	0	0	0	0	0	0	0	0	0	0	0	0.0168	0.0717
$C_{15}H_{30}$	0	0	0	0	0	0	0	0	0	0	0	0	0	0	0.0155

Table 2: Default thermal cracking parameters

II.2. Mapping Alkene Cracking

Alkene cracking has two aspects to consider; one is that alkenes themselves participate in thermal decomposition reactions via transfers of hydrogen atoms and even oligomerization [20], and the other is that competitive inhibition of alkane cracking by alkenes has been reported [23, 24]. Both of these processes are best understood in terms of radical mechanisms, which is a complex field of modeling necessarily beyond the scope of this work. The model constructed here to simulate reactor networking does not purport to be a perfectly realistic representation of the Fischer-Tropsch process and subsequent cracking, but since networking and recycling effects clearly take advantage of the availability and adsorption of such building blocks as ethene in the reactor unit, it must in good faith also take into account the inhibiting effects of alkenes in the cracking unit.

To model the thermal decomposition of alkenes, it assumed that with some probability, an alkene will be rendered radical by the cracker via either scissioning of a single C–C bond or dehydrogenation as a precursor to subsequent oligomerization. Subsequent chain propagation reactions can shed carbon as well as agglomerate longer olefins. Since the feedstock for the thermal alkene cracking inherently contains hydrogen and carbon in a strictly 2:1 ratio, net hydrogen production could only accompany the production of alkynes, which while industrially evident is excluded from the present study which is restricted to alkanes and alkenes. Therefore, to reflect the production of methane and ethane which is industrially observed [30], some H_2 is consumed in the modeled alkene decomposition, the origins of which are assumed to be ambient hydrogen atoms produced from alkane decomposition and not from incoming H_2 left on the table

by the Fischer-Tropsch reactor. The inhibition of alkane decomposition by alkenes is reflected in the model by the presence of such alkene "cracking" reactions as

$$\mathrm{C}_n\mathrm{H}_{2n} + \mathrm{H}_2 \rightarrow \mathrm{C}_n\mathrm{H}_{2n+2} \tag{63}$$

$$\mathrm{C}_n\mathrm{H}_{2n} + \mathrm{CH}_4 \rightarrow \mathrm{C}_{n+1}\mathrm{H}_{2n+4} \tag{64}$$

which effectively reverses these same reactions that are simultaneously occurring as an alkane decompositions. (The rates of decomposition are low enough that it is unlikely to impossible to net-produce alkanes in the cracker, even though this reaction suggests that numerical possibility.) Consider the example of ethene, whose thermal inhibition behavior can be represented as:

$$\mathrm{C}_2\mathrm{H}_4 + \mathrm{H}_2 \rightarrow \mathrm{C}_2\mathrm{H}_6 \tag{65}$$

$$3\ \mathrm{C}_2\mathrm{H}_4 + 2\mathrm{H}_2 \rightarrow 2\ \mathrm{C}_3\mathrm{H}_8 \tag{66}$$

$$\vdots$$

$$k\ \mathrm{C}_2\mathrm{H}_4 + 2\mathrm{H}_2 \rightarrow 2\ \mathrm{C}_k\mathrm{H}_{2k+2} \tag{67}$$

$$\mathrm{C}_2\mathrm{H}_4 + \mathrm{CH}_4 \rightarrow \mathrm{C}_3\mathrm{H}_8 \tag{68}$$

$$\vdots$$

$$k\ \mathrm{C}_2\mathrm{H}_4 + \mathrm{CH}_4 \rightarrow \mathrm{C}_{2k+1}\mathrm{H}_{4k+4} \tag{69}$$

Similarly, propene inhibition can be represented as

$$k\ \mathrm{C}_3\mathrm{H}_6 + 3\mathrm{H}_2 \rightarrow 3\ \mathrm{C}_k\mathrm{H}_{2k+2} \tag{70}$$

$$k\ \mathrm{C}_3\mathrm{H}_6 + \mathrm{CH}_4 \rightarrow \mathrm{C}_{3k+1}\mathrm{H}_{6k+4} \tag{71}$$

Although it appears to be a dramatic consumption of H_2, note that in each possibility there is only one H_2 or CH_4 consumed per alkane produced, as was the case for the implied alkane decomposition being inhibited. Inhibition reactions aside, the thermal decomposition of alkenes in the cracker unit assumes the following possibilities for the cracking of one or more C_nH_{2n} compounds into two pieces of carbon lengths *x* and *y*:

$$x + y = n \tag{72}$$

$$\mathrm{C}_n\mathrm{H}_{2n} \rightarrow \mathrm{C}_x\mathrm{H}_{2x} + \mathrm{C}_y\mathrm{H}_{2y} \tag{73}$$

$$2\ \mathrm{C_nH_{2n}} \rightarrow 2\ \mathrm{C_xH_{2x}} + \mathrm{C_{2y}H_{4y}} \tag{74}$$

$$2\ \mathrm{C_nH_{2n}} \rightarrow \mathrm{C_{2x}H_{4x}} + 2\ \mathrm{C_yH_{2y}} \tag{75}$$

$$2\ \mathrm{C_nH_{2n}} \rightarrow \mathrm{C_{2x}H_{4x}} + \mathrm{C_{2y}H_{4y}} \tag{76}$$

$$2\ \mathrm{C}_n\mathrm{H}_{2n} \rightarrow \mathrm{C}_x\mathrm{H}_{2x} + \mathrm{C}_{n+y}\mathrm{H}_{2n+2y} \tag{77}$$

$$2\ \mathrm{C}_n\mathrm{H}_{2n} \rightarrow \mathrm{C}_{n+x}\mathrm{H}_{2n+2x} + \mathrm{C}_y\mathrm{H}_y \tag{78}$$

$$2\ \mathrm{C}_n\mathrm{H}_{2n} \rightarrow \mathrm{C}_{2n}\mathrm{H}_{4n} \tag{79}$$

$$\mathrm{C}_n\mathrm{H}_{2n} + \mathrm{H}_2 \rightarrow \mathrm{C}_{n-1}\mathrm{H}_{2n-2} + \mathrm{CH}_4 \tag{80}$$

$$\mathrm{C}_n\mathrm{H}_{2n} + \mathrm{CH}_4 \rightarrow \mathrm{C}_{n+1}\mathrm{H}_{2n+2} + \mathrm{H}_2 \tag{81}$$

III. References

1. Van der Laan, G.P. and A. Beenackers, *Kinetics and selectivity of the Fischer-Tropsch synthesis: A literature review.* Catalysis Reviews-Science and Engineering, 1999. **41**(3-4): p. 255-318.

2. Botes, F.G., *Proposal of a new product characterization model for the iron-based low-temperature Fischer-Tropsch synthesis.* Energy & Fuels, 2007. **21**(3): p. 1379-1389.

3. de Klerk, A., *Thermal cracking of Fischer-Tropsch waxes.* Industrial & Engineering Chemistry Research, 2007. **46**(17): p. 5516-5521.

4. Schulz, H. and M. Claeys, *Reactions of alpha-olefins of different chain length added during Fischer-Tropsch synthesis on a cobalt catalyst in a slurry reactor.* Applied Catalysis a-General, 1999. **186**(1-2): p. 71-90.

5. van der Laan, G.P. and A.A.C.M. Beenackers, *alpha-Olefin readsorption product distribution model for the gas-solid Fischer-Tropsch synthesis.* Natural Gas Conversion V, 1998. **119**: p. 179-184.

6. Shi, B.C. and B.H. Davis, *Fischer-Tropsch synthesis: The paraffin to olefin ratio as a function of carbon number.* Catalysis Today, 2005. **106**(1-4): p. 129-131.

7. James, O.O., et al., *Reflections on the chemistry of the Fischer-Tropsch synthesis.* Rsc Advances, 2012. **2**(19): p. 7347-7366.

8. Van der Laan, G.P., *Kinetics, selectivity and scale up of the Fischer-Tropsch synthesis.* 1999, University of Groningen: Groningen, The Netherlands.

9. Aaserud, C., et al., *Hydrogenation of propene on cobalt Fischer-Tropsch catalysts.* Catalysis Letters, 2004. **94**(3-4): p. 171-176.

10. Iglesia, E., S.C. Reyes, and R.J. Madon, *TRANSPORT-ENHANCED ALPHA-OLEFIN READSORPTION PATHWAYS IN RU-CATALYZED HYDROCARBON SYNTHESIS.* Journal of Catalysis, 1991. **129**(1): p. 238-256.

11. Schulz, H., B.R. Rao, and M. Elstner, *C-14-STUDIES FOR EVALUATION OF REACTION MECHANISM OF FISCHER-TROPSCH SYNTHESIS.* Erdol Und Kohle Erdgas Petrochemie Vereinigt Mit Brennstoff-Chemie, 1970. **23**(10): p. 651-&.

12. Snel, R. and R.L. Espinoza, *SECONDARY REACTIONS OF PRIMARY PRODUCTS OF THE FISCHER-TROPSCH SYNTHESIS .1. THE ROLE OF ETHENE.* Journal of Molecular Catalysis, 1987. **43**(2): p. 237-247.

13. Boelee, J.H., J.M.G. Custers, and K. Vanderwiele, *INFLUENCE OF REACTION CONDITIONS ON THE EFFECT OF CO-FEEDING ETHENE IN THE FISCHER-TROPSCH SYNTHESIS ON A FUSED-IRON CATALYST IN THE LIQUID-PHASE.* Applied Catalysis, 1989. **53**(1): p. 1-13.

14. Iglesia, E., Advances in catalysis, 1993. **39**: p. 345.

15. Kuipers, E.W., I.H. Vinkenburg, and H. Oosterbeek, *CHAIN-LENGTH DEPENDENCE OF ALPHA-OLEFIN READSORPTION IN FISCHER-TROPSCH SYNTHESIS.* Journal of Catalysis, 1995. **152**(1): p. 137-146.

16. Voge, H.H. and G.M. Good, *THERMAL CRACKING OF HIGHER PARAFFINS.* Journal of the American Chemical Society, 1949. **71**(2): p. 593-597.

17. Kossiakoff, A. and F.O. Rice, *Thermal decomposition of hydrocarbons, resonance stabilization and isomerization of free radicals.* Journal of the American Chemical Society, 1943. **65**: p. 590-595.

18. Rice, F.O., *The thermal decomposition of organic compounds from the standpoint of free radicals. I. Saturated hydrocarbons.* Journal of the American Chemical Society, 1931. **53**(2): p. 1959-1972.

19. Rice, F.O. and W.R. Johnston, *The thermal decomposition of organic compounds from the standpoint of free radicals V The strength of bonds in organic molecules.* Journal of the American Chemical Society, 1934. **56**: p. 214-219.

20. Sundaram, K.M. and G.F. Froment, *MODELING OF THERMAL-CRACKING KINETICS .3. RADICAL MECHANISMS FOR PYROLYSIS OF SIMPLE PARAFFINS, OLEFINS, AND THEIR MIXTURES.* Industrial & Engineering Chemistry Fundamentals, 1978. **17**(3): p. 174-182.

21. de Klerk, A., *Fischer-Tropsch fuels refinery design.* Energy & Environmental Science, 2011. **4**(4): p. 1177-1205.

22. Safarik, I. and O.P. Strausz, *The thermal decomposition of hydrocarbons .1. n-alkanes (C>=5).* Research on Chemical Intermediates, 1996. **22**(3): p. 275-314.

23. Dombi, A. and P. Huhn, *EFFECTS OF OLEFINS ON THE THERMAL-DECOMPOSITION OF PROPANE .4. INFLUENCE OF PROPYLENE.* International Journal of Chemical Kinetics, 1986. **18**(3): p. 301-312.

24. Dombi, A. and P. Huhn, *EFFECTS OF OLEFINS ON THE THERMAL-DECOMPOSITION OF PROPANE .2. INFLUENCE OF ETHYLENE.* Magyar Kemiai Folyoirat, 1985. **91**(1): p. 27-31.

25. Froment, G.F., et al., *THERMAL-CRACKING OF ETHANE AND ETHANE-PROPANE MIXTURES.* Industrial & Engineering Chemistry Process Design and Development, 1976. **15**(4): p. 495-504.

26. Froment, G.F., B.O. Vandesteene, and A.G. Goossens, *THERMAL-CRACKING OF HYDROCARBON MIXTURES.* Abstracts of Papers of the American Chemical Society, 1976. **172**(SEP3): p. 70-70.

27. Froment, G.F., et al., *THERMAL-CRACKING OF LIGHT-HYDROCARBONS AND THEIR MIXTURES.* Aiche Journal, 1977. **23**(1): p. 93-106.

28. Ranzi, E., et al., *INITIAL PRODUCT DISTRIBUTIONS FROM PYROLYSIS OF NORMAL AND BRANCHED PARAFFINS.* Industrial & Engineering Chemistry Fundamentals, 1983. **22**(1): p. 132-139.

29. Arai, Y., et al., *SIMULATION OF PRODUCT DISTRIBUTIONS FROM PYROLYSIS OF NORMAL AND BRANCHED ALKANE MIXTURES OVER A WIDE-RANGE OF CONVERSIONS.* Journal of Chemical Engineering of Japan, 1977. **10**(4): p. 303-307.

30. Belohlav, Z., P. Zamostny, and T. Herink, *The kinetic model of thermal cracking for olefins production.* Chemical Engineering and Processing, 2003. **42**(6): p. 461-473.

Chapter 5

Configurations of Simple Separators for Greater Spectrum Sharpening

The Gaussian separator produces biased but imperfect separation, and a crucial aspect of networked reactor systems is the ability to preferentially direct and re-direct chemical traffic. The more rigorous the separation selectivity of the system, the more efficiently the throughputs can be delivered to where they belong. Just as reactors and crackers can be judiciously networked, can unremarkable separators be networked to produce remarkably precise separation?

I. A Linear Separator Network

One possible arrangement of crude Gaussian separators that was studied is the linear network, in which each set of separators performs some sort of sharpening of a distribution, and that distribution is passed on to the next set. The system is initiated by a single merging unit that directs streams into a simple Gaussian separator, which outputs the "preferred" central peak of the distribution to one side, and the remainder to the other side. These streams are each then fed into another simple Gaussian separator. Any stream from the preferred or "good" side that

emerges from the "good" central peak of the second separator as well is considered doubly good, or "GG" in the diagram, as it has been twice sharpened. Anything emerging from the second separator on the "bad" side is similarly doubly bad or "BB" in the diagram. The remaining streams, which were outside the peak on the preferred side and inside the peak on the disfavored side are "GB" and "BG" respectively, and these are fed back up to the original input merger.

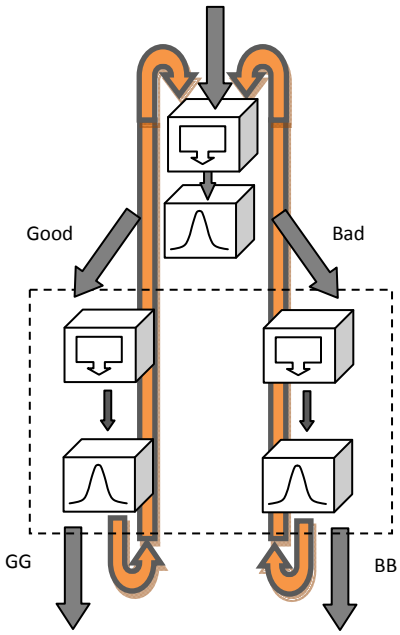

Figure 5.1: An assembly of Gaussian separators

Such a scheme can be propagated forward in an expanding linear network of separators, with each stream that survives a level of separation is more pure (or more filtered as impure) than it was the level before, and any middling outputs are sent back up to be re-filtered. Theoretically, a "bad" molecule on the good side is filtered out by being sent back up to the unit above repeatedly until it is filtered out through the bad side. To analyze such a linear cascade with recycling, first consider a configuration in which all of the recycle loops from subsequent pairs of left and right

separators are directed all the way to the front end instead of to the previous subassembly. Let G_i be the fraction of chemical *n* that emerges from a linear assembly of *n* consecutive pairs of units *following the first single unit*, each of which recycle the rejected fraction outside of the Gaussian to the front of the chain. Let x_i be the sum of the recycled fractions of component *i* from the left and right units in the array. Thus the top unit has an incoming flow of $1 + x_i$ of chemical component *i*, and if ε_i is fraction of component *i* that survives each Gaussian, then the top unit transmits $(1 + x_i)\varepsilon_i$to the left separator of the first assembly and $(1 + x_i)(1 - \varepsilon_i)$ to the right separator.

	Left separators		Right separators	
	Pure fraction	Recycled fraction	Recycled fraction	Impure fraction
Unit *n* = 1 produces:	$(1 + x_i)\varepsilon_i^2$	$(1 + x_i)\varepsilon_i(1 - \varepsilon_i)$	$(1 + x_i)(1 - \varepsilon_i)\varepsilon_i$	$(1 + x_i)(1 - \varepsilon_i)^2$
Unit *n* = 2 produces:	$(1 + x_i)\varepsilon_i^3$	$(1 + x_i)\varepsilon_i^2(1 - \varepsilon_i)$	$(1 + x_i)(1 - \varepsilon_i)^2\varepsilon_i$	$(1 + x_i)(1 - \varepsilon_i)^3$
Unit *n* = 3 produces:	$(1 + x_i)\varepsilon_i^4$	$(1 + x_i)\varepsilon_i^3(1 - \varepsilon_i)$	$(1 + x_i)(1 - \varepsilon_i)^3\varepsilon_i$	$(1 + x_i)(1 - \varepsilon_i)^4$
Unit *n* produces:	$(1 + x_i)\varepsilon_i^{n+1}$	$(1 + x_i)\varepsilon_i^n(1 - \varepsilon_i)$	$(1 + x_i)(1 - \varepsilon_i)^n\varepsilon_i$	$(1 + x_i)(1 - \varepsilon_i)^{n+1}$

Table 5.1: Purities of a linear separator network

Some conservation laws must be satisfied by these relations. Since the recycling was internal and only unit quantities of each component entered the assembly, the pure and impure fractions emerging the separators must obey

$$1 = (1 + x_i) \cdot \varepsilon_i^{n+1} + (1 + x_i) \cdot (1 - \varepsilon_i)^{n+1} = (1 + x_i) \cdot [\varepsilon_i^{n+1} + (1 - \varepsilon_i)^{n+1}]$$

$$x_i = \frac{1}{\varepsilon_i^{n+1} + (1-\varepsilon_i)^{n+1}} - 1 \tag{1}$$

The sum of the recycled fractions x_i returning to the top separator from the left separators is a geometric series

$$x_{i_{\text{left}}} = (1+x_i)\cdot\varepsilon_i\cdot(1-\varepsilon_i) + (1+x_i)\cdot\varepsilon_i^2\cdot(1-\varepsilon_i) + \cdots + (1+x_i)\cdot\varepsilon_i^n\cdot(1-\varepsilon_i)$$

$$x_{i_{\text{left}}} = \frac{(1+x_i)\cdot\varepsilon_i\cdot(1-\varepsilon_i)}{1-\varepsilon_i}(1-\varepsilon_i^n) \tag{2}$$

while the fraction returning from the right is similarly

$$x_{i_{\text{right}}} = (1+x_i)\cdot\varepsilon_i\cdot(1-\varepsilon_i) + (1+x_i)\cdot\varepsilon_i\cdot(1-\varepsilon_i)^2 + \cdots + (1+x_i)\cdot\varepsilon_i\cdot(1-\varepsilon_i)^n$$

$$x_{i_{\text{right}}} = \frac{(1+x_i)\cdot\varepsilon_i\cdot(1-\varepsilon_i)}{1-(1-\varepsilon_i)}[1-(1-\varepsilon_i)^n] \tag{3}$$

which must satisfy

$$x_i = x_{i_{\text{left}}} + x_{i_{\text{right}}} = \frac{(1+x_i)\cdot\varepsilon_i\cdot(1-\varepsilon_i)}{1-\varepsilon_i}(1-\varepsilon_i^n) + \frac{(1+x_i)\cdot\varepsilon_i\cdot(1-\varepsilon_i)}{1-(1-\varepsilon_i)}[1-(1-\varepsilon_i)^n]$$

$$x_i = (1+x_i)\cdot\varepsilon_i\cdot(1-\varepsilon_i)\cdot\left[\frac{1-\varepsilon_i^n}{1-\varepsilon_i} + \frac{1-(1-\varepsilon_i)^n}{1-(1-\varepsilon_i)}\right] \tag{4}$$

If all has gone well, the previously solved expression for $x_i(\varepsilon_i, n)$ satisfies this relationship, and indeed it does:

$$\frac{1}{\varepsilon_i^{n+1} + (1-\varepsilon_i)^{n+1}} - 1 \quad =? \quad \left(\cancel{1} + \frac{1}{\varepsilon_i^{n+1} + (1-\varepsilon_i)^{n+1}} - \cancel{1}\right)\cdot\varepsilon_i\cdot(1-\varepsilon_i)\cdot\left[\frac{1-\varepsilon_i^n}{1-\varepsilon_i} + \frac{1-(1-\varepsilon_i)^n}{1-(1-\varepsilon_i)}\right]$$

$$\frac{1-(\varepsilon_i^{n+1} + (1-\varepsilon_i)^{n+1})}{\cancel{\varepsilon_i^{n+1} + (1-\varepsilon_i)^{n+1}}} \quad =? \quad \left(\frac{1}{\cancel{\varepsilon_i^{n+1} + (1-\varepsilon_i)^{n+1}}}\right)\cdot\varepsilon_i\cdot(1-\varepsilon_i)\cdot\left[\frac{1-\varepsilon_i^n}{1-\varepsilon_i} + \frac{1-(1-\varepsilon_i)^n}{\varepsilon_i}\right]$$

$$1-(\varepsilon_i^{n+1} + (1-\varepsilon_i)^{n+1}) \quad =? \quad \varepsilon_i\cdot(1-\varepsilon_i)\cdot\left[\frac{1-\varepsilon_i^n}{1-\varepsilon_i} + \frac{1-(1-\varepsilon_i)^n}{\varepsilon_i}\right]$$

$$1-\varepsilon_i^{n+1}-(1-\varepsilon_i)^{n+1} \stackrel{?}{=} \varepsilon_i\cdot(1-\varepsilon_i^n)+(1-\varepsilon_i)\cdot(1-(1-\varepsilon_i)^n)$$

$$1-\varepsilon_i^{n+1}-(1-\varepsilon_i)^{n+1} \stackrel{?}{=} \varepsilon_i-\varepsilon_i^{n+1}+1-\varepsilon_i-(1-\varepsilon_i)^n+\varepsilon_i(1-\varepsilon_i)^n$$

$$-(1-\varepsilon_i)^{n+1} \stackrel{?}{=} -(1-\varepsilon_i)^n+\varepsilon_i(1-\varepsilon_i)^n$$

$$-(1-\varepsilon_i)^{n+1} \stackrel{?}{=} (-1+\varepsilon_i)\cdot(1-\varepsilon_i)^n$$

$$-(1-\varepsilon_i)^{n+1} \stackrel{?}{=} -(1-\varepsilon_i)\cdot(1-\varepsilon_i)^n$$

$$-(1-\varepsilon_i)^{n+1} = -(1-\varepsilon_i)^{n+1} \tag{5}$$

Thus the linear chain of separators recycles $x_i(\varepsilon_i,n)$ to produce a pure fraction $(1+x_i)\varepsilon_i^{n+1}$ according to

$$\mathrm{G}_i(\varepsilon,n)=(1+x_i)\cdot\varepsilon_i^{n+1}=\left(1+\frac{1}{\varepsilon_i^{n+1}+(1-\varepsilon_i)^{n+1}}-1\right)\varepsilon_i^{n+1}$$

$$\mathrm{G}_i(\varepsilon,n)=(1+x_i)\cdot\varepsilon_i^{n+1}=\frac{\varepsilon_i^{n+1}}{\varepsilon_i^{n+1}+(1-\varepsilon_i)^{n+1}}$$

$$\mathrm{G}_i(\varepsilon,n)=(1+x_i)\cdot\varepsilon_i^{n+1}=\frac{1}{1+\left(\frac{1}{\varepsilon_i}-1\right)^{n+1}} \tag{6}$$

What happens in the infinite limit, in which a very large number of such paired separators are consecutively linked in a chain? By assumption,

$$0<\varepsilon_i<1$$

$$1<\frac{1}{\varepsilon_i}<\infty$$

$$0<\left(\frac{1}{\varepsilon_i}-1\right)<\infty \tag{7}$$

Therefore

$$\lim_{n\to\infty} G_i(\varepsilon, n) = \lim_{n\to\infty} \frac{1}{1+\left(\frac{1}{\varepsilon_i}-1\right)^{n+1}} = \begin{cases} 1 & \text{if} \quad 0 < \left(\frac{1}{\varepsilon_i}-1\right) < 1 \\ 0 & \text{if} \quad 1 < \left(\frac{1}{\varepsilon_i}-1\right) < \infty \end{cases} \tag{8}$$

For a chemical component to be guaranteed to emerge from the pure fraction in the infinite limit, its Gaussian peak probability must satisfy

$$\left(\frac{1}{\varepsilon_i}-1\right) < 1$$

$$\frac{1}{\varepsilon_i} < 2$$

$$\varepsilon_i > \frac{1}{2} \tag{9}$$

Likewise, in the infinite limit, any chemical with a Gaussian probability of less than ½ emerges only from the impure fraction, and any chemical whose probability equals ½ will be equally divided between the outgoing ports.

This is a difficult space in which to operate if the base separator units are not siphoning off more than half of an impure chemical in a single pass-through, but it does not strain belief to assume that even an unremarkable separator unit or subassembly of units would be able to extract more than half of a desired chemical of a certain mass.

Now consider the more complex configuration described above in which the throughput is looped to the previous subassembly instead of all the way back to the front of the network:

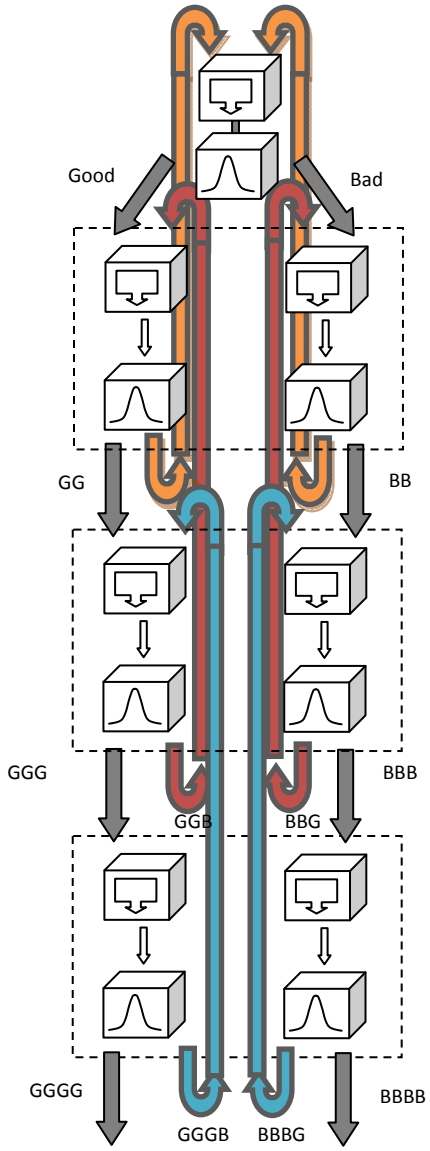

Figure 5.2: A linear assembly of Gaussian separators

Let n represent the subassemblies *after* the first separator, let $\{L_1, L_2, L_3, \ldots L_n \ldots L_N\}$ represent the recycled loops on the left hand side, and let $\{R_1, R_2, R_3, \ldots R_n \ldots R_N\}$ represent the recycled loops on the right hand side. For example, L_3 recycles the rejected chemicals from the left-hand

separator of the third subassembly which are re-fed into the left-hand separator of the second subassembly.

The very top separator is separating an incoming stream made up of the initial amount of a given chemical taken to be unity, the amount of that chemical looped up from the first left-hand separator recycle L_1, and the amount recycled up from the first right-hand separator recycle R_1. That amount, $(1 + L_1 + R_1)$, passes through the left-hand "good" side with probability ε, so of that original amount, $(1 + L_1 + R_1) \cdot \varepsilon$ enters the left separator of the first subassembly. Recycled amount L_2 from the second subassembly just underneath is also fed into the first subassembly, which therefore receives a total left-side input of $(1 + L_1 + R_1) \cdot \varepsilon + L_2$ the proportion of this, L_1, that is looped back to the very top separator is $(1 - \varepsilon)$, and so is

$$\big((1 + L_1 + R_1) \cdot \varepsilon + L_2\big) \cdot (1 - \varepsilon) = L_1 \tag{10}$$

For the subsequent left-hand separators, consider that unit $n = 2$ receives two inputs, the recycle from the unit $n = 3$, L_3, and the "good" output from $n = 1$. Now if the "bad" output from $n = 1$ was L_1, then the total output from $n = 1$ was $\frac{L_1}{1-\varepsilon}$, and the fraction of that output as "good" into the $n = 2$ unit was $\frac{L_1}{1-\varepsilon} \cdot \varepsilon$. Thus the total input into $n = 2$ is $\frac{L_1}{1-\varepsilon} \cdot \varepsilon + L_3$, of which the "bad" fraction is recycled up as L_2 and we have the relation

$$\left(\frac{L_1}{1-\varepsilon} \cdot \varepsilon + L_3\right) \cdot (1 - \varepsilon) = L_2$$

$$L_1 \cdot \varepsilon + L_3 \cdot (1 - \varepsilon) = L_2 \tag{11}$$

The preceding analysis holds for subsequent units, leading to the generalization

$$L_{n-1} \cdot \varepsilon + L_{n+1} \cdot (1 - \varepsilon) = L_n \tag{12}$$

The final N^{th} unit does not receive a recycle loop from below, i.e. $L_{N+1} = 0$, and so

$$L_{N-1} \cdot \varepsilon = L_N \tag{13}$$

If G_N is the amount emerging from the final N^{th} unit while L_N is recycled from it, then the total output was $\frac{L_N}{1-\varepsilon}$ and ε of that was considered "good", so

$$\frac{L_N}{1-\varepsilon} \cdot \varepsilon = G_N \tag{14}$$

The system of equations for the left-hand separators is therefore

$$\big((1 + L_1 + R_1) \cdot \varepsilon + L_2\big) \cdot (1 - \varepsilon) = L_1$$

$$L_{n-1} \cdot \varepsilon + L_{n+1} \cdot (1 - \varepsilon) = L_n$$

$$(N - 2 \text{ equations for } 2 \le n \le N - 1)$$

$$L_{N-1} \cdot \varepsilon = L_N$$

$$\frac{L_N}{1-\varepsilon} \cdot \varepsilon = G_N \tag{15}$$

The same analysis holds for the right-hand-side separators, only the ε and $(\varepsilon - 1)$ terms are interchanged:

$$\big((1 + L_1 + R_1) \cdot (1 - \varepsilon) + R_2\big) \cdot \varepsilon = R_1$$

$$R_{n-1} \cdot (1 - \varepsilon) + R_{n+1} \cdot \varepsilon = R_n$$

$$(N - 2 \text{ equations for } 2 \le n \le N - 1)$$

$$R_{N-1} \cdot (1 - \varepsilon) = R_N$$

$$\frac{R_N}{\varepsilon} \cdot (1 - \varepsilon) = B_N \tag{16}$$

There are $2 \times \{1 + (N - 2) + 1 + 1\} = 2N + 2$ equations in this system for the $2N + 2$ variables $\{L_1, L_2, L_3, \ldots L_n \ldots L_N\}$, $\{R_1, R_2, R_3, \ldots R_n \ldots R_N\}$, G_N, and B_N. While these would be a cumbersome analytical system to solve, it is well-suited to numerical solution by constructing

matrices according to these equations for various values of N, i.e. for various numbers of linearly configured subassemblies. These simulations demonstrated however that recycling backwards one subassembly at a time produced precisely the same output spectra that were produced when all of these loops were recycled to the front-end separator as derived previously; there is no advantage in this case to intermediate recycle that can be observed in the output chemical spectrum. The results are graphed for various subassembly chain lengths.

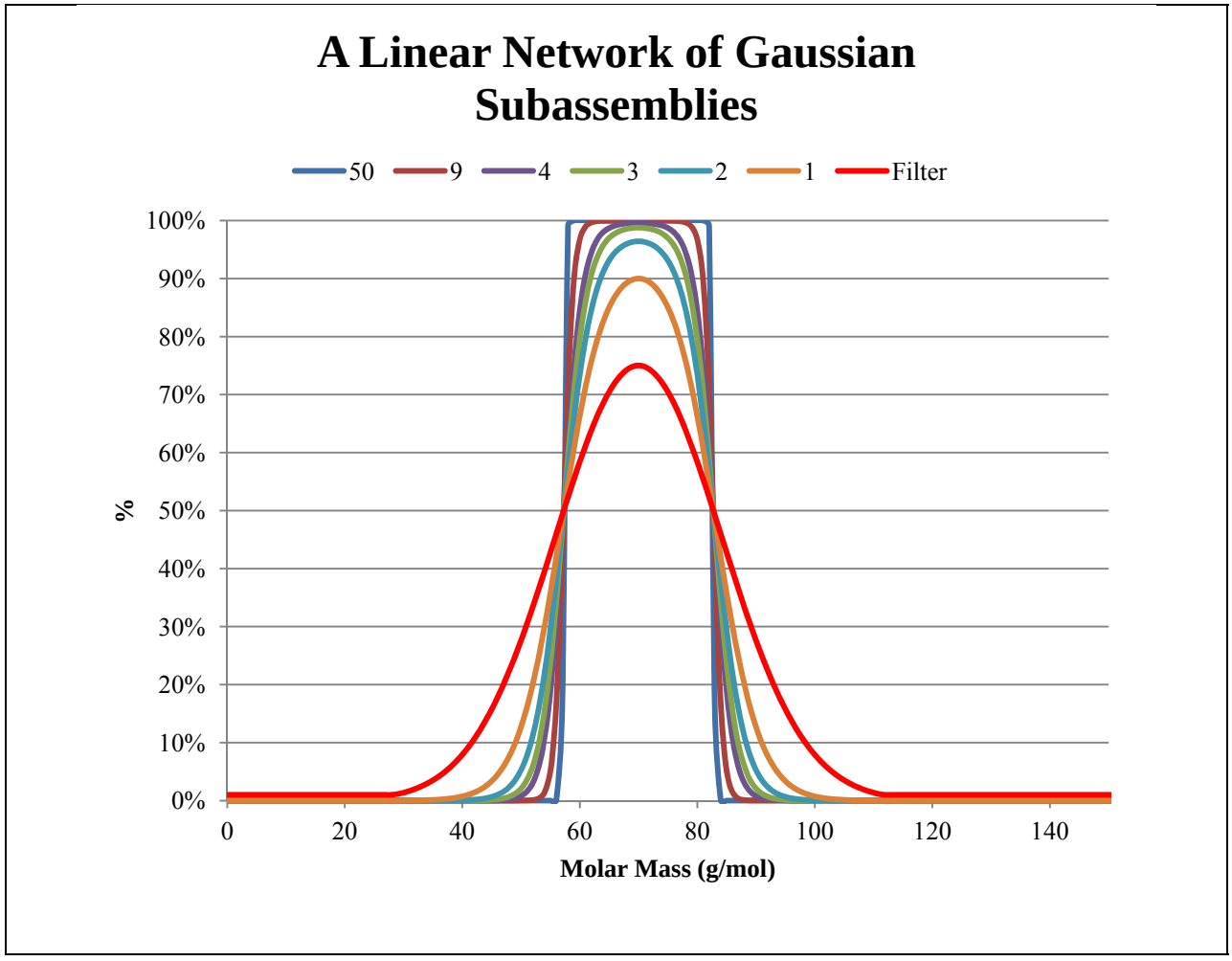

Figure 5.3: Simulations of a linear assembly of Gaussian separators

As the graph makes clear, the linear chain of subassemblies produces a sharpening that pivots about the point on either side of the Gaussian peak at which the probability of being filtered through either outgoing port is 50%. As the number of separators increases, the shape of the chemical spectrum approaches a "delta" function that selects perfectly for all chemicals of a mass within that range and 0% for those outside of it. To construct a configuration that would function as a delta separator, one would need to ensure that the probability of chemicals within a monomer of the desired mass pass through just below the critical threshold of 50%. Alkanes and alkenes are within far less than that for a given chain length, but alkenes are much more readily selected for under the reactor maps used here, and can be readily hydrocracked into saturated chains if need be.

II. A Fractal Network

Another way to frame a network of simple, unremarkable Gaussian separators which combine to produce a sharper spectrum than the individual units ever could we be to lay out a self-similar network. The basic subassembly of such a network would contain three simple separators and two mergers in a recycle scheme similar to that studied above, in which the rejected stream from the second run at the central peak filter is merged with the central peak filter of the rejected stream ("good-bad" and "bad-good") and recycled back to the front of the subassembly as per the diagram below.

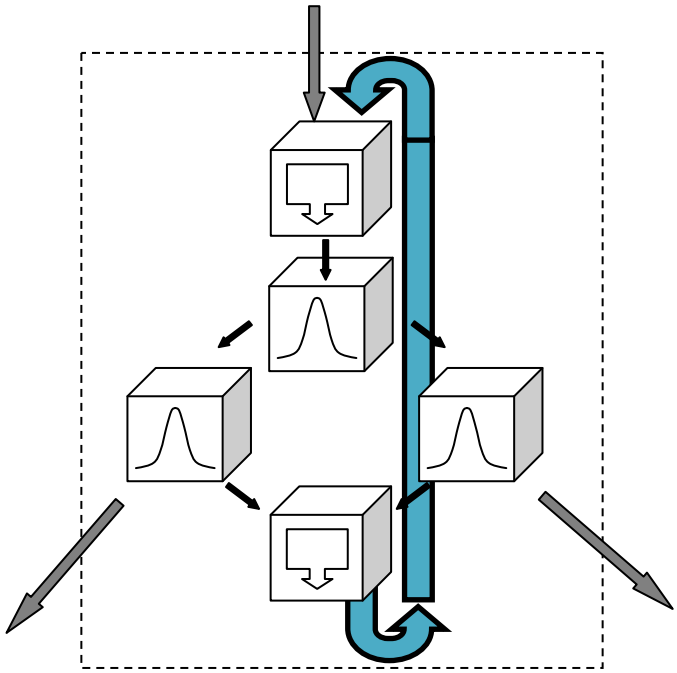

Figure 5.4: A sample Flowsheet Block of a self-similar Gaussian assembly

In essence, therefore, this subunit can be networked as if were itself a simple separator, with one input stream being filtered into one output emphasizing those chemicals favored by the central peak of the Gaussian, and the other output stream emphasizing those chemicals outside of the central peak. Since this subassembly itself has the port behavior of a simple separator, it can replace a simple separator in a configuration just like this one, with separators within separators. This self-similar network can be repeated if each separator is replaced with a subassembly of separators as described here. The array of course becomes rapidly numerous, since one level deep would contain 9 separators, and if each of those were replaced with a subassembly to create a third level then there would be 27 separators.

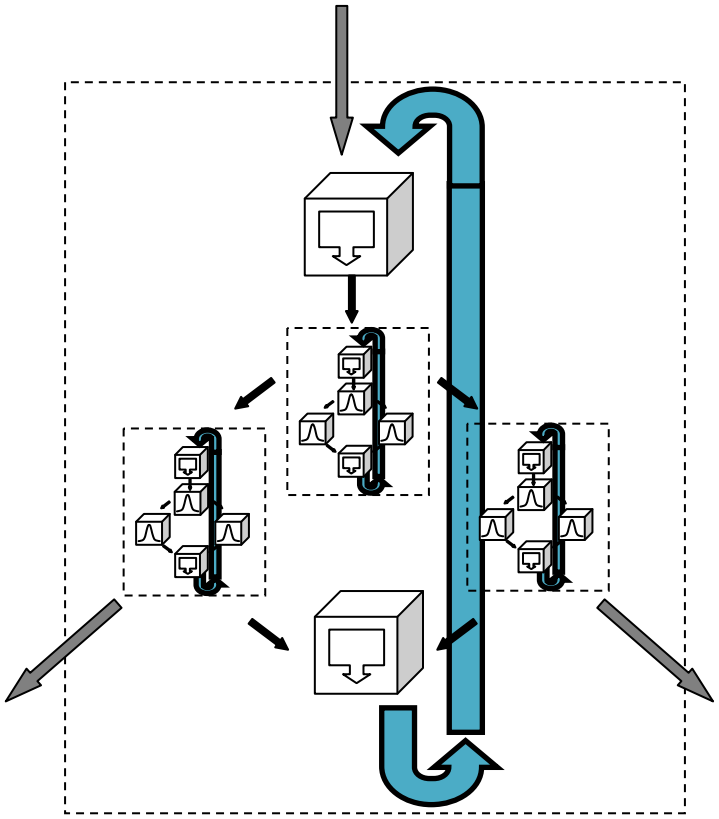

Figure 5.5: A sample Flowsheet of a self-similar Gaussian assembly

Does this improve upon the results of the linear assemblies? This self-similar design can also be analyzed analytically. Consider one such sub-assembly, with three simple separators in it. Let the input to the top separator be called T, with added recycle stream x from the left and right separator beneath it. This stream is sent through the "good" side in the amount $(T + x) \cdot \varepsilon$ and then recycled by the left separator in the amount $(T + x) \cdot \varepsilon \cdot (1 - \varepsilon)$. Meanwhile the input stream is sent through the "bad" side in the amount $(T + x) \cdot (1 - \varepsilon)$ and then recycled by the right separator in the amount $(T + x) \cdot (1 - \varepsilon) \cdot \varepsilon$. Thus the recycle satisfies

$$(T + x) \cdot \varepsilon \cdot (1 - \varepsilon) + (T + x) \cdot (1 - \varepsilon) \cdot \varepsilon = x$$

$$2 \cdot (T + x) \cdot \varepsilon \cdot (1 - \varepsilon) = x$$

$$x = \frac{2 \cdot T \cdot \varepsilon \cdot (1 - \varepsilon)}{1 - 2 \cdot \varepsilon \cdot (1 - \varepsilon)} \tag{17}$$

The input stream $T + x$ survives the second separator as "good" in the amount

$$G = (T + x) \cdot \varepsilon^2$$

$$G = \left(T + \frac{2 \cdot T \cdot \varepsilon \cdot (1 - \varepsilon)}{1 - 2 \cdot \varepsilon \cdot (1 - \varepsilon)}\right) \cdot \varepsilon^2$$

$$G = T\left(\frac{1}{1 - 2 \cdot \varepsilon \cdot (1 - \varepsilon)}\right) \cdot \varepsilon^2 \tag{18}$$

Therefore the effective "epsilon", ε_3, of this three-separator assembly that multiplies the input T, in terms of the epsilon ε of the underlying three separators, is given by

$$\varepsilon_3 = \frac{\varepsilon^2}{1 - 2 \cdot \varepsilon \cdot (1 - \varepsilon)} \tag{19}$$

From here it is a simple matter to understand what would happen if the underlying simple separators were replaced by such a subassembly; their underlying multipliers ε would become ε_3 and the overlying assembly would now have an effective ε of

$$\varepsilon_9 = \frac{{\varepsilon_3}^2}{1 - 2 \cdot \varepsilon_3 \cdot (1 - \varepsilon_3)} \tag{20}$$

This pattern repeats itself indefinitely. Such a system grows far more rapidly than a linear assembly, however one can compare what 27 separators would do in one of these self-similar networks (three layers deep) compared to 27 separators in a chain of subassemblies described above (one in front plus 13 pairs), and the linear case has actually purified "good" chemicals and filtered out "bad" chemicals ever so slightly more effectively. This observation, compared with

how rapidly this exponential arrangement grows, favors the linear chain as being more finely tune-able. The self-similar network also demonstrates the now familiar property that chemicals with an ε of less than 50% are filtered to approach zero, and chemicals with an ε greater than 50% are filtered to approach one, and so the simple separator of the base unit must exhibit that quality of favoring only the selected chemical with greater than 50% probability in order for a network of such separators to improve the output tuning.

III. A Cascading Network

A common thread in the results described above is that while throughput is aggressively looped, it is looped with minimal extraction of pure output. What if pure output were more frequently extracted, leaving behind a spectrum that can be re-filtered without that pure output and therefore be forced to become a different spectrum compared to what it was before that extraction?

For a given Gaussian profile defined by some molar-mass dependent bias $\varepsilon(m) = \varepsilon_m$, there are two variables behind the cascading network, n and k. A single sub-assembly of this flavor of network contains a series of separators and mergers which are applied repeatedly to the throughput and produce three output streams which are maximally pure, maximally impure, and blended. If there are n separations in this sub-assembly it would contain $(2n - 1)$ separators and the maximally pure stream results from applying $\varepsilon_m^{\,n}$ to the incoming unfiltered stream, the maximally impure stream results from appling $(1-\varepsilon_m)^n$, and the blended remainder has been effectively applied a map of $1 - \varepsilon_m^{\,n} - (1-\varepsilon_m)^n$.

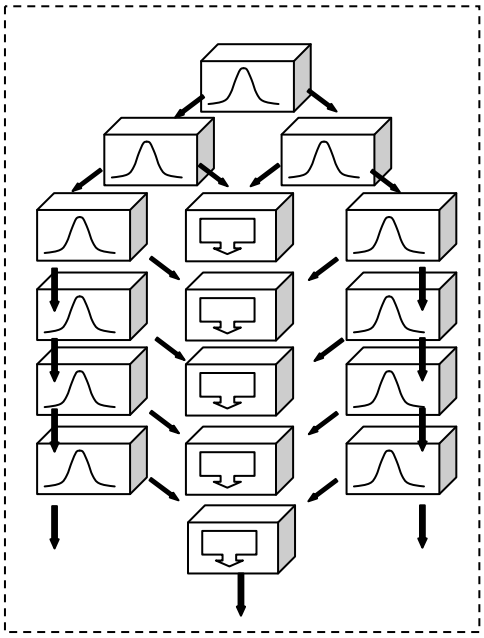

Figure 5.6: A sample Flowsheet Block of a cascading network for $n = 6$

The importance of the value of n is that the more times n is applied, the more purely filtered the stream becomes but also the more reduced the stream; as n approaches infinity, $\varepsilon_m{}^n$ approaches zero and nothing escapes as pure.

Each subassembly produces a pure stream, an impure stream, and a blended stream, and this blended stream can be fed into the next subassembly for further purification according to the "good", "middle", and "bad" maps

$$G = \varepsilon_m^n$$

$$M = 1 - \varepsilon_m^n - (1 - \varepsilon_m)^n$$

$$B = (1 - \varepsilon_m)^n$$

$$G + M + B = 1 \qquad (21)$$

If the middle stream from the first subassembly M_1 is fed into a second subassembly, it will produce three new streams

$$G_{\varepsilon,n,2} = \varepsilon_m^n \cdot M_1$$

$$M_{\varepsilon,n,2} = (1 - \varepsilon_m^n - (1 - \varepsilon_m)^n) \cdot M_1$$

$$B_{\varepsilon,n,2} = (1 - \varepsilon_m)^n \cdot M_1 \tag{22}$$

Collecting the "good" streams, the "bad" streams, and the final "middle" stream (and recalling that $G + B = 1 - M$) yields

$$(G_1 + G_2) + M_2 + (B_1 + B_2) =$$

$$G + GM + M^2 + B + BM = (1 + M)(G + B) + M^2 =$$

$$(1 + M)(1 - M) + M^2 = 1 - M^2 + M^2 = 1 \tag{23}$$

confirming conservation of mass. In general, after *k* subassemblies,

$$G_{\varepsilon,n,k} = G \cdot M^{k-1} = \varepsilon_m^n \cdot M^{k-1}$$

$$M_{\varepsilon,n,k} = M^k = (1 - \varepsilon_m^n - (1 - \varepsilon_m)^n)^k$$

$$B_{\varepsilon,n,k} = B \cdot M^{k-1} = (1 - \varepsilon_m)^n \cdot M^{k-1} \tag{24}$$

and since the net mapping is a geometric sequence in the case of the final middle stream and a geometric series in the case of the pure and impure streams,

$$\sum_{i=1}^{k} G_{\varepsilon,n,k} + M_{\varepsilon,n,k} + \sum_{i=1}^{k} B_{\varepsilon,n,k} = \sum_{i=1}^{k} G \cdot M^{k-1} + M^k + \sum_{i=1}^{k} B \cdot M^{k-1} =$$

$$\frac{G \cdot (1 - M^k)}{1 - M} + M^k + \frac{B \cdot (1 - M^k)}{1 - M} = \frac{(G + B) \cdot (1 - M^k)}{1 - M} + M^k =$$

$$\frac{(1 - M) \cdot (1 - M^k)}{1 - M} + M^k = (1 - M^k) + M^k = 1 \tag{25}$$

For an infinite set of subassemblies, we have

$$\lim_{k\to\infty}\sum_{i=1}^{k} G_{\varepsilon,n,k} = \frac{G}{1-M} = \frac{\varepsilon_m^n}{\varepsilon_m^n + (1-\varepsilon_m)^n} = \frac{1}{1+\left(\frac{1}{\varepsilon_m}-1\right)^n}$$

$$\lim_{k\to\infty}\sum_{i=1}^{k} M_{\varepsilon,n,k} = \lim_{k\to\infty}\sum_{i=1}^{k} M^k = 0$$

$$\lim_{k\to\infty}\sum_{i=1}^{k} B_{\varepsilon,n,k} = \frac{B}{1-M} = \frac{(1-\varepsilon_m)^n}{\varepsilon_m^n + (1-\varepsilon_m)^n} = \frac{1}{1+\left(\frac{1}{\varepsilon_m}-1\right)^{-n}}$$

$$\lim_{k\to\infty}\sum_{i=1}^{k} G_{\varepsilon,n,k} + \lim_{k\to\infty}\sum_{i=1}^{k} M_{\varepsilon,n,k} + \lim_{k\to\infty}\sum_{i=1}^{k} B_{\varepsilon,n,k} =$$

$$\frac{G}{1-M} + 0 + \frac{B}{1-M} = \frac{1-M}{1-M} = 1 \tag{26}$$

These maps for the infinite set of subassemblies are important because they represent the best-case separation scenarios for a given (ε_m, n). The number of units a mole of a given chemical must pass through to be produced in the proportion $\varepsilon_{m,n,k}$ is equal to nk, and that final proportion is

$$\varepsilon_{m,n,k} = \sum_{i=1}^{k} G_{\varepsilon,n,k} = \frac{\varepsilon_m^n \cdot (1-(1-\varepsilon_m^n-(1-\varepsilon_m)^n)^k)}{\varepsilon_m^n + (1-\varepsilon_m)^n} \tag{27}$$

Chemical spectra filtered from inputs of unity are graphed below for one through five subunits. Worth noting here is that the ability to nest separators within a unit in this way leads to a shrinking of the filtered curve, which may seem undesirable, but since the above results offer ways of networking simple separators into delta separators for a user-specified chemical contingent upon the ability to keep the wanted and unwanted filter probabilities on either side of

50%, a chain of simple separators such as this effectively accomplishes that. In the figure below, for example, it only takes 3 separations for the central peak to just barely peek above 50% and be therefore eligible as a base unit in a delta separation assembly of separators.

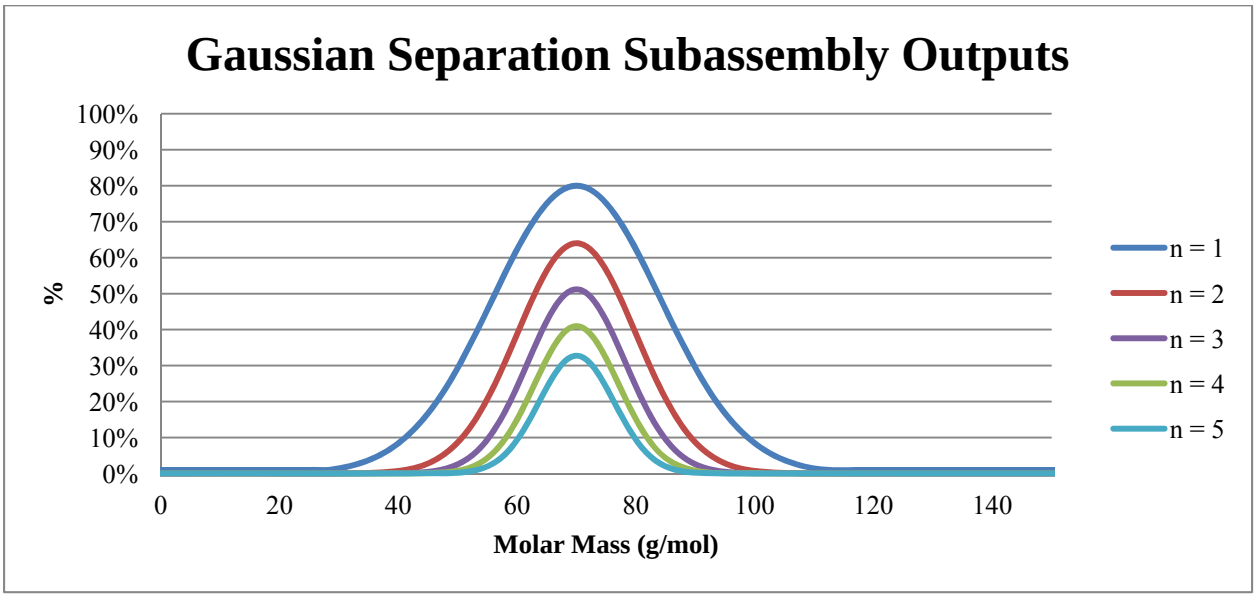

Figure 5.7: The effect of multiple separators on subassembly output

Chapter 6

The Benefits of Networking

Recycling of syngas to increase conversion is an existing and well-established practice of Fischer-Tropsch fuel synthesis, as outlined in the reactor review above. Naturally the fuel synthesis network modeled here might be similarly positioned to take advantage of recycling. To recycle a stream through a network unit is to reapply the process map, and if the recycle is applied through the same unit from which that stream emerged then it is as if the same unit map is repeatedly applied, with the important constraint that the recycled stream, once merged with the incoming stream, is mapped to the same output port from which it was recycled. This is not a chemical constraint, since in a true time-dependent system one can re-route outputs to the front-end input stream and try again indefinitely. It is rather a numerical user-specified constraint, reflecting that this network model sought after and discovered steady-state solutions. This is critically important for the stability of the solutions, as even a modest departure from steady-state behavior will amplify over time. Even a periodicity that is numerically stable is to be avoided, as per earlier remarks about the suboptimal effect of periodicity on the reaction noted in the fuel

synthesis literature. In a network replete with knobs that the operator (or automated algorithm) can turn in order to tune the distribution to a desired outcome, there would of course be disruptions to a steady state as the system adjusted from, say, producing hexene to producing dodecane, but once it is producing a given chemical, a steady state is desired.

I. Selectivity & Partial Recycling

Simulating a convergent recycle scheme proved numerically challenging, and required manipulation of weighting schemes discussed above in order to prevent the code from running away with the solutions, either towards infinity or zero. To feel out the behavior of the network and work towards complete recycle with perfectly tuned output, partial recycling schemes were studied with following configuration:

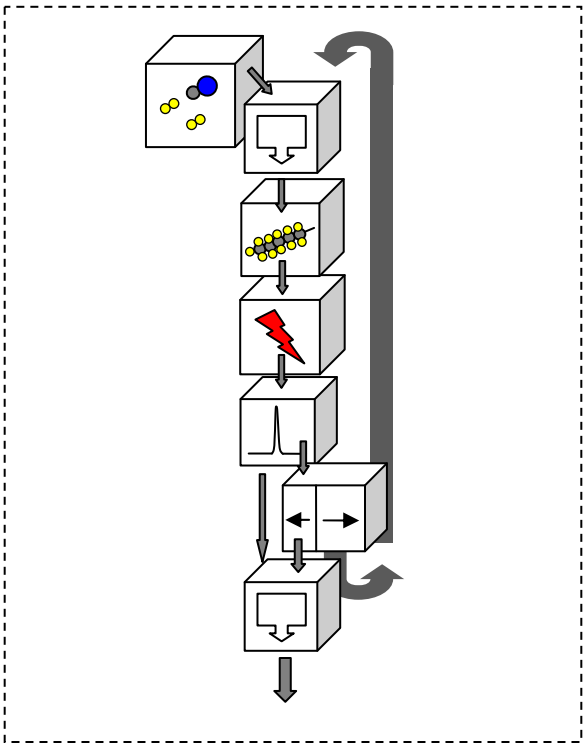

Figure 6.1: Partially recycled production: Layout

This schematic represents the following simulated processing of the chemical streams:

1. The syngas enters on the upper left, where the graphics represent a composition of two H_2 molecules per CO molecule coming in.
2. The syngas enters a merger unit, which merges that syngas with a recycled stream of chemicals looped back from the bottom of the assembly.
3. That merged stream is fed into a fuel synthesis reactor that grows carbon chains.
4. The synthesized chemical stream flows into a cracking unit (illustrated with a lightning bolt).

5. The cracked chemical stream is then fed through a separation filter, referred to in this work as a delta filter and illustrated with a crudely drawn Dirac delta function, which separates the user-specified chemical from the remainder of the stream.
6. The remainder passes through a simple splitter which directs some user-specified fraction of the output through one outgoing port and the remaining fraction of the output through the other outgoing recycling port.
7. The recycled chemicals flow back to the merging unit at the top of the assembly, while the un-recycled chemicals flow into a merging unit at the bottom of the assembly where they are re-combined with the user-specified filtered chemicals for a final output product.

Simulations were run for all alkanes and alkenes from chain length 2 through 14, and for recycled fractions from 0% to 95%, in which a 95% recycled fraction indicates that 95% of the post-filtered product is recycled back to the front of the assembly while 5% is merged with the user-specified product. The purpose of this experiment was to study how the system responds to increasing demands on what is or is not permitted to leave the assembly while the network manipulates streams coming in and out of single units. For the entire Flowsheet to reconcile, the outgoing moles of carbon, hydrogen, and oxygen must match the inputs. If all but the user-specified product chemical is considered “waste”, then the greater the proportions of “waste” chemical fractions recycled back, the greater proportion that user-specified chemical will comprise of the final product. There is no mass constraint on how much must be recycled to reach a steady-state solution, and indeed that amount varied depending on which chemical the user-specified.

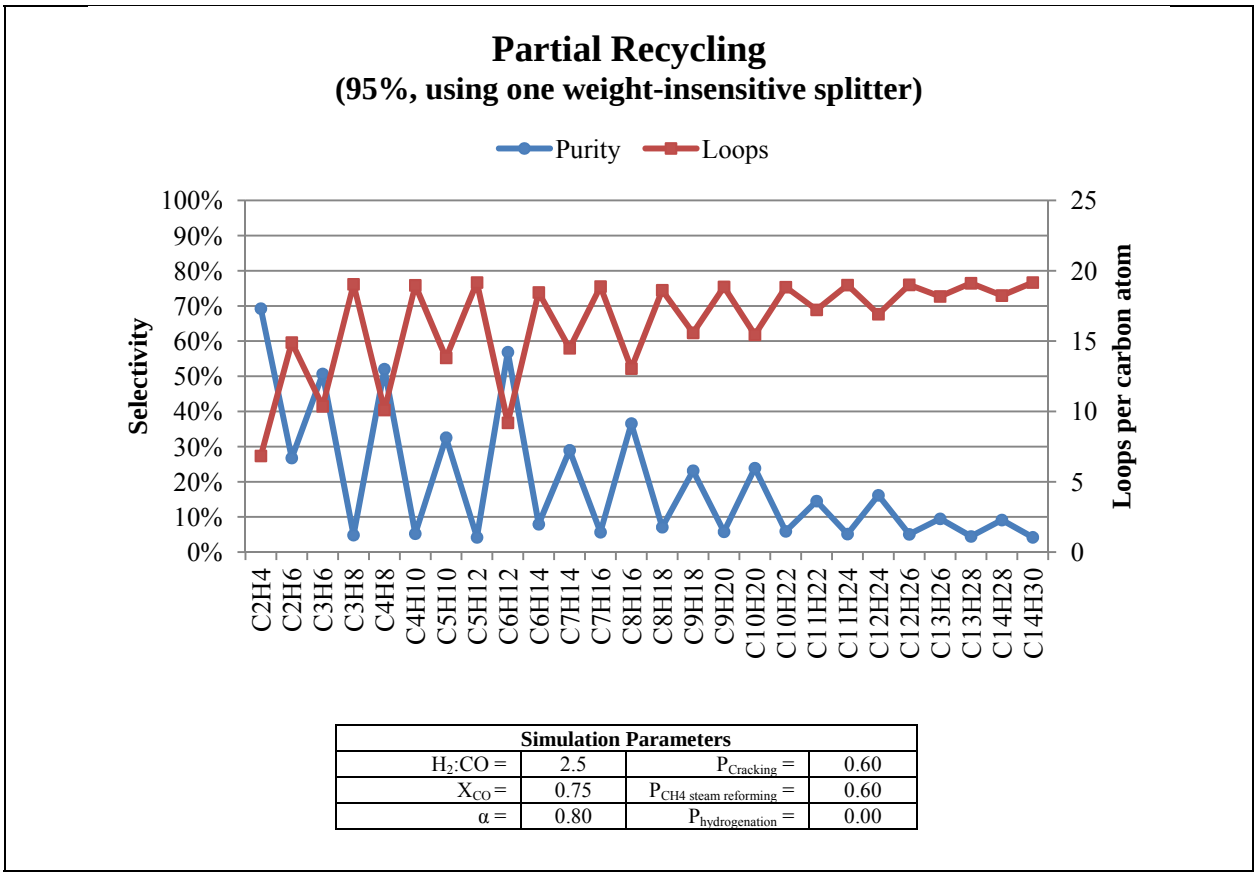

Simulation Parameters			
H_2:CO =	2.5	$P_{Cracking}$ =	0.60
X_{CO} =	0.75	$P_{CH4\ steam\ reforming}$ =	0.60
α =	0.80	$P_{hydrogenation}$ =	0.00

Figure 6.2: Partially recycled production: Selectivity and penalties

These results make clear that user-specified alkenes are much easier to select for than user-specified alkanes. Either is possible, however the reactor produces alkanes relative to alkenes depending on the H_2:CO ratio coming in, and as discussed in the justification of the maps, the cracker heavily favors alkenes, and so it is much more difficult to raise alkane selectivity and requires a greater recycled stream to do so; even at the 95% recycle ratio shown above, alkanes were selected for at only single-digit percentages of the incoming carbon atoms, and consistently required almost 20 loops per carbon atom to get there. Predictably, the shorter chain carbon lengths required fewer loops to accumulate, since the cracker harvests the longer chains and the

reactor grows them relatively more slowly. As explained in the discussion of the simulation algorithms, the solutions arrived at here are not necessarily unique; there could be other steady states available for the system that satisfy all pertinent conservations and unit maps, but the solutions arrived at here are available steady states which would persist once initiated, and the trends observed as the recycle ratio is varied inform closed loop and expanded network designs to further optimize fuel synthesis. Below are examples of the behavior of select chemicals as they approach (but do not yet reach) complete recycle of unspecified chemicals.

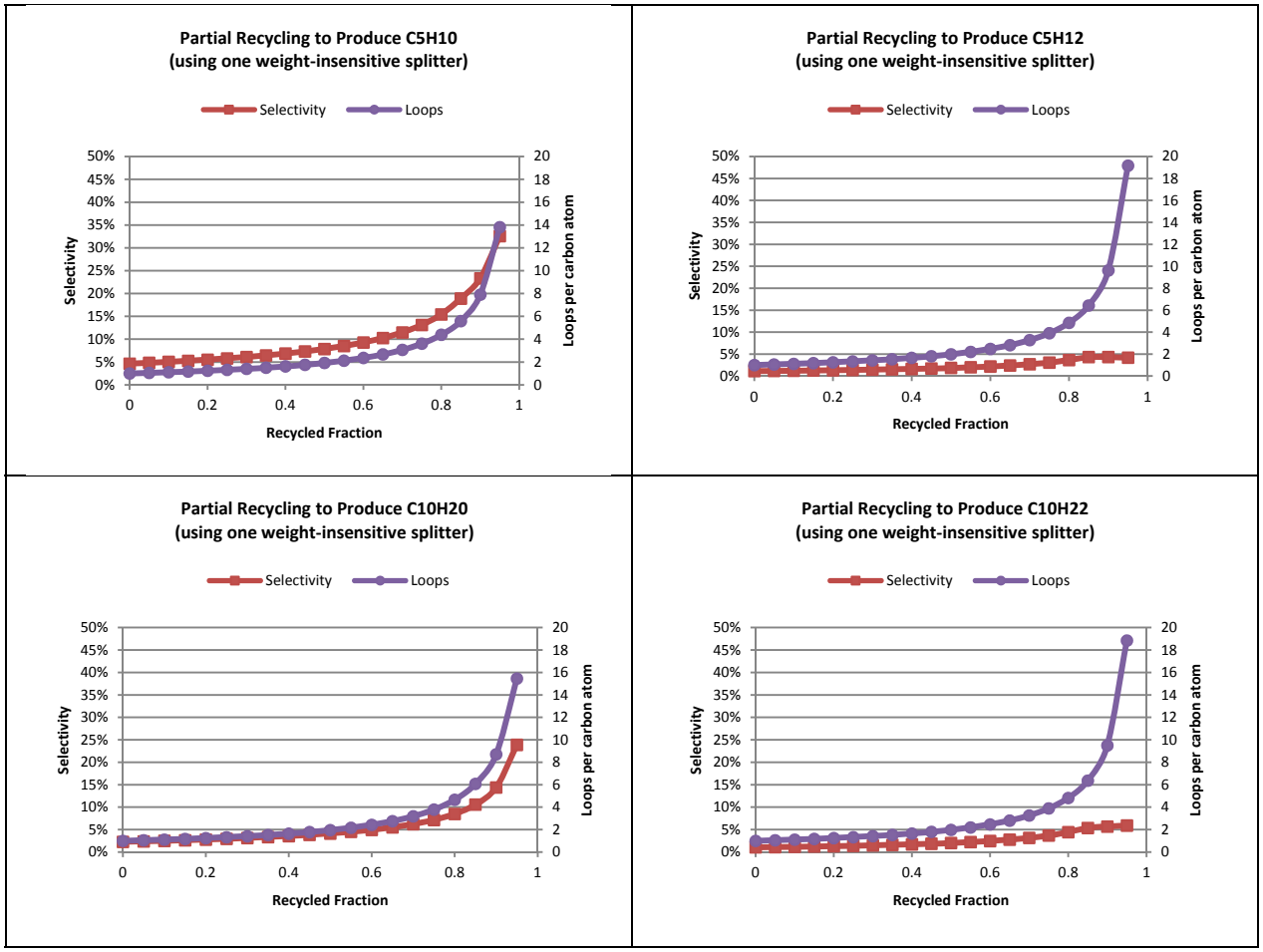

Simulation Parameters			
H_2:CO =	2.5	$P_{Cracking}$ =	0.60
X_{CO} =	0.75	$P_{CH4\ steam\ reforming}$ =	0.60
α =	0.80	$P_{hydrogenation}$ =	0.00

Figure 6.3: Partially recycled production: Selectivity and penalties for C_5, C_{10}

II. Unidirectional Product Sharpening

In order to understand how well streams of different flavors might be favored by smart networking of the chemical throughput, a non-looping unidirectional network was designed and simulated to show how the outputs might be sharpened. In the same way that a recycled stream is being re-mapped front to back each time it passes through, a set of linear subassemblies can accomplish sequential mapping while the effect of decision-making as to which stream is directed where is studied.

The unidirectional configuration consists of Flowsheet Blocks within Flowsheet Blocks within Flowsheet Blocks, taking full advantage of the hierarchical facilities of the code:

1. Each trafficking block consists of three erf separators, each set to a different separation mean, that turn a single incoming chemical stream into four streams filtered by mass. The top separator splits the incoming stream into a heavy stream and a light stream, each of which flow into their own respective sub-separators that separate them once more into two fuel synthesis reactors and two crackers. This Flowsheet Block has one input and four outputs.
2. Each reaction block consists of two fuel synthesis reactors and two crackers, each with parameters that are customizable from unit to unit. The fuel synthesis reactor itself is a Flowsheet Block which internally has the option of connecting to a syngas generator to supplement the incoming chemical stream. There is one reactor for the lighter fraction of the light stream and one reactor for the heavier fraction of light stream. Similarly, there is

one cracker for the lighter fraction of the heavy stream and one cracker for the heavier fraction of the heavy stream. The reaction block has four inputs and four outputs.

3. The merging block consists of three mergers, which consolidate the four outgoing streams from the previous units into a single stream. The merging block has four inputs and one output.

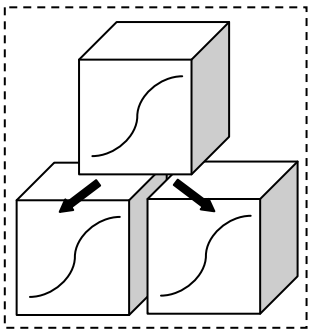

Figure 6.4: Unidirectional Network Trafficker

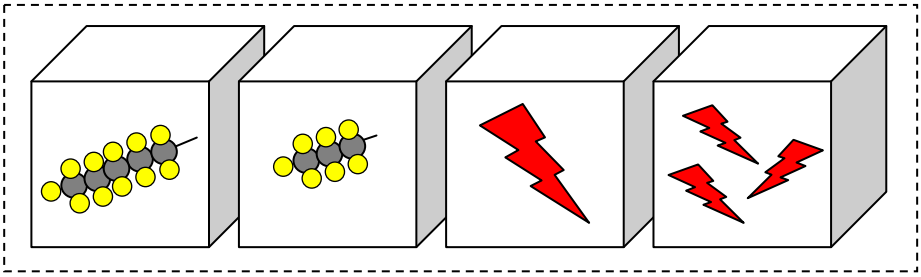

Figure 6.5: Unidirectional Network Reactor/Cracker

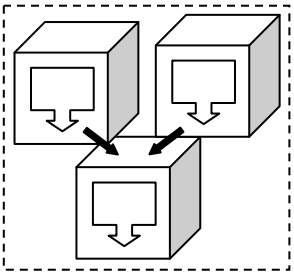

Figure 6.6: Unidirectional Network Merger

These three Flowsheet Blocks are part of a subassembly which is itself a Flowsheet Block. This subassembly feeds the incoming stream through a delta separator so as not to scavenge and re-process the user-specified chemical that the network aims to produce. The remaining stream is fed into the erf-separating block, the reacting block, and then the merging block, from which the outgoing stream is merged with the user-specified chemicals previously sequestered for entry into the subsequent subassembly. Thus each such subassembly has one input and one output and can be laid end-to-end as much as desired. Feeding this chain of subassemblies at the very beginning will be a single fuel synthesis reactor, so that there is a diverse suite of chemicals, albeit largely unconverted, entering the network for mass-dependent trafficking.

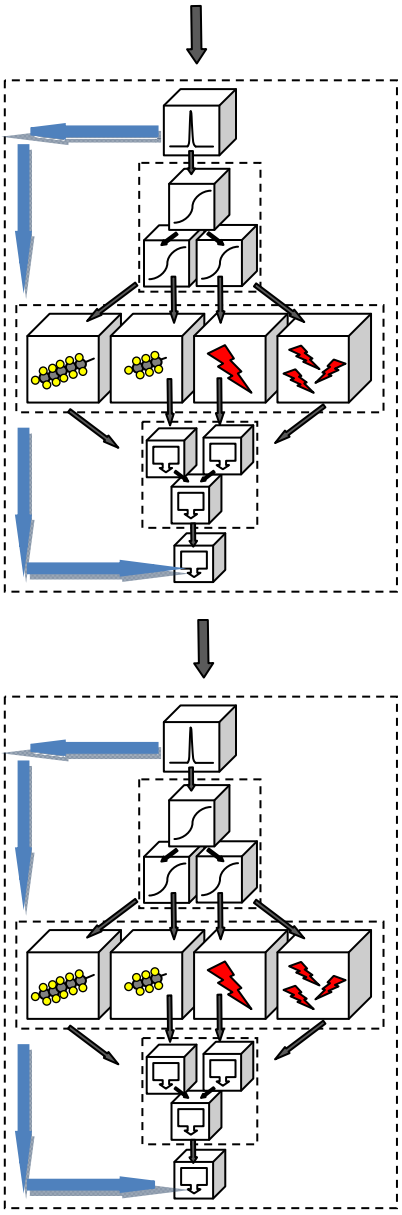

Figure 6.7: Unidirectional Network Layout

It is important to note that while this design was implemented for computational convenience and symmetry, a real network would not elect to mix the user-specified product back into the

chemical throughput only to be separated back out in the next block. This would be a wasteful step unless there were opportunities for further sharpening.

Simulations were conducted of chains of varying numbers of such subassemblies. As more subassemblies were linked together, they were assumed to convert less of the syngas coming through. This is because the basis of comparison will be between the performance of greater numbers of lower-converting units imitating small ones and the performance of lower numbers of higher-converting units imitating large ones. Chemical throughput passing through a smaller unit will have a lower residence time, and so the assumption of lower conversion of CO is valid.

For the studied chemicals, the parameters of these units – the knobs that the operator of such a network would be able to turn – were varied in order to demonstrate the strongest performance possible relative to the single unit base case. Varied parameters included the chain growth probabilities of the reactors, whether or not the chemicals to be thermally cracked were hydrocracked with some probability first, and the mass parameters assigned to the three erf separators as a basis of separation.

Having run thousands of permutations of possible parameter values for different chemicals, it is clear that the chain growth probability for the fuel synthesis reactor need not vary very much to affect the outcome, and that far more significant parameters are the decision to hydrocrack the chemical streams and the mean molar masses about which the erf separators are

centered. The effect that hydrocracking has on the proceedings is that the products of cracking alkanes and the products of cracking alkenes are in practice quite different. As discussed in the justification of the cracker maps, alkanes do not tend to recombine into longer carbon chains when undergoing cracking reactions whereas olefins do, and so the chemical streams most in need of being pared down will most likely do so if they are saturated with hydrogen. A logical supposition going into these simulations might have been that for the top erf separator of the trafficking subunit, the logical mean about which to separate might be the mean of the desired chemical, such that chemicals larger than that user-specified product would be sub-divided into the two crackers and chemicals smaller than that product would be sub-divided between the two fuel synthesis reactors. In practice however the optimum mean for the chemicals studied tended to be significantly less than that of the user-specified chemical. This could be a result of the fact that the fuel synthesis units grow carbon chains aggressively enough that they must begin significantly below the desired mass and not just slightly below. Another contributing factor to the same conclusion could be that, again, thermal cracking of olefins can grow them and this would explain why the optimum erf centers direct a significant quantity of chemicals that are lighter than the desired product into a stream that enters the thermal cracker unsaturated.

These simulation studies produced subsets of parameters that produce favorable results, where in this case favorability is measured as having a greater fraction of the incoming carbon atoms converted to the chemical of choice than a single traditional unit with the same inputs and core parameters would have. With these parameters, it was then possible to study what the effect on the output would be if greater numbers of less aggressive (i.e. smaller) units were used in

place of fewer but more aggressive (i.e. larger and more traditional) units were used. These simulations were run with the following assumptions:

1. For the sake of relative simplicity and consistency for a basis of comparison, each of the subassemblies in a given chain used the same three erf centers. In other words, the top erf separators in each trafficking subunit of each subassembly would all separate about the same mean molar mass, as would the left and right sub-separators beneath them. (Note that a value of 0 for an erf center does not mean that the erf directed chemicals about a mean of zero, but rather that it was an erf that simply split the incoming chemicals about their own mean and not a predetermined mean.)
2. All fuel synthesis reactors would produce the same chain growth probability of 0.8, with the exception that the last subassembly in the chain would produce a more modest chain growth probability of 0.7.
3. The sum of the CO conversion rates along a particular path of reactors is 90%. Side-by-side reactors are assumed to act in parallel, but the sum of the rates of reactors in series is what is counted. For example, if there are two subassemblies, then an incoming carbon has gone through the front-end reactor and these two subassemblies for a total of three, and so each of the reactors converts one third of 90%, or 30%. Nine subassemblies and one front-end reactor each convert 0.9 % of the incoming CO, again totaling 90%.

The second assumption regarding growth probabilities is informed by the multivariate simulations which consistently produced optima in which the very last reactors were slightly less

aggressive in growing carbon chains. This is a logical result since the network configuration being studied here lays the reactors and the crackers in parallel, so the final reactors will not have a chance to be cracked, so they had better not overdo it. In the looped scenarios discussed above and below this not necessarily true since unfavorable products can be rerouted to the beginning, but this network is designed as a one-way street to track how these streams evolve the first time through. Thus the best-case scenario depends on having done things right the first time. The results of such simulations for C_6H_{12} and $C_{10}H_{20}$ are graphed as a function of the number of consecutive subassemblies on the *x*-axis. The percentage of incoming carbons referred to on the *y*-axis represent how many carbon atoms emerged as C_6H_{12} or $C_{10}H_{20}$ compared to how many entered the system. The reference lines in each graph indicate what a single reactor followed by a single cracker would produce with these parameters. Note that the leftmost entries for *one* subassembly refer to chemicals passing through *two* reactors, as discussed above, since the network contains an $n = 0$ initial reactor. This may explain why the entry for one subassembly is actually below the reference line; chemicals in that configuration pass through only one reactor of relatively weak conversion (45%) before their only opportunity to be grown further or cracked.

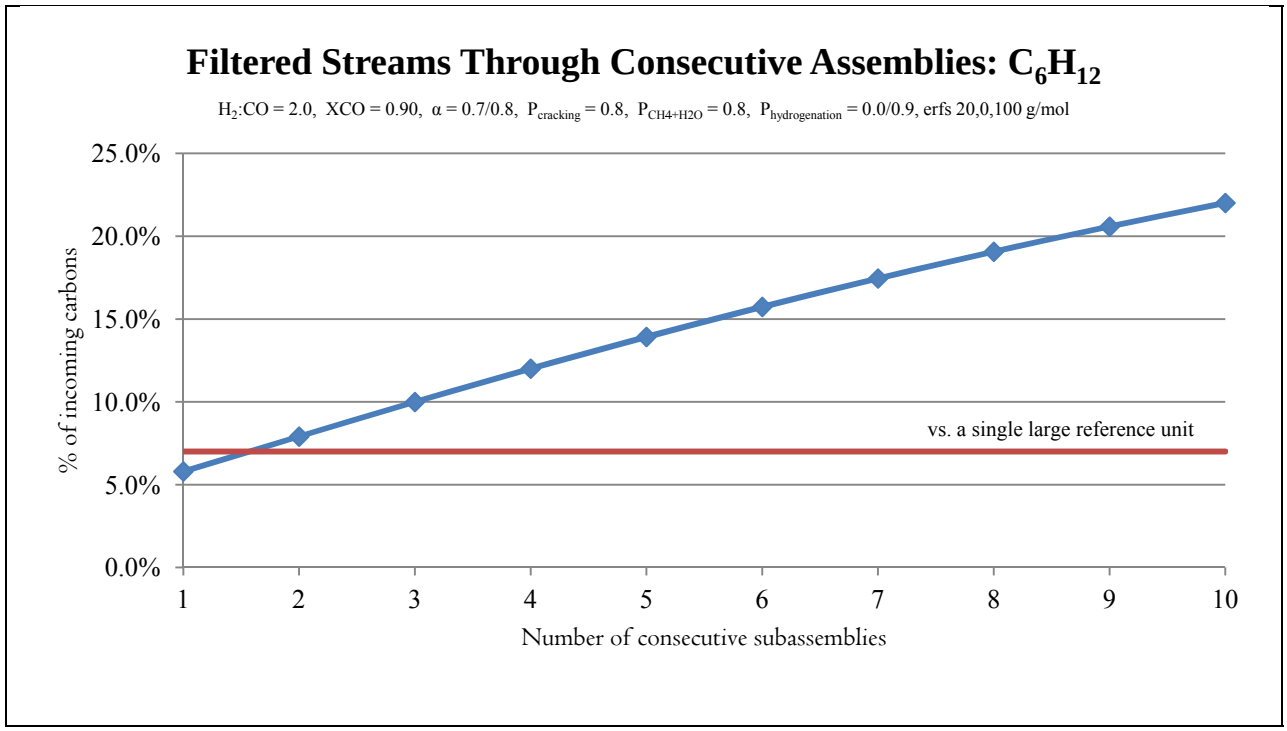

Figure 6.8: Unidirectional Network Layout for C_6H_{12}

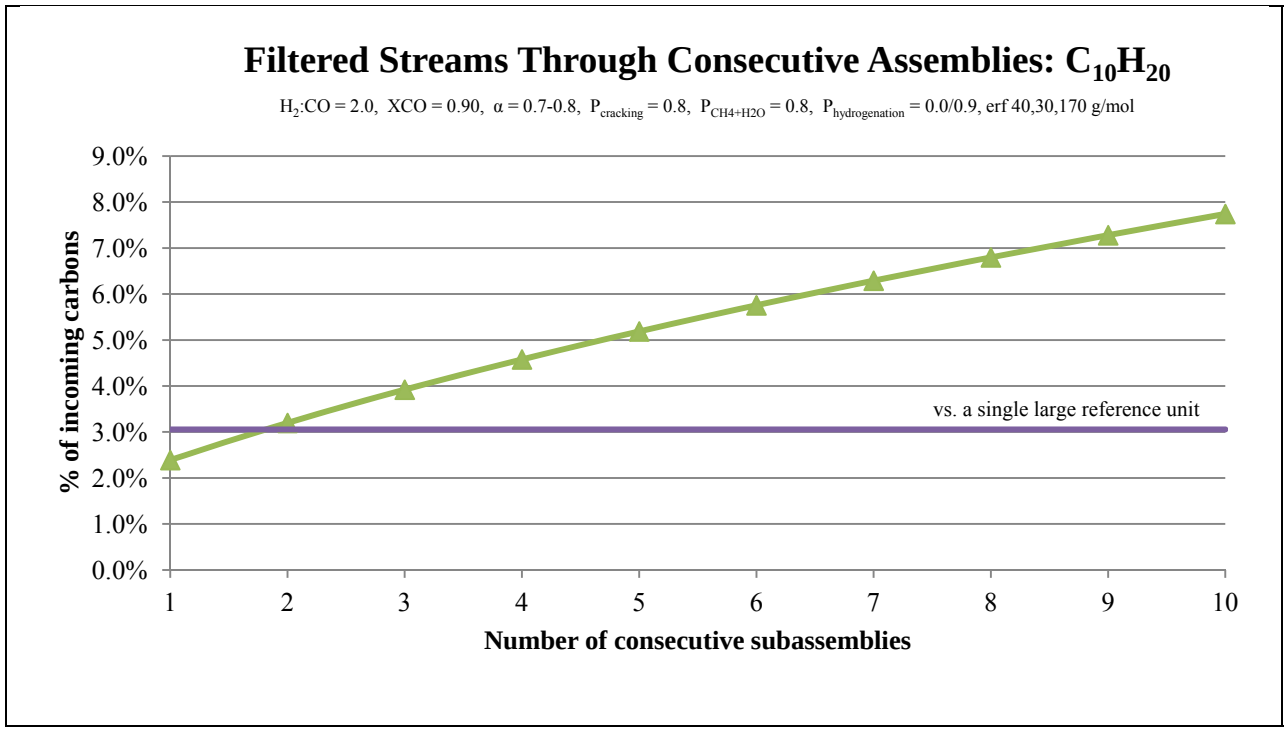

Figure 6.9: Unidirectional Network Layout for $C_{10}H_{20}$

Both graphs demonstrate increasingly superior conversion for 2 or more subassemblies, along curves that look linear but are ever so slightly concave down with second order curve-fitting indicating a quadratic coefficient of order 10^{-4}. Running the chemical flows through ten subassemblies produced more than triple the reference amount of carbon content in C_6 olefins and more than double the reference amount of carbon content in C_{10} olefins. This is an exciting result that indicates real and substantial returns to small scale and specificity. Also important to note is that the parameters used for the C_6 simulations versus those for the C_{10} simulations differed only in the mean centers of the erf separators. In other words, the same reactors and crackers can produce either enhanced C_6 or enhanced C_{10} based only on the way in which the streams are trafficked, and not on going into the reactor and cracker units themselves and altering

their fundamental characteristics. The ability to tune distributions by turning knobs of traffic flow rather than customizing and re-customizing more costly and specific catalytic units is a powerful statement in favor of producing hydrocarbons from cleverly networked arrays of standard chemical processing units.

The graphs above were generated from sensible values, with how "sensible" a value is informed by the effect on the output spectrum from previous simulations. Parameters were by no means completely exhaustively permuted, but trends in which values were favored for certain flavors of output chemical were readily apparent. As an example, consider the following figure in which C_6H_{12} was selected as the output chemical for over 18,000 different permutations of parameters that were near those used for the above simulations. It is clear from the figure that while once in the neighborhood of favorable parameters, the networked output is usually dramatically better than the reference case, but it's also clear that how much better it can be yet depends on those choices, and that optimization of output against those choices better informs how the network should be configured.

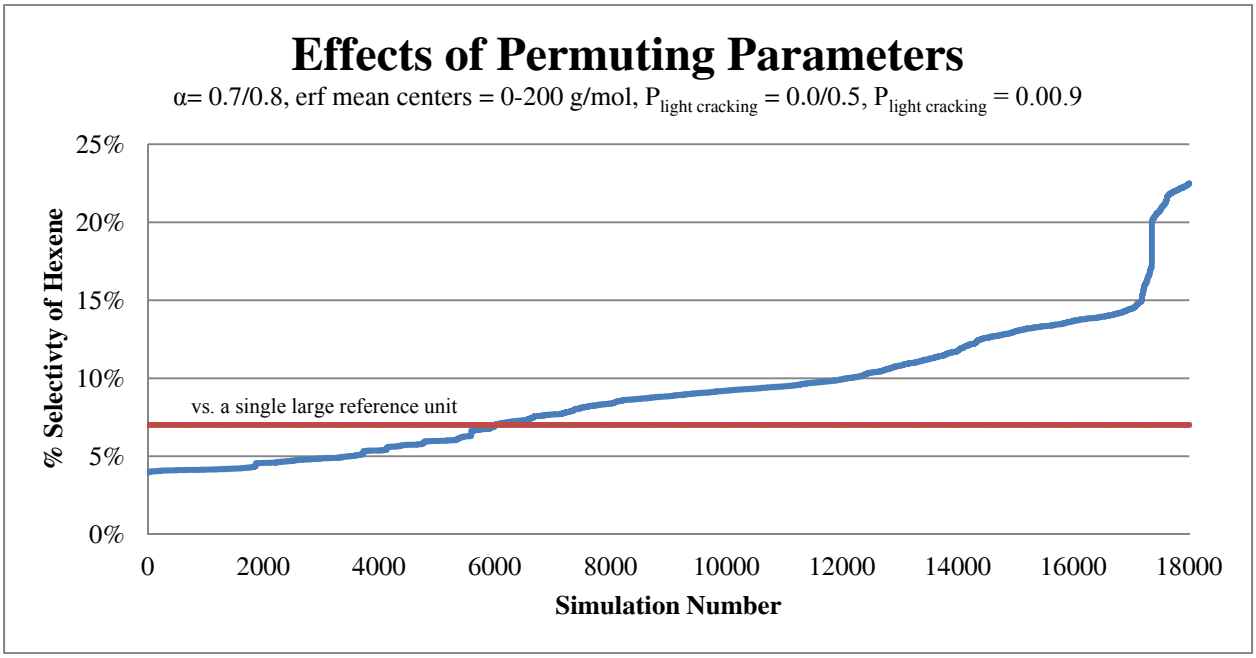

Figure 6.10: The effect of parameter variation on output

III. Perfectly Tuned Production

III.1. Simulating One Flowsheet Block

Simulating a convergent recycle scheme proved more challenging as greater demands were placed on the output, but once the eigenvalues of the error mapping described above were nudged below unity, the fuel synthesis network was able to converge to solutions of a system in which the output was constrained to be only water and a particular hydrocarbon. The inclusion of water was necessary in order to obey mass conservation, since every carbon converted to hydrocarbon originally entered the system as a CO molecule, and so for every outgoing carbon atom there must be one outgoing oxygen atom. The 2:1 ratio of incoming H_2:CO present in the syngas is perfectly mapped to a 2:1 ratio of carbon atoms to H_2O in the output; the molecular

ratio simply depends on how long the olefin chain is. For example, a five carbon chain would emerge with H_2O in a ratio of 1:5:

$$5\ CO + 10\ H_2 \rightarrow C_5H_{10} + 5\ H_2O \quad (1)$$

Once the output of a single unit of reactor and cracker consists entirely of the desired product, the selectivity is 100% and the variable of interest becomes the size of the recycled stream in order to accomplish this, which answers the question of how many times a carbon atom must cycle through the system in order to emerge as the desired product. The more carbon atoms are recycled, the more carbons live in the system at any given time. The likelihood that a carbon exist the system at all in a give pass-through simply depends on the ratio of product, say, pentene in the case suggested above, to reacted and cracked carbon

$$exit\ probability = \frac{5 \times n_{C_5H_{10}}}{5 \times n_{C_5H_{10}} + N_{recycled\ carbon\ atoms}} \quad (2)$$

More generally, noting that these simulations all assumed that 100 carbon atoms were input and therefore that the perfectly restricted output must contain 100 carbon atoms,

$$Exit\ probability = \frac{100}{100 + N_{recycled\ carbon\ atoms}} \quad (3)$$

$$Number\ of\ loops\ = \frac{1}{Exit\ probability} = \frac{100 + N_{recycled\ carbon\ atoms}}{100} \quad (4)$$

In order to take fuller advantage of networking, and to support the algorithm with as much user-specified help to converge to a solution, the layout of the units was more sophisticated here than simply recycling 100% of the unspecified chemical to the front of the unit. Instead of running the

reacted and cracked chemical streams through a simple splitter, they were instead run through an erf separator that was balanced about a mean equal to the mass of the user-specified chemical. On average, within the Gaussian accuracy, chemicals lighter than the user-specified product were routed back to the reactor in need of further growth, while chemicals heavier than the user-specified product were routed back to the cracker in need of breakage for the chance of reaching the desired chain length or then being re-routed again back to either the reactor or cracker for further processing on the next loop. The network model was run to simulate perfectly pure output selectivity for olefins of carbon chain lengths 2 through 14, and each of these runs converged to a solution, so that the selectivity of unit was by definition 100%, and the pertinent variable with chain length was the number of loops per carbon atom and probability of exit as defined above.

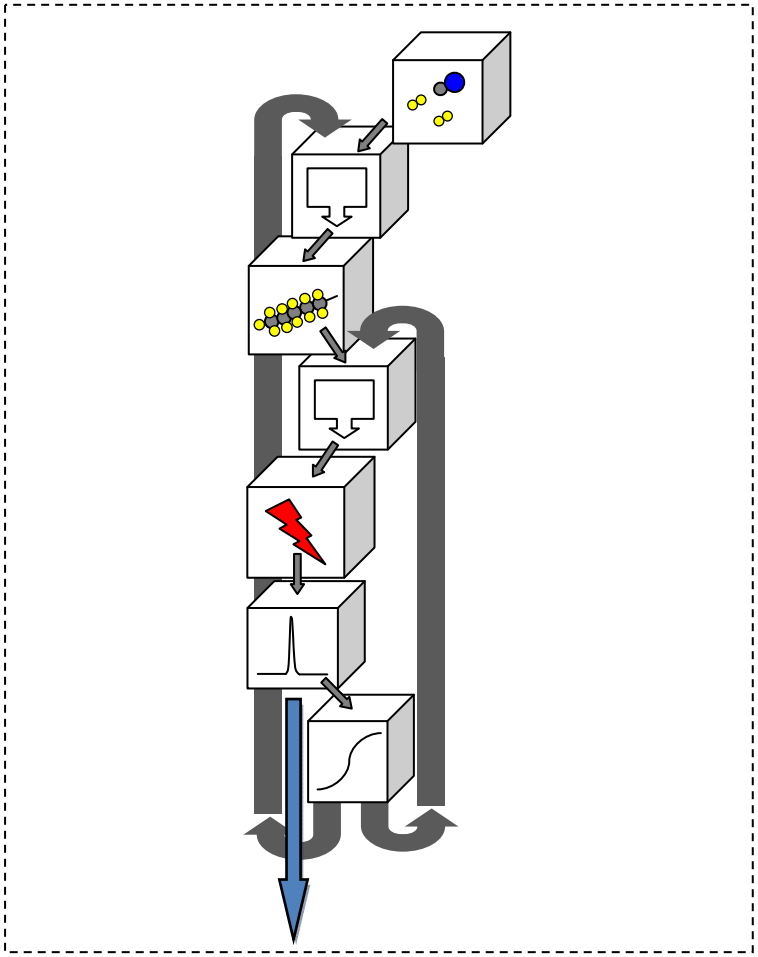

Figure 6.11: Perfectly tuned production with one assembly: Layout

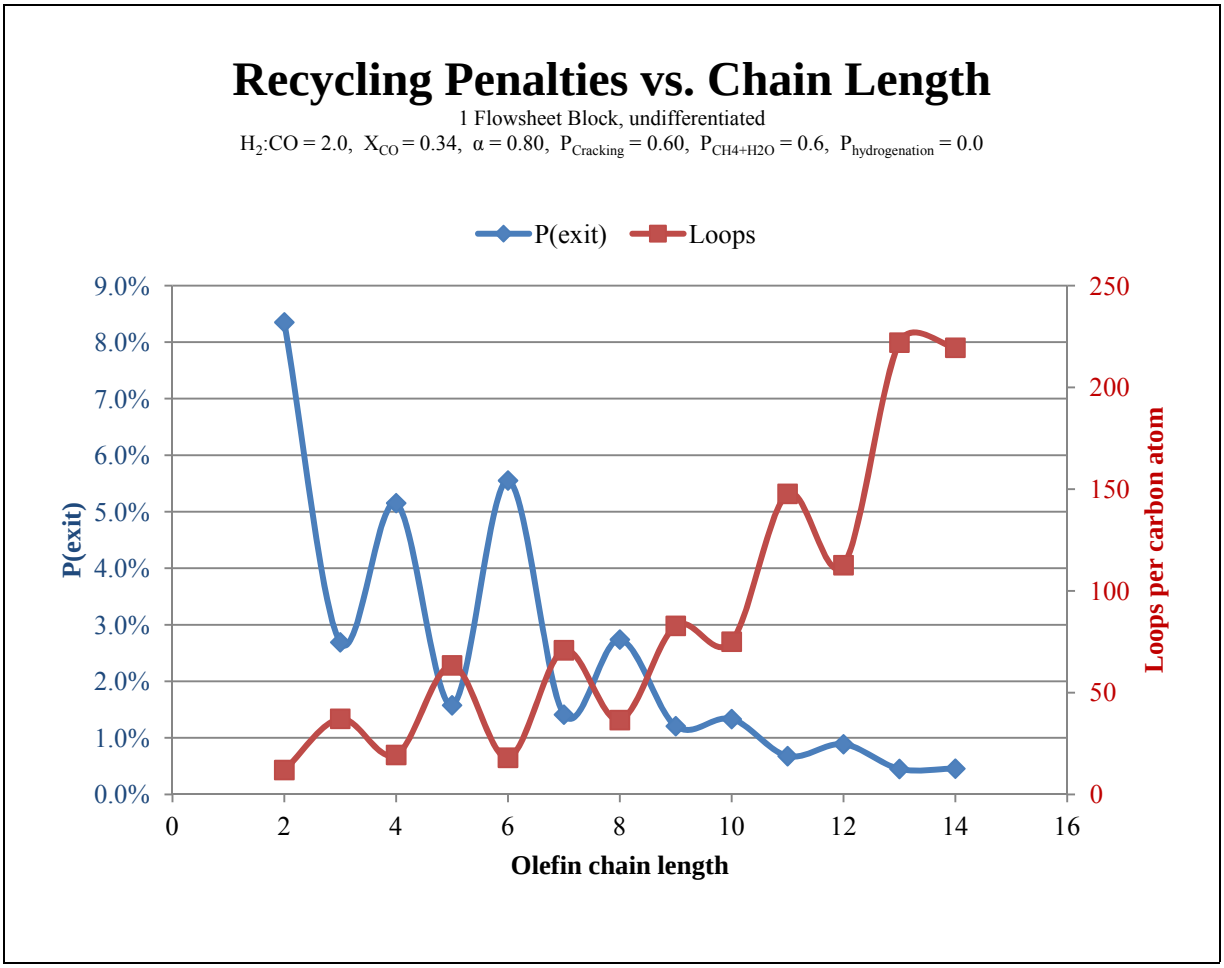

Figure 6.12: Perfectly tuned production with one assembly: Looping penalties

In the resulting figure, the overall trend is observed that as the length of the selected chemical increased, the number of loops per carbon atom required to attain perfect purity also increased. This stands to reason since if longer carbon chains are desired, more growth cycles through the reactor unit will be required. Also evident in the figure is that while the number of loops per *even* carbon number and the number of loops per *odd* carbon number increased, these two flavors

were very differently favored. For every even carbon chain of length n, the network required fewer passes per carbon atom than it did for every adjacent carbon chain of length $n \pm 1$. This is likely a reflection of the bias introduced into the cracker mapping for speedier computational convergence discussed above, but also due to the fact that the ethylene was present in such high quantities relative to the others, and can only build upon itself via olefin growth in the cracker to form even chains.

III.2. Simulating a Chain of Flowsheet Blocks

Having successfully produced 100% selectivity for a user-specified chemical in a single Flowsheet Block, the next step was to understand what might happen if multiple Flowsheet Blocks were strung together in a chain. The Flowsheet Blocks were the same as that described above, with cracked chemicals from a reactor-cracker chain having the user-specified chemical separated out and the remainder split by mass according to an erf separator, only instead of feeding back to the same block, the light and heavy streams feed forwards to the next reactor and cracker, respectively. At each successive Flowsheet Block, the desired products are extracted and the remaining chemicals sorted by mass into the subsequent unit until the last unit is reached. They are then recycled back to the very beginning of the chain of Flowsheet Blocks.

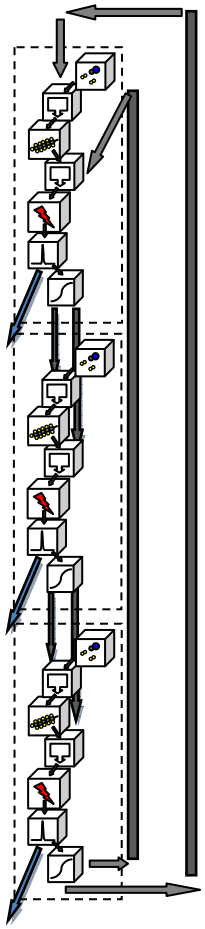

Figure 6.13: Perfectly tuned production with multiple assemblies: Layout

When the assemblies were simply laid down consecutively with their internal parameters unchanged, the system was still constrained by mass conservation to produce 100 carbon atoms worth of the selected chemical. However with multiple assemblies feeding into one another and extracting the products of value after each one, there was a reduced burden on each individual assembly to produce that chemical and therefore less throughput per unit. It is unsurprising, then,

that with each successive Flowsheet Block in the assembly, with inter-block product extraction and mass-based networking, fewer carbons needed to be recycled to back to the beginning of the assembly.

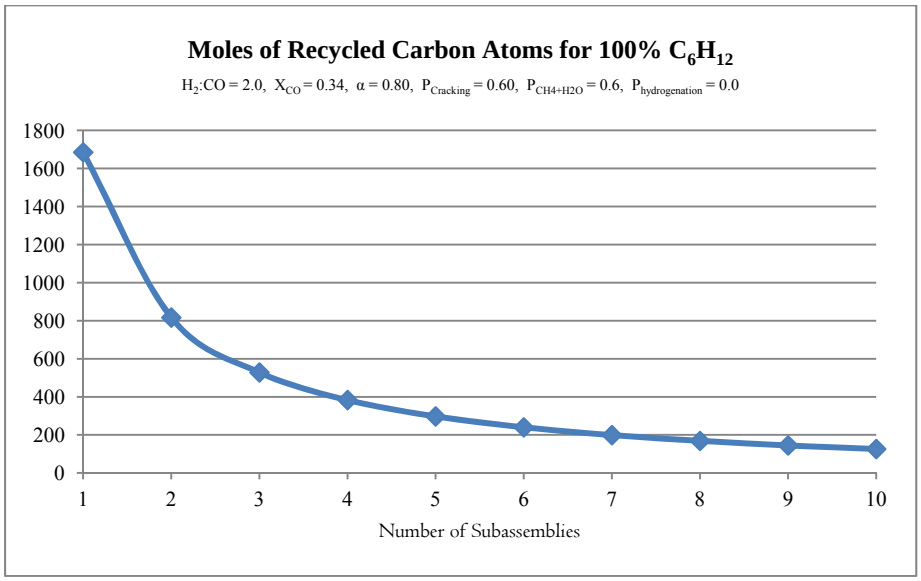

Figure 6.14: Perfectly tuned production with multiple assemblies: C_6H_{12}

Upon closer inspection of the data, however, a key observation emerged, which was that if the throughput in each unit was summed up, which would be 3 throughputs when there were 3 sub-assemblies in a row and 6 throughputs when there were 6 assemblies in a row, the sum of these throughputs was invariant and equal to the amount recycling required in a single assembly indicated on the previous graph.

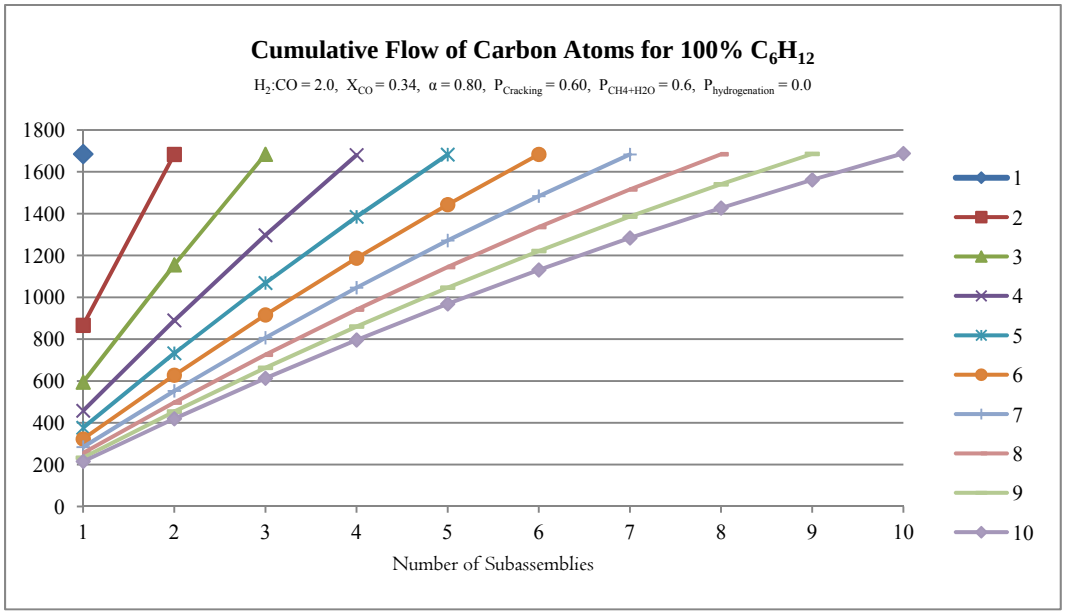

Figure 6.15: Perfectly tuned production with multiple assemblies

The implication here is that the numerical solver preserved the previous solution, and simply spread it out across equal blocks. If the user permits them to, 5 units can do with 100 moles of carbon exactly what a single unit can do, only at a more leisurely pace. This is by no means necessarily a unique solution, but one to which the code is gravitating. This comparison, however, is not what the present work is after. The present work isn't meant to compare one unit to 5 units, however, but rather one large unit to 5 smaller units of equivalent capacity. As a crude approximation of a smaller unit that is less ambitious with its throughput than a large unit is, the carbon conversion rate is proportionally reduced; if one unit would have converted 90% of its incoming CO, than 9 units must each convert 10% of its incoming CO. If smart and automated inter-unit networking redirects traffic, what can 9 of the 10% units do compared to a single 90% unit? The output demand is still for 100% purity of the user-specified chemical, so the pertinent

variable is still the recycle rate; how aggressively must carbon be recycled through the assemblies to accomplish the demanded purity? This question was studied for three olefins produced from network configurations ranging from 1 to 10 subassemblies such that the greater the number of subassemblies, the less CO was converted in each subassembly. The CO and H_2 syngas was injected in the front of the chain of subassemblies but not re-injected in subsequent units except to conserve volumetric throughput. Each subassembly produced, reacted and cracked chemicals that were redirected to a reactor or a cracker in the next unit on the basis of mass, and the reacted and cracked chemicals that were not user-specified were looped back to the beginning of the chain.

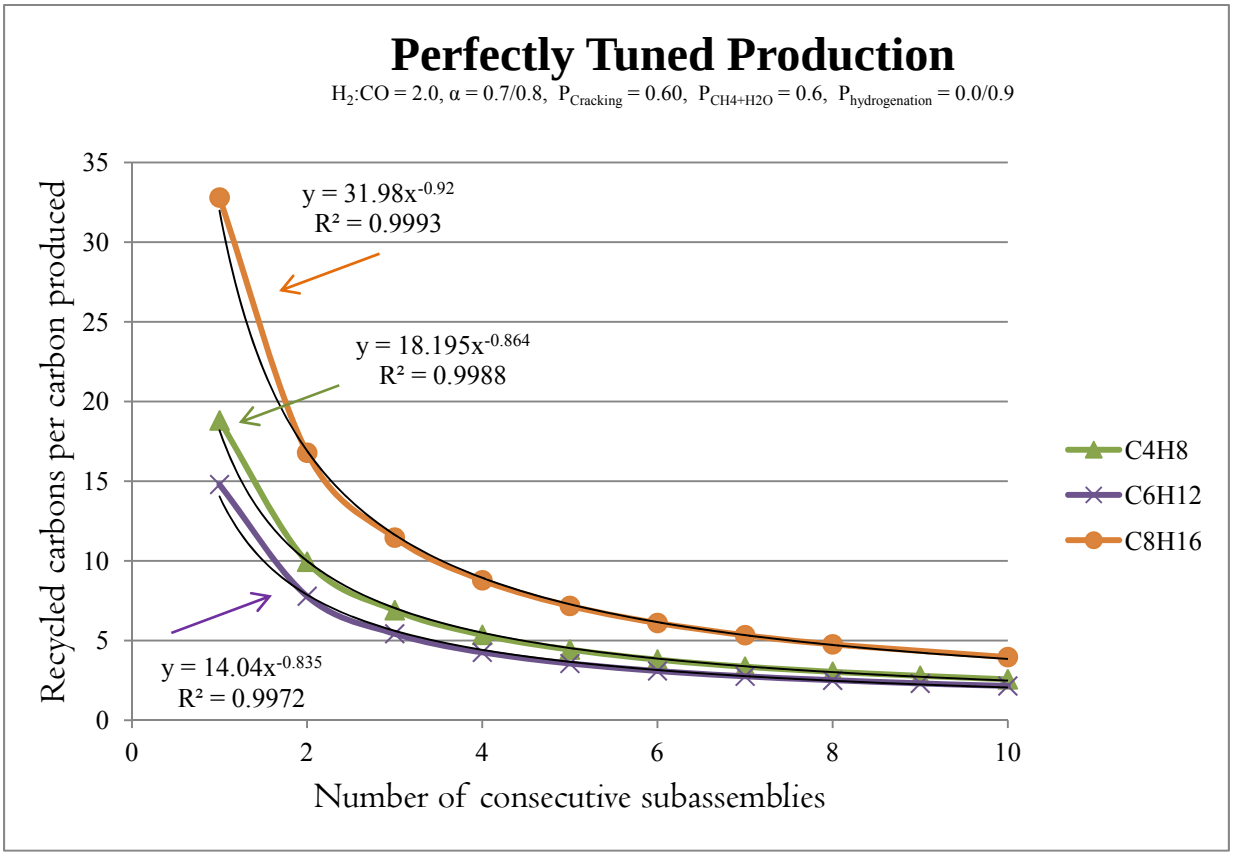

Figure 6.16: Perfectly tuned production with multiple assemblies

The results of the simulations were that while each of the three chemicals studied required different quantities of recycled carbon to produce the perfect spectrum desired, they all displayed an unambiguously decreasing power law as a function of the number of subassemblies. In other words, the more units of decreasing size were used, the less needed to be recycled to the front of the network for another pass. These simulations only included configurations as numerous as 10 reactors and crackers, but this was sufficient networking to push the recycle loop required down to 2-4 carbon atoms per carbon atom of product produced.

Chapter 7

Conclusion

This dissertation developed a modeling code capable of simulating and optimizing a hierarchical network of complex interacting units and subassemblies of such units in a robust and novel way. Advanced Flowsheet Block library-building and memory management permitted greater flexibility in stream and block connectivity, as well as manipulation of the parameters of the units, subunits, and further on down this structure from within any level of the hierarchy. Global manipulation of these parameters from the very top level in order to permute and optimize their values enabled many more possible configurations to be efficiently assessed and compared. Adjustments to weighting schemes permitted much more aggressive constraint and convergence of solutions, in which the rigorously looped and purified output streams were simulated. The code has wider ranging applications than those tested here, and would stand up to a more detailed model of fuel synthesis, thermal cracking or any other modular engineering process. Modeling would play an important role in the implementation of networks such as those investigated here since the steady state recycle loops must be carefully calibrated in order to conserve mass in the system; the response to inputs of the units involved would have to be understood in rigorous detail and manipulated in real time, which is why automation is such an

important component of small-scale networking. The code already interacts with a deep database of steam tables, and can draw from any other existing or user-provided modules and data in the same way that existing numerical modeling software can, but with the flexibility and sophistication discussed above.

The fuel synthesis network modeled in this dissertation demonstrated that a chemical process in which a spectrum of inputs is mapped into a spectrum of outputs can be vastly improved upon when networked into a variety of units processing judiciously trafficked streams. This trafficking is performed by separators which themselves need not to extraordinary, as it was analytically demonstrated that simple off-the-shelf separators can be configured in subassemblies which produce sharpening of output spectra that the individual separators could never have accomplished. This idea extended to the fuel synthesis network itself as well; the individual units need not be custom-made case by case, which would undermine the benefits of mass production, although this work demonstrated improvements that can be achieved when there are different flavors of simple units. The most powerful customization here comes not from the tailoring of each individual unit but rather the decision-making applied to the chemical streams being processed by these units. This is the great advantage of the network, that the same units which may have been previously applied to uniform chemical streams can be wholly outperformed by their application to a filtered variety of streams. The simulations here demonstrated not only that unidirectional flow through a series of units can dramatically increase the share of the user-specified product without the aid of recycled loops, but even more remarkably that recycled configurations of units can sharpen the spectrum in the steady state to a single user-specified

molecule, without a single carbon atom going to waste and with less than an order of magnitude in the number of passes per carbon atom to get there.

Future research applying these results and more rigorously understanding these benefits would entail bench scale reactor studies in order to observe true parameters of particular reacting and cracking units. This code is agnostic as to a particular chain growth value or cracking value, but empirically verified values are necessary in order to optimally direct chemical streams. The pertinent parameters are well understood in the literature, and their measurement is straightforward. What would follow is an iterative process by which simulation informs bench-scale experimentation, and experimental results inform simulations of more complex arrangements. This dissertation explored the small-scale paradigm to a specific fuel synthesis process, but the promise and possibilities of networking small modules that are sensitive to inputs is by no means restricted to Fischer-Tropsch, nor are the applications of such a robust modeling code limited to chemical conversion processes. There was already reason to believe that automation and mass production can turn traditional energy scaling paradigms on their heads. There is now reason to believe that additional networking advantages await the small-scale regime.